

INFRARED STUDIES OF HYDROGEN BONDING OF  
METHANOL WITH AROMATIC HYDROCARBONS

INFRARED SPECTRUM AND MOLECULAR  
STRUCTURE OF NITROUS ACID

INFRARED SPECTRA AND MOLECULAR STRUCTURE OF  
ISOCYANIC ACID, AND ISOTHIOCYANIC ACID

Thesis by

Llewellyn H. Jones

In Partial Fulfillment of the Requirements  
For the Degree of  
Doctor of Philosophy

California Institute of Technology  
Pasadena, California

1951

## ACKNOWLEDGMENTS

It is with great pleasure that I express my sincere appreciation for the guidance and instruction received from Professor Richard M. Badger.

I wish to acknowledge a stipend received as an Atomic Energy Commission predoctoral fellow during the year 1949-50.

With deepest gratitude, I thank my wife, Jean Jones, for her invaluable aid in preparing this thesis.

## ABSTRACT

Part I of this thesis presents the results of an investigation of hydrogen bonding of methanol with aromatic hydrocarbons. The infrared spectra of methanol in various solvents indicate that the methanol molecules form weak hydrogen bonds with aromatic hydrocarbons, probably at the center of the aromatic ring.

Part II of this thesis presents the results of an investigation of the infrared spectrum of nitrous acid. The spectrum indicates that there are two isomeric forms of nitrous acid, a cis and a trans form. The rotational structure of the hydrogen stretching band of the cis form indicates that the  $O=N-O$  angle of cis nitrous acid is  $113 \pm 2^\circ$ . A normal coordinate treatment of HONO and DONO indicates that the strongest band in the spectrum out to fifteen microns is the overtone of the  $O=N-O$  bending vibration. On the basis of this treatment the frequencies of the five in plane vibrations of trans nitrous acid have been assigned as 3590, 1696, 1270, 825, and  $413 \text{ cm}^{-1}$ .

In Part III the results of an investigation of the infrared spectrum of isocyanic acid and isothiocyanic acid are presented. For isocyanic acid the fundamental vibrational frequencies are 3534, 2280, 1340, 779, 650, and  $550 \text{ cm}^{-1}$ . The last two frequencies were obtained from combination bands. For isothiocyanic acid the fundamental vibrational frequencies are 3530,

1972, 1000, 660, 616, and 543  $\text{cm}^{-1}$ . The last three were obtained from combination bands. From the rotational structure of the N-H stretching bands of these two molecules we have calculated that the effective H-N-C angle in the ground vibrational state is  $128^{\circ}19' \pm 40'$  for HNCO and  $138^{\circ}40' \pm 1^{\circ}$  for HNCS.

Introduction . . . . . 1  
 Experimental . . . . . 2  
 Frequency and Assignment of Bands . . . . . 3  
 Rotational Structure of Bands . . . . . 4  
 Effect of Temperature on the Rotational Structure . . . . . 5

11 The Rotational Structure of the N-H Stretching Bands of  
 Methylamine . . . . . 11

12 The Rotational Structure of the N-H Stretching Bands of  
 Methylamine . . . . . 12  
 13 The Rotational Structure of the N-H Stretching Bands of  
 Methylamine . . . . . 13  
 14 The Rotational Structure of the N-H Stretching Bands of  
 Methylamine . . . . . 14  
 15 The Rotational Structure of the N-H Stretching Bands of  
 Methylamine . . . . . 15  
 16 The Rotational Structure of the N-H Stretching Bands of  
 Methylamine . . . . . 16  
 17 The Rotational Structure of the N-H Stretching Bands of  
 Methylamine . . . . . 17  
 18 The Rotational Structure of the N-H Stretching Bands of  
 Methylamine . . . . . 18  
 19 The Rotational Structure of the N-H Stretching Bands of  
 Methylamine . . . . . 19  
 20 The Rotational Structure of the N-H Stretching Bands of  
 Methylamine . . . . . 20

21 The Rotational Structure of the N-H Stretching Bands of  
 Methylamine . . . . . 21

22 The Rotational Structure of the N-H Stretching Bands of  
 Methylamine . . . . . 22  
 23 The Rotational Structure of the N-H Stretching Bands of  
 Methylamine . . . . . 23  
 24 The Rotational Structure of the N-H Stretching Bands of  
 Methylamine . . . . . 24  
 25 The Rotational Structure of the N-H Stretching Bands of  
 Methylamine . . . . . 25  
 26 The Rotational Structure of the N-H Stretching Bands of  
 Methylamine . . . . . 26  
 27 The Rotational Structure of the N-H Stretching Bands of  
 Methylamine . . . . . 27  
 28 The Rotational Structure of the N-H Stretching Bands of  
 Methylamine . . . . . 28  
 29 The Rotational Structure of the N-H Stretching Bands of  
 Methylamine . . . . . 29  
 30 The Rotational Structure of the N-H Stretching Bands of  
 Methylamine . . . . . 30

31 The Rotational Structure of the N-H Stretching Bands of  
 Methylamine . . . . . 31  
 32 The Rotational Structure of the N-H Stretching Bands of  
 Methylamine . . . . . 32  
 33 The Rotational Structure of the N-H Stretching Bands of  
 Methylamine . . . . . 33  
 34 The Rotational Structure of the N-H Stretching Bands of  
 Methylamine . . . . . 34  
 35 The Rotational Structure of the N-H Stretching Bands of  
 Methylamine . . . . . 35  
 36 The Rotational Structure of the N-H Stretching Bands of  
 Methylamine . . . . . 36  
 37 The Rotational Structure of the N-H Stretching Bands of  
 Methylamine . . . . . 37  
 38 The Rotational Structure of the N-H Stretching Bands of  
 Methylamine . . . . . 38  
 39 The Rotational Structure of the N-H Stretching Bands of  
 Methylamine . . . . . 39  
 40 The Rotational Structure of the N-H Stretching Bands of  
 Methylamine . . . . . 40

41 The Rotational Structure of the N-H Stretching Bands of  
 Methylamine . . . . . 41  
 42 The Rotational Structure of the N-H Stretching Bands of  
 Methylamine . . . . . 42  
 43 The Rotational Structure of the N-H Stretching Bands of  
 Methylamine . . . . . 43  
 44 The Rotational Structure of the N-H Stretching Bands of  
 Methylamine . . . . . 44  
 45 The Rotational Structure of the N-H Stretching Bands of  
 Methylamine . . . . . 45  
 46 The Rotational Structure of the N-H Stretching Bands of  
 Methylamine . . . . . 46  
 47 The Rotational Structure of the N-H Stretching Bands of  
 Methylamine . . . . . 47  
 48 The Rotational Structure of the N-H Stretching Bands of  
 Methylamine . . . . . 48  
 49 The Rotational Structure of the N-H Stretching Bands of  
 Methylamine . . . . . 49  
 50 The Rotational Structure of the N-H Stretching Bands of  
 Methylamine . . . . . 50

51 The Rotational Structure of the N-H Stretching Bands of  
 Methylamine . . . . . 51  
 52 The Rotational Structure of the N-H Stretching Bands of  
 Methylamine . . . . . 52  
 53 The Rotational Structure of the N-H Stretching Bands of  
 Methylamine . . . . . 53  
 54 The Rotational Structure of the N-H Stretching Bands of  
 Methylamine . . . . . 54  
 55 The Rotational Structure of the N-H Stretching Bands of  
 Methylamine . . . . . 55  
 56 The Rotational Structure of the N-H Stretching Bands of  
 Methylamine . . . . . 56  
 57 The Rotational Structure of the N-H Stretching Bands of  
 Methylamine . . . . . 57  
 58 The Rotational Structure of the N-H Stretching Bands of  
 Methylamine . . . . . 58  
 59 The Rotational Structure of the N-H Stretching Bands of  
 Methylamine . . . . . 59  
 60 The Rotational Structure of the N-H Stretching Bands of  
 Methylamine . . . . . 60

TABLE OF CONTENTS

<u>PART</u>	<u>TITLE</u>	<u>PAGE</u>
I	Infrared Studies of Hydrogen Bonding of Methanol with Aromatic Hydrocarbons	
	Introduction. . . . .	1
	Experimental. . . . .	3
	Presentation of Results . . . . .	4
	Discussion of Results . . . . .	5
	Effect of Temperature on the Hydrogen Bond. . . . .	10
II	Infrared Spectrum and Molecular Structure of Nitrous Acid	
	Introduction. . . . .	12
	Experimental Procedure. . . . .	13
	Experimental Results and Interpretation . . . . .	15
	A. Recorded Spectra. . . . .	15
	B. Molecular Structure of Nitrous Acid . . . . .	19
	C. Cis-trans Equilibrium and Intensity Relations . . . . .	33
	D. Analysis of Normal Vibrations of HONO . . . . .	38
	E. Comparison of $2\nu_{\text{O-H}}$ of Formic Acid with $2\nu_{\text{O-H}}$ cis-HONO. . . . .	52
III	Infrared Spectra and Molecular Structure of Isocyanic Acid, and Isothiocyanic Acid	
	Introduction. . . . .	54
	Experimental Procedure. . . . .	57
	Normal Modes of Vibration of HNCO and HNCS. . . . .	58
	Presentation and Discussion of Results. . . . .	59
	A. Vibrational Frequencies of HNCO and DNCO. . . . .	59
	B. Rotational Structure of the First Overtone of the N-H Stretching Vibration. . . . .	68
	C. Molecular Structure of HNCO . . . . .	81
	D. Rotational Structure of the N-H Fundamental Absorption Band. . . . .	83
	E. Rotational Structure of the Combination Band, $\nu_1 + \nu_4$ , of HNCO . . . . .	87
	F. Calculation of $X_{01}$ for Hydrogen Bonding Vibration . . . . .	90
	G. Perturbations in the Upper Level of the Band at $5790\text{ cm}^{-1}$ , ( $\nu_1 + \nu_2$ ) . . . . .	92

<u>PART</u>	<u>TITLE</u>	<u>PAGE</u>
H.	Vibrational Frequencies of Isothiocyanic Acid . . . . .	96
I.	Rotational Structure of the First Overtone of the N-H Stretching Vibration of HNCS. . . . .	101
J.	Molecular Structure of HNCS . . . . .	102
 Appendices:		
	Appendix I. . . . .	105
	Appendix II . . . . .	108
	Appendix III. . . . .	110
	Appendix IV. . . . .	113
	Appendix V. . . . .	119
	Appendix VI . . . . .	128
	Appendix VII. . . . .	130
	Appendix VIII . . . . .	134
	Appendix IX . . . . .	137
	Appendix X. . . . .	140
	Appendix XI . . . . .	143
References . . . . .		147
Propositions . . . . .		150



## Introduction.

The vibration-rotation spectrum of methanol vapor was investigated in the photographic infrared by Badger and Bauer (1). They observed the third harmonic of the O-H vibration with its center at 9490 Å. Badger and Bauer (2) also investigated, in the photographic infrared, the spectra of liquid methanol and of dilute solutions of methanol in carbon tetrachloride. For the third harmonic of the O-H vibration in the pure liquid they observed a band at 10,068 Å, while in dilute solutions in carbon tetrachloride the absorption band was at 9577 Å.

The above observations illustrate two classes of frequency shifts. The first shift, from 9490 to 10,068 is ascribed mainly to hydrogen bonding, the hydrogen atom of the O-H group of one alcohol molecule forming a weak bond with the oxygen atom of another molecule. The much smaller shift, from 9490 to 9577, is due to the interaction of the O-H group with the dielectric field of the solvent. Kirkwood, from his theory of solutions containing zwitterions (3), has developed a theoretical formula for this shift, assuming a simple electrostatic interaction of an oscillating dipole with its surroundings of dielectric constant  $D$ . He found that the relative shift to lower frequencies should be approximately proportional to  $(D-1)/(2D+1)$ . This simple derivation has not been published and is therefore presented in Appendix I.

Gordy (4) has made a considerable number of investigations of the shift in the O-H frequency due to hydrogen bonding with

oxygenated and with nitrogenated solvents. He also investigated the shift in the O-D frequency of  $\text{CH}_3\text{OD}$  due to "hydrogen" bonding with various solvents (5). In most of his work Gordy used benzene as an "inert" solvent; that is, a solvent in which the O-H band of the methanol is unshifted since no association occurs. However, Kreuzer and Mecke (6) observed that the O-H band of methanol in benzene solution is appreciably shifted to longer wavelengths and considerably broadened, as compared with the O-H band of methanol dissolved in carbon tetrachloride. The shift of the O-H frequency in benzene as a solvent appears to be due to some sort of association, as it is much greater than that expected from the dielectric constant of benzene, and the broadening of the band resembles the association bands of alcohols investigated by Badger and Bauer (2) and also by Fox and Martin (7). Fox and Martin speak of the broad association band as a distribution curve showing the proportion of molecules with any given strength of binding; thus, the stronger the hydrogen bond is, the more shifted will be the O-H vibrational frequency.

We have undertaken an investigation of the third harmonic of the O-H band of methanol in three groups of solvents: (a) carbon tetrachloride, normal hexane, and cyclohexane; (b) pentachloroethane, sym-tetrachloroethane, and chloroform; (c) aromatic hydrocarbons. The members of the first group are nonpolar and appear to be "inert", exhibiting a small frequency shift proportional to  $(D-1)/(2D+1)$  where D is the dielectric constant of the

solvent. The second group exhibits a shift somewhat less than expected from the dielectric constants of the solvents. However, the aromatic hydrocarbons exhibit a shift much greater than that expected and indicate some sort of association of the O-H hydrogen atom with the aromatic ring.

### Experimental.

The instrument used was a large Littrow spectrograph with a glass prism giving a dispersion of about 64 wave numbers per mm. The spectra were recorded on Eastman 1Z plates, sensitized with 3% ammonia.

Since the association bands of the O-H vibration in aromatic solvents are quite broadened it was sometimes difficult to assign the maximum. However, it is believed that where a maximum is given it is accurate to within 10 wave numbers. In the more highly substituted aromatic solvents very broad association bands were obtained which did not exhibit a pronounced maximum, but appeared to have two small maxima at either end of the broad band. All maxima listed were measured from microphotometer tracings of the photographic plate transmission. The expansion of the microphotometer tracings is eight times that of the original photographic plates.

The wavelengths were determined by photographing an arc spectrum of known lines alongside the absorption spectrum. A carbon arc was used, operated at 160 volts and 6 amps. On the lower electrode were placed salts of  $Ba^{++}$ ,  $Na^+$ ,  $K^+$ ,  $Ca^{++}$ ,  $Sr^{++}$ ,

and  $\text{Cr}^{+++}$  which gave 15-20 lines distributed between 0.8 and 1.2  $\mu$ . Longer exposure brought out more lines. The wavelengths of these standard lines were taken from the Handbook of Chemistry and Physics (1947).

The solutions used were 1 volume formal in methanol. Path lengths were 19 cm. The times of exposure varied from two to three minutes. A five hundred watt tungsten lamp was used as the source.

Aromatic hydrocarbons have weak C-H bands near the third harmonic of the O-H band of methyl alcohol. In order to make a satisfactory comparison, the following procedure was used. In each case three exposures were taken, using two cells of the same path length in series.

- 1) 19 cm. of 1 vf methanol in carbon tetrachloride and 19 cm. of the aromatic hydrocarbon;
- 2) 19 cm. of carbon tetrachloride and 19 cm. of 1 vf methanol in the aromatic hydrocarbon;
- 3) 19 cm. of carbon tetrachloride and 19 cm. of the aromatic hydrocarbon.

#### Presentation of Results.

The third harmonic of the O-H vibration has been redetermined for methyl alcohol vapor and found to be at  $9490 \text{ \AA}$ , ( $10,537 \text{ cm}^{-1}$ ), as determined by Badger and Bauer (1). This same absorption band was studied in various solvents with the following results. In carbon tetrachloride, n-hexane, and cyclohexane for the O-H band

a relatively sharp peak was observed at 9590, 9570, and 9580 Å respectively. In chloroform, pentachloroethane, and symtetrachloroethane the O-H band was also a relatively sharp peak at 9623, 9613, and 9633 Å respectively. The solutions of methanol in the aromatic hydrocarbons exhibit an O-H band not only shifted to longer wavelengths, but also considerably broadened. Furthermore, for the substituted benzenes there appear to be two overlapping O-H bands. The O-H bands for methanol in aromatic hydrocarbons are shown in Fig. I, together with the O-H band of methanol in carbon tetrachloride for comparison. In Table I are listed the observed O-H frequencies of solutions of methanol in the various solvents, the shift in these frequencies from the frequency in the vapor ( $10,537 \text{ cm}^{-1}$ ), the dielectric constant,  $D$ , of the solvent, and the value of  $(D-1)/(2D+1)$ . In Fig. II is plotted the frequency shift, from methanol vapor to solution, as a function of  $(D-1)/(2D+1)$ .

#### Discussion of Results.

From Fig. II we see that for the aromatic hydrocarbons as solvents the proportionality of  $\Delta\nu$  to  $(D-1)/(2D+1)$  fails badly. The frequency shift is much greater than we would expect from the dielectric constant alone. Thus we are led to believe that the methanol molecules are bonded to the aromatic hydrocarbon molecules through a weak hydrogen bond involving the O-H hydrogen atom.

For methanol in the more highly substituted hydrocarbons,

Fig. I. Absorption spectra of one volume-formal methanol in the indicated solvent, compared in each case with the single sharp peak of methanol in  $\text{CCl}_4$ .

The dotted line represents solvent background.

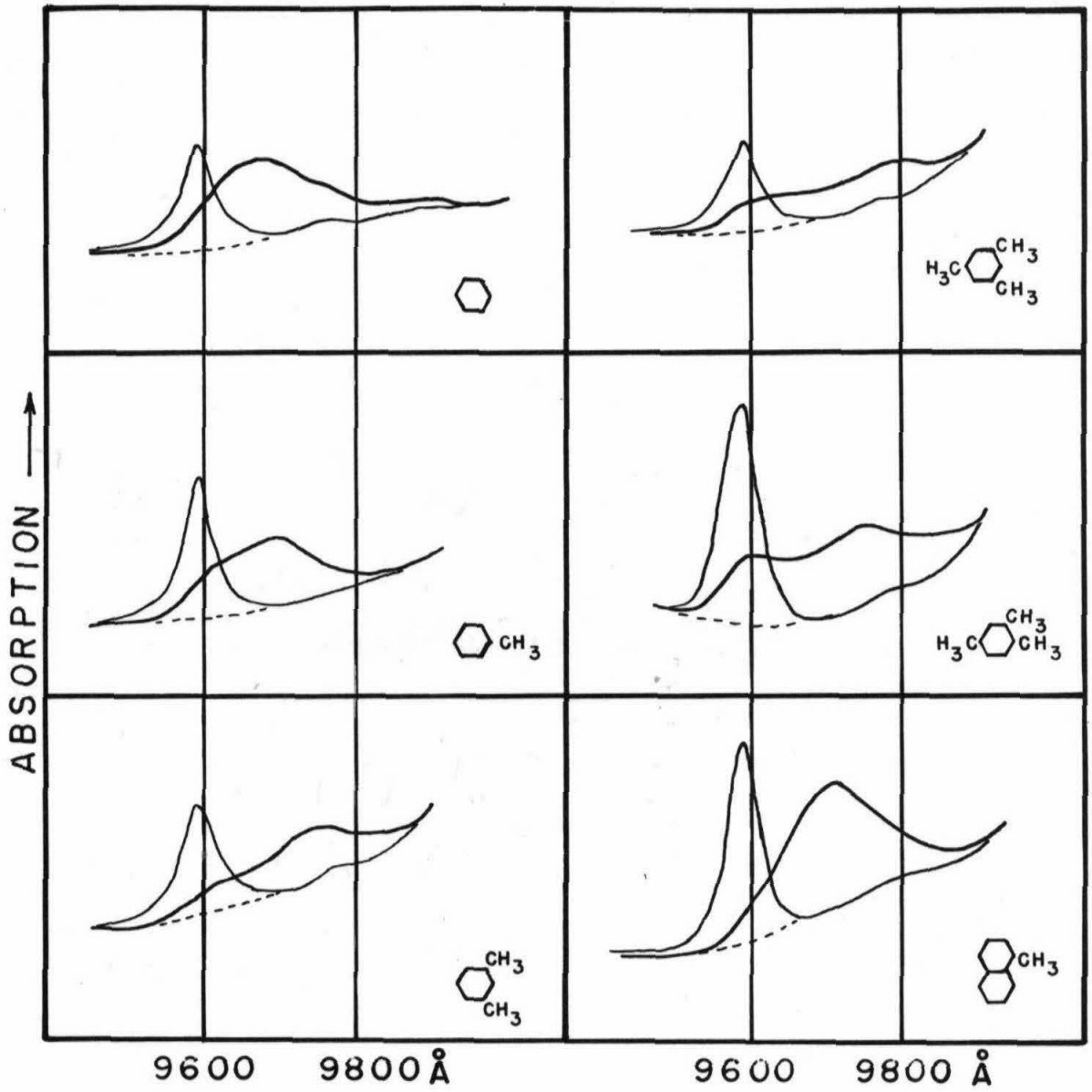


Fig. II. Frequency shift of the third-harmonic O-H absorption band of methanol plotted against the indicated function of the dielectric constant of the solvent.

The small solid circles are for the high frequency maxima where two occur.

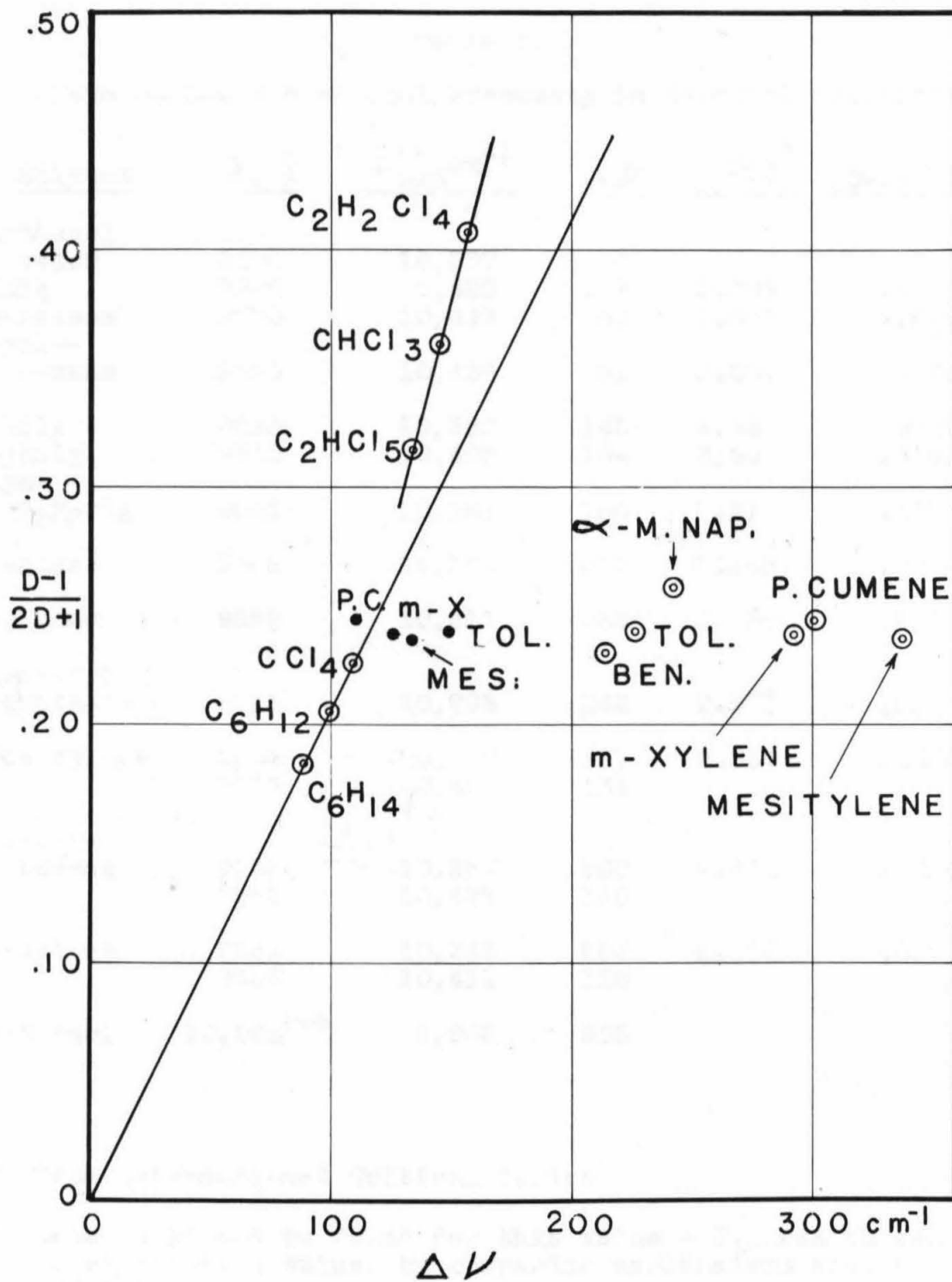


Table I.

Data on O-H Vibrational Frequency in Methanol Solutions.

<u>Solvent</u>	$\lambda, \text{\AA}$	$\nu_{\text{max}} \text{cm}^{-1}$	$\Delta\nu$	$D_{28}^*$	$(D-1)/(2D+1)$
methanol vapor	9490	10,537	0		
CCl <sub>4</sub>	9590	10,428	109	2.229	.2252
n-hexane	9570	10,449	88	1.865	.1829
cyclo- hexane	9580	10,438	99	2.039	.2046
CHCl <sub>3</sub>	9623	10,392	145	4.85	.3598
C <sub>2</sub> HCl <sub>5</sub>	9613	10,403	134	3.55	.3148
sym- C <sub>2</sub> H <sub>2</sub> Cl <sub>4</sub>	9633	10,381	156	7.61	.4075
benzene	9686	10,324	213	2.268	.2291
toluene	9698	10,311	226	2.369	.2386
$\alpha$ -methyl naphthalene	9713	10,295	242	2.6**	.258
mesitylene	9804	10,200	337	2.337	.2356
	9613	10,403	134		
pseudo- cumene	9768	10,237	300	2.414	.2426
	9592	10,427	110		
m-xylene	9761	10,245	292	2.359	.2377
	9605	10,411	126		
methanol	10,068***	9,932	605		

\* From International Critical Tables

\*\* Data could not be found for this value - 2.6 was chosen as an approximate value, by comparing naphthalene with benzene and toluene.

\*\*\* From Badger and Bauer (2).

mesitylene, pseudo-cumene, and meta-xylene, there appear to be two maxima for the O-H band. Even for toluene as a solvent the spectrum suggests that there are two maxima overlapping. The presence of two O-H bands suggests that some of the methanol molecules are not associated. Where two maxima appear the frequency shift for the short wave length maximum lies close to the curve of Fig. II, indicating that this absorption arises from unassociated methanol molecules. Thus it appears that increasing the number of methyl groups on the benzene ring increases the strength of the association, but at the same time decreases the probability of association.

The formation of a hydrogen bond by methanol with aromatic hydrocarbons indicates that there is a concentration of negative charge on the hydrocarbons, probably at the center of the benzene ring. Methyl groups on the benzene ring apparently increase the negative charge at the center of the ring, but also make it more difficult for the alcohol molecule to approach this hydrogen bonding site.

Mesitylene exhibits stronger association than its unsymmetrical isomer pseudocumene. The symmetrical addition of methyl groups would cause the greatest increase of negative charge at the center of the aromatic ring. The unsymmetrical addition, as in pseudo-cumene, would show the greatest concentration of negative charge at a point away from the center of the ring. These facts further suggest that the O-H bond of the alcohol associates with the aromatic molecule at the center of the aromatic ring.

Effect of Temperature on the Hydrogen Bond.

The effect of temperature on the O-H association band was briefly investigated. An 0.4 volume formal solution of cyclohexanol in pseudo-cumene was investigated. The absorption spectrum was taken at various temperatures, as shown in Fig. III. As the temperature is increased the broad, shifted band reverts to the narrower, less-shifted band, similar to the O-H band of cyclohexanol in carbon tetrachloride solution.

This observation serves to substantiate the idea that the alcohol molecules are associated with the aromatic ring, as association would be expected to decrease as the temperature is raised, as observed by Fox and Martin (7).



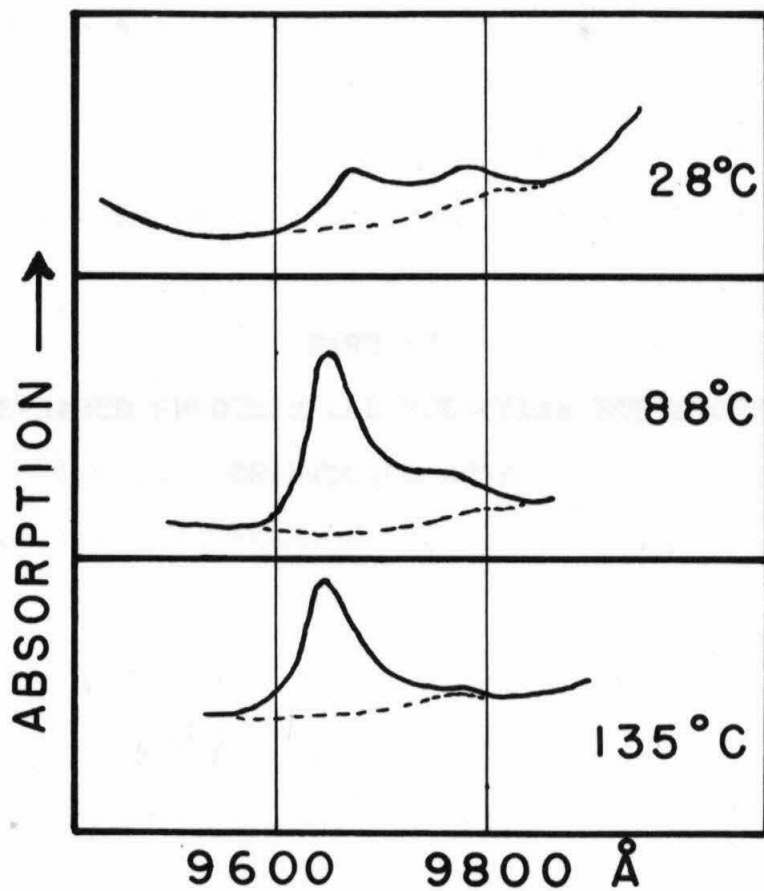


Fig. III. Absorption spectra of 0.4 volume-formal solutions of cyclohexanol in pseudocumene at different temperatures.



## Introduction.

Nitrous acid is a rather weak and unstable acid, which unfortunately cannot be isolated. To maintain an appreciable concentration in the vapor phase a large excess of nitric oxide is necessary, as well as appreciable amounts of nitrogen dioxide and water vapor. Thus its structure does not lend itself to electron diffraction investigation. In studying the ultraviolet absorption spectra of mixtures of nitric oxide, nitrogen dioxide, and water vapor, Melvin and Wulf (8) observed bands which they attributed to nitrous acid. E. J. Jones (9) observed absorption in the near infrared, between 7000 and 7025  $\text{cm}^{-1}$ , which was attributed to the first overtone of the O-H vibration in nitrous acid.

Prior to this investigation little was known of the molecular structure of nitrous acid. If the valence formula for nitrous acid is  $\text{H-O-N=O}$  it is expected that its structure would be similar to that of formic acid. Formic acid approximates a symmetric top well enough to give characteristic parallel and perpendicular type bands, with regular fine structure from which the effective moments of inertia in the ground state have been calculated (10, 11). It was hoped that the spectrum of nitrous acid would exhibit absorption bands with similar rotational fine structure. Indeed it was found that one band exhibits characteristic structure from which the large rotational constant in the ground state has been calculated.

After a brief description of the experimental procedure, the

observed spectra are presented. There follows a discussion of the rotational structure of one of the bands. In order to aid in assigning the fundamental vibrational frequencies a normal coordinate treatment of HONO is presented.

#### Experimental Procedure.

Nitrous acid was prepared by introducing nitric oxide, nitrogen dioxide, and water vapor into the absorption cell. NO was used in large excess; NO<sub>2</sub> and N<sub>2</sub>O<sub>4</sub> were kept low as they contribute several intense absorption bands. A typical mixture was 600 mm NO added to 40 mm of an NO<sub>2</sub>, N<sub>2</sub>O<sub>4</sub> mixture at 25°C. To the resulting mixture water vapor was added to saturation at 25°C. As shown in Appendix II, this procedure gave an equilibrium mixture with a pressure of about 21 mm Hg for the nitrous acid present, calculated on the basis of equilibrium constant of Verhoek and Daniels (12), Wayne and Yost (13), and Forsythe and Giaque (14). A few drops of water added to the cell dissolved most of the NO<sub>2</sub> and N<sub>2</sub>O<sub>4</sub> as well as some of the nitrous acid. Indeed this procedure decreased the nitrous acid absorption, but also caused the NO<sub>2</sub> and N<sub>2</sub>O<sub>4</sub> bands to almost disappear.

Absorption cells with pyrex windows were used for mapping the spectrum out to 2.7 microns, and cells with silver chloride windows were used for longer wavelengths.

The vacuum spectrograph designed by Badger, Zumwalt, and Giguere (15) was used for mapping the spectrum from 1 to 3.2 microns. This spectrograph employed a replica grating of 7500

lines per inch, and a lead sulfide photoconductive cell to measure the intensity of light transmitted. This instrument will resolve water lines slightly more than one wave number apart at 2 microns. The spectrograph was calibrated with argon lines (16) emitted from a sodium arc, and with water vapor absorption lines as reported by R. C. Nelson (17). It was found possible to use the lead sulfide cell out to 3.2 microns by cooling it to dry ice temperature. Cooling the cell greatly increased its sensitivity throughout the spectrum. The photoconductive cell rested in a hollow end of a solid copper rod which was projected about a foot outside of the vacuum spectrograph. The external portion of the rod was completely immersed in a dry ice-methanol bath. The temperature of the lead sulfide cell under these conditions was believed to be between  $-50^{\circ}\text{C}$  and  $-60^{\circ}\text{C}$ . Special Army Navy low temperature O-rings were used to maintain a vacuum seal about the copper rod. Of several lead sulfide cells investigated, only a few showed marked response to cooling.

The spectrum of nitrous acid was also mapped from 2 to 15 microns using a Beckman IR-2 spectrometer, with a sodium chloride prism. This spectrograph has a resolution of about  $3\text{ cm}^{-1}$  at 9 microns. The wavelength drive and slit control are coupled in such a fashion that the intensity background is reasonably constant.

For each of the spectrographs described above a Brown recorder gives a continuous plot of wavelength versus transmission.

Slit widths are given with the high dispersion spectra. These are the effective slit widths - the width of an absorption line at half-height calculated from the geometry of the spectrographs, assuming the grating is perfect.

In the absorption spectra shown, the broken line represents the background intensity, including water vapor absorption.

#### Experimental Results and Interpretation.

##### A. Recorded Spectra

The low dispersion spectra of nitrous acid and deuterio-nitrous acid, from 2 to 15 microns, are shown in Fig. IV.

The two hydrogen stretching fundamentals were observed also with the grating spectrograph. Their spectrum is shown in Fig. V.

The high dispersion spectra of HONO and DONO were also observed from 1 to 2.7 microns. The complete spectra will not be shown here but the frequencies, relative intensities, and character of the observed bands, together with those of Figs. IV and V, are given in Table II.

In Table II the relative intensities given are only qualitative but give the correct order of magnitude. An intensity of 100 is assigned to the strongest band in the HONO spectrum and also to the strongest band in the DONO spectrum. These bands are of approximately equal intensity. The character of the bands listed in Table II refers to their appearance as

Fig. IV. Absorption spectra of HONO and DONO

	Pressure	Path Length
A. DONO	2-3 mm	5 cm
B. DONO	2-3 mm	50 cm
C. HONO	2-3 mm	5 cm
D. HONO	2-3 mm	50 cm

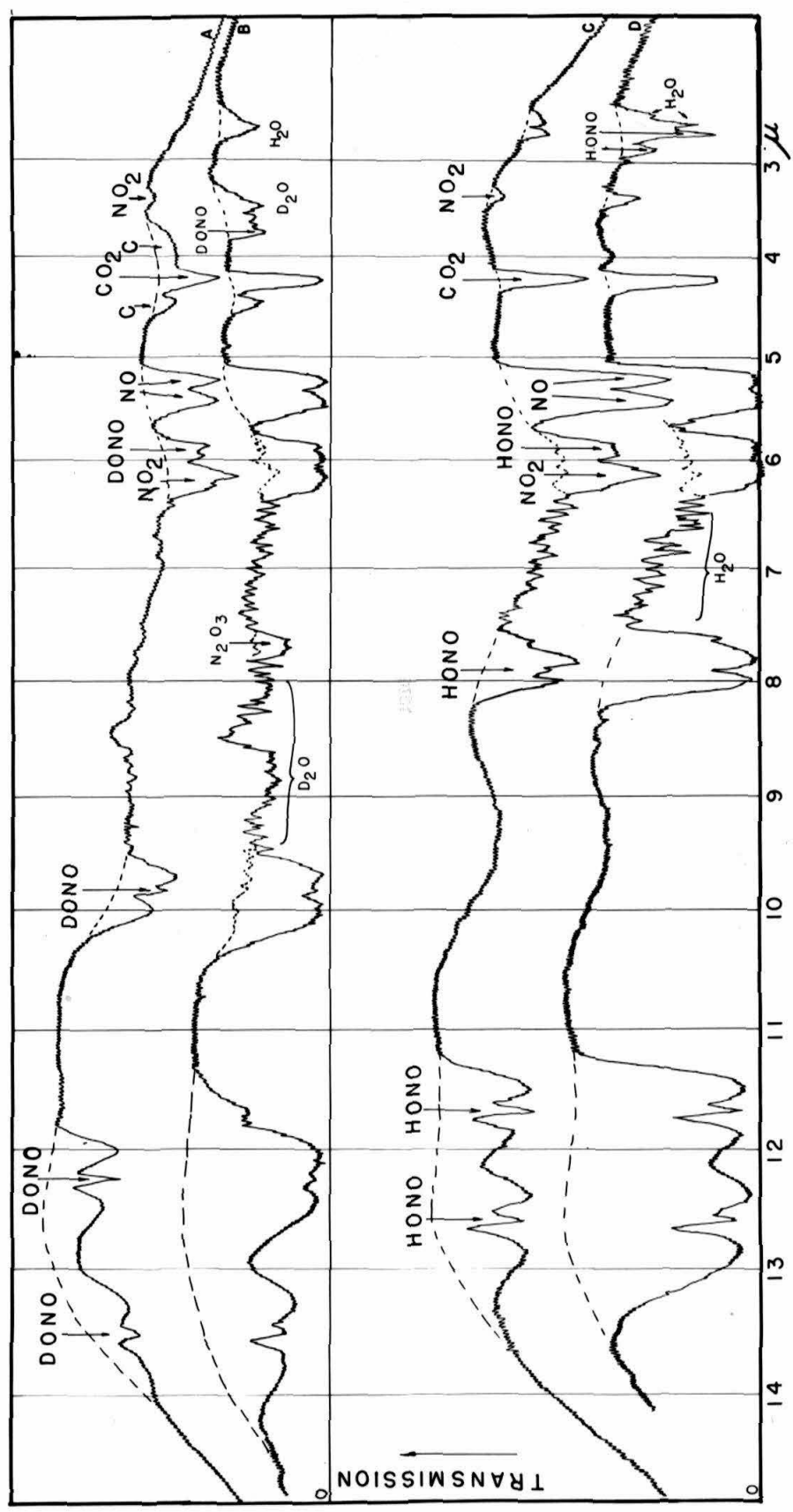


Fig. V. Absorption spectrum of hydrogen stretching fundamentals of cis and trans nitrous acid.

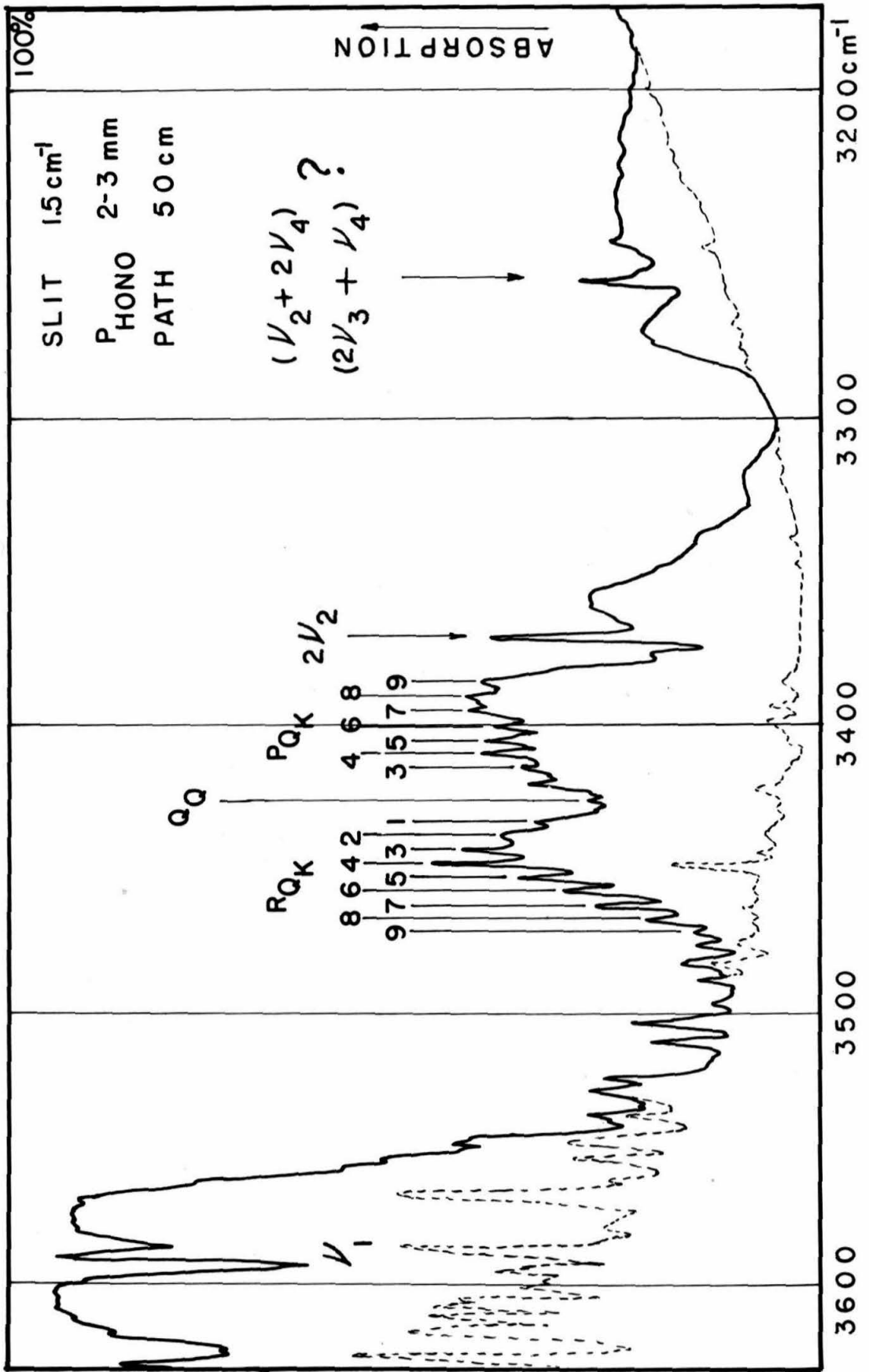


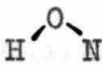
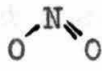
Table II.

Observed Infrared Absorption Bands for HONO and DONO  
from 1 to 15 Microns.

Assignment	$\nu$ cm <sup>-1</sup>	HONO		$\nu$ cm <sup>-1</sup>	DONO	
		Int	Character		Int	Character
$\nu_4$ (N-O)	794 $\pm$ 1	100	parallel	739 $\pm$ 1	40	parallel
$2\nu_5$ (O-N=O)	856 $\pm$ 1	100	" "	816 $\pm$ 1	100	" "
$\nu_3$ (H-O-N)	1270 $\pm$ 1	50		1018 $\pm$ 1	60	
$\nu_2$ (N=O)	1696 $\pm$ 1	20		1690 $\pm$ 5	20	
$2\nu_3$	2505 $\pm$ 10	2				
$\nu_2 + 2\nu_4$ or $2\nu_3 + \nu_4$	3257 $\pm$ 1	1	" "			
$2\nu_2$	3372 $\pm$ 1	1.5	" "	3361 $\pm$ 1		" "
$\nu_1$ cis (O-H)	3426 $\pm$ .3	1.5	hybrid	2530 $\pm$ 10	1	
$\nu_1$ trans (O-H)	3590 $\pm$ 1	5	parallel	2650 $\pm$ 10	3	
$(2\nu_3 + \nu_2)$	4124 $\pm$ 1	.0005	" "			
$\nu_1^t + \nu_4$	4378 $\pm$ 1	.001	" "			
$\nu_1^t + \nu_3$	4830 $\pm$ 1	.02	" "			
$3\nu_2$	5038 $\pm$ 1	.002		4999 $\pm$ 1		hybrid
$\nu_1^t + 2\nu_3$	6050 $\pm$ 1	.001	" "			
$2\nu_1^c$	6664.8 $\pm$ .5	.03	hybrid	4963 $\pm$ 1		" "
$2\nu_1^t$	7015 $\pm$ 1	0.10	parallel	5212 $\pm$ 1		parallel

compared with parallel and perpendicular bands of a symmetric top molecule. The hybrid bands appear to have both parallel and perpendicular structure.

Assignments of fundamental vibrational frequencies were made on the basis of a normal coordinate treatment, presented in section II-D. The assignments given in Table I are characterized as follows:

$\nu_1$	O-H	stretching
$\nu_2$	-N=O	stretching
$\nu_3$		bending
$\nu_4$	-N-O-	stretching
$\nu_5$		bending

$\nu_1^t$  is attributed to the hydrogen stretching vibration of a "trans" form of nitrous acid.  $\nu_1^c$  is attributed to the hydrogen stretching vibration of a "cis" form of nitrous acid. The reasons for these assignments are discussed in section II-B. Neither  $\nu_1^c$  nor  $\nu_1^t$  can be attributed to combination or overtone bands as they both exhibit overtones,  $2\nu_1^c$  and  $2\nu_1^t$ . These frequencies give the expected isotopic shift for hydrogen stretching frequencies when deuterium is substituted for hydrogen. Furthermore, they both exhibit the usual degree of anharmonicity found in O-H stretching vibrations.

#### B. Molecular Structure of Nitrous Acid

As mentioned above, at both 3 microns and 1.5 microns two

bands appear which it seems necessary to describe as hydrogen stretching fundamentals and overtones respectively. In each region one band has P, Q, and R envelopes while the other shows rotational structure from which we can obtain the largest rotational constant of the molecule.

Figure VI shows the high dispersion spectra of  $2\nu_1^c$  and  $2\nu_1^t$  for HONO, and Fig. VII shows the high dispersion spectra of  $2\nu_1^c$  and  $2\nu_1^t$  for DONO.

These bands will be treated as perpendicular bands of a prolate symmetric top, assuming the maxima in the bands to be Q branches arising from transitions with  $\Delta K = \pm 1$ ,  $\Delta J = 0$ . In Appendix III we shall consider the more exact energy expression for the asymmetric top, and show that the error introduced by using the relations for the approximate symmetric top is negligible. Table III gives the measured frequencies of Figs. VI and VII. The band  $2\nu_1^c$  for DONO has indeed poorly resolved structure, however, the recorded maxima were observed on several different tracings of the same band and are thus believed to be real.

For the approximate symmetric top, neglecting centrifugal stretching, we use the usual expression (18) for the energy levels:

$$W = \frac{1}{2} (B_V + C_V) J(J + 1) + \left[ A_V - \frac{1}{2} (B_V + C_V) \right] K^2 + G(v) \quad (1)$$

$$A > B > C, \quad A = \frac{h}{8\pi^2 c I_A}, \text{ etc.}$$

Fig. VI. Second harmonic of O-H stretching of cis and trans HONO.

Fig. VII. Second harmonic of O-D stretching of cis and trans DONO.

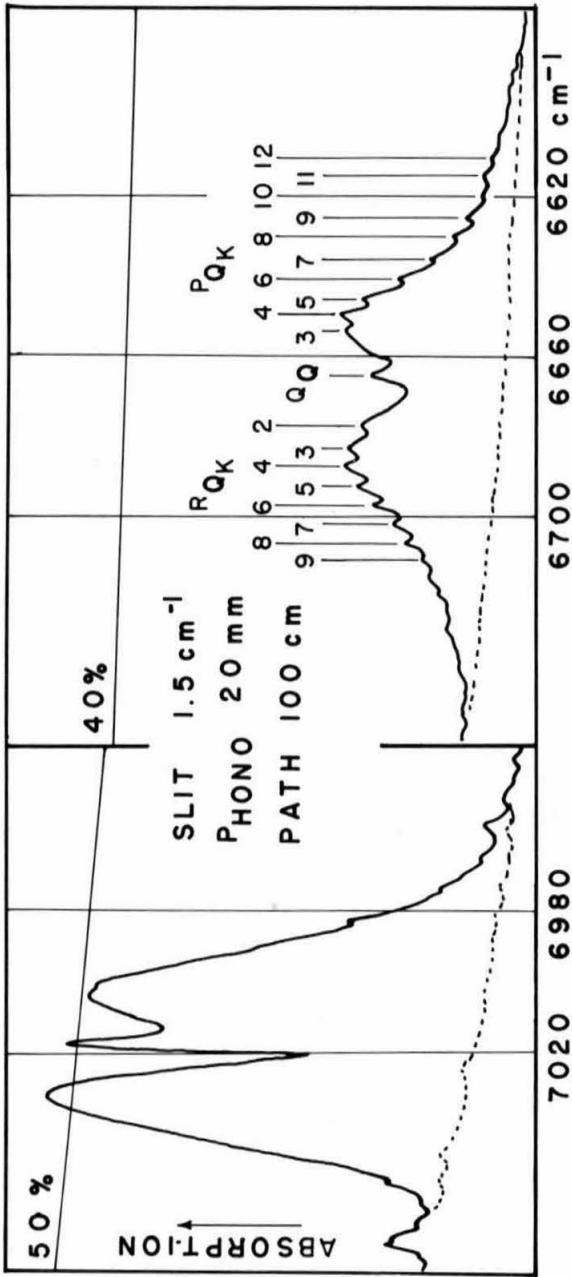


Fig. VI

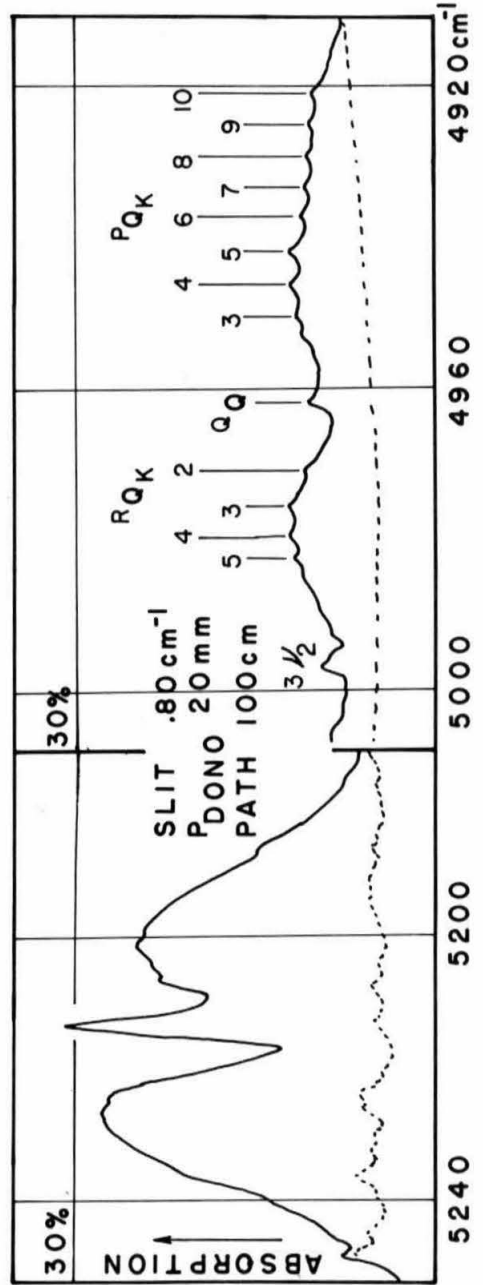


Fig. VII

Table III.

Observed Frequencies of Vibration-Rotation Maxima In  
Hydrogen Stretching Bands of Cis-nitrous Acid

K''	HONO		DONO	
	$\nu_1^c$ cm <sup>-1</sup>	$2\nu_1^c$ cm <sup>-1</sup>	$2\nu_1^c$ cm <sup>-1</sup>	
R Q K	9	3470.86	6709.98	
	8	3466.54	6705.19	
	7	3461.69	6700.51	
	6	3456.86	6695.63	
	5	3452.29	6691.18	4983.44
	4	3447.24	6685.90	4979.88
	3	3442.71	6680.84	497.23
	2	3437.11	6675.46	4972.11
	1	3432.84		
	0			
P Q K	1		6658.19	
	2			
	3	3414.09		4953.65
	4	3409.52	6648.06	4949.68
	5	3405.17	6644.08	4945.43
	6	3400.19	6638.98	4940.99
	7	3395.17	6633.59	4936.65
	8	3390.53	6628.50	4932.52
	9	3385.56	6623.64	
	10	3380.97	6618.67	
	11	3375.70	6613.70	

K'' refers to lower vibrational state.

Letting  $\left[ A_v - \frac{1}{2}(B_v + C_v) \right] = X_v$  we can make combinations to solve for  $X_v$  as:

$$\begin{bmatrix} R \\ Q \\ K \end{bmatrix}_v - \begin{bmatrix} P \\ Q \\ K \end{bmatrix}_v = 4KX_v$$

$$\begin{bmatrix} R \\ Q \\ K-1 \end{bmatrix}_v - \begin{bmatrix} P \\ Q \\ K+1 \end{bmatrix}_v = 4KX_0$$

$X_v$  is the rotational constant in the upper state and  $X_0$  is the rotational constant in the lower state. The subscripts on  $Q$  in the above combinations refer to the value of the rotational quantum number  $K$  in the lower vibrational state. The superscripts  $R$  and  $P$  refer to transitions for which  $\Delta K = +1$  and  $\Delta K = -1$  respectively. From the data of Table III and the above combinations, values of  $X_1$ ,  $X_2$ , and  $X_0$  have been determined for HONO, and  $X_2$  and  $X_0$  for DONO. These results are given in Table IV.

Table IV.

Experimental Rotational Constants for HONO and DONO

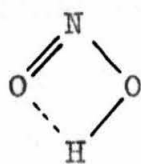
K	HONO			DONO		
	$X_0$ cm <sup>-1</sup> Calculated from $\nu_1^c$	$X_0$ cm <sup>-1</sup> Calculated from $2\nu_1^c$	$X_1$ cm <sup>-1</sup>	$X_2$ cm <sup>-1</sup>	$X_0$ cm <sup>-1</sup>	$X_2$ cm <sup>-1</sup>
1						
2						
3	2.30	2.28	2.39		1.87	1.88
4	2.35	2.30	2.36	2.37	1.92	1.89
5	2.35	2.35	2.36	2.36	1.94	1.90
6	2.38	2.40	2.36	2.36	1.95	
7	2.37	2.40	2.38	2.39		
8	2.38	2.40	2.38	2.40		
9	2.38	2.40	2.37	2.40		
10	2.38	2.41				

Since HONO is a slightly asymmetric top the  $+$  and  $-$  K levels of the symmetric top are split. This splitting increases with increasing J but decreases with increasing K. Since the most populated J levels for HONO will be fairly high (between 15 and 20), the levels of low K are widely split and are not expected to even approximate Equation (1). However, for higher K values Equation (1) becomes better. Indeed, for HONO for levels K = 6 and higher, Table IV shows quite constant values for  $X_0$ . The value for  $X_0$  from the band  $\nu_1^c$  is slightly lower than that from  $2\nu_1^c$  - probably because half of the band  $\nu_1^c$  coincides with half of the band  $2\nu_2^c$ , which displaces

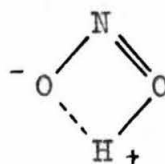
the  $P_Q$  branches. Therefore, the value of  $2.40 \text{ cm}^{-1}$  is probably the more reliable value for  $X_0$  obtained from Equation (1). Since  $X_0$  varies very little from  $K = 6$  to  $K = 10$  it seems that our neglect of the centrifugal stretching was justifiable and that we should assign  $2.40 \pm .02 \text{ cm}^{-1}$  to  $X_0$  for the nonrotating molecule.

For DONO the data is rather poor. We have not observed sufficient  $P_{Q_K}$  and  $R_{Q_K}$  maxima to determine  $X_0$  for  $K > 6$  where Equation (1) is more accurate. For HONO the value of  $X_0$  calculated at  $K = 6$  is the correct value so the value for DONO calculated at  $K = 6$  is probably close to the correct value. Thus  $X_0$  for DONO is probably between  $1.95$  and  $2.00 \text{ cm}^{-1}$ . We shall report it as  $1.95 \pm .05 \text{ cm}^{-1}$ .

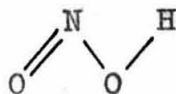
We have determined that  $A_0 - \frac{1}{2}(B_0 + C_0) = 2.40 \pm .02 \text{ cm}^{-1}$  for HONO and  $1.95 \pm .05 \text{ cm}^{-1}$  for DONO. Before attempting to interpret this constant we shall discuss the possible structures for nitrous acid. Four structures must be considered, all having an equal number of bonds. These possibilities are indicated in Fig. VIII, with probable resonant structures.



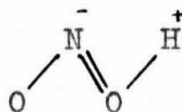
I-A



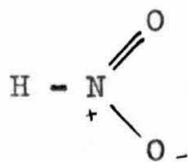
I-B



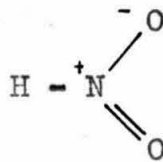
II-A



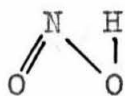
II-B



III-A



III-B



IV

Fig. VIII. Possible Structures of Nitrous Acid

Structure I we shall call the "cis" structure, structure II the "trans" structure, and structure III the "nitro" structure. Structures I, II, and III are all planar to gain the indicated resonances. Structure IV is non-planar and cannot gain the double bond resonance energy. Furthermore, if the hydrogen is not held in the trans position we should expect the terminal oxygen atom to pull the hydrogen atom into the plane. We believe that structure IV need not be considered further.

The frequency of the hydrogen stretching vibration,  $\nu_1^c$ , is  $3426 \text{ cm}^{-1}$ . This is normal for an N-H frequency but is indeed quite low for an O-H frequency. This fact favors structure III. Therefore, we shall investigate first the possibility of the nitro structure giving rise to the band at  $3426 \text{ cm}^{-1}$ . Due to the double bond we expect the nitro model to be planar. Therefore, the largest axis of inertia must be perpendicular to the plane of the molecule. The least axis of inertia will be parallel to the line through the two oxygen atoms unless the O-N=O angle is below  $65^\circ$ . Actually we expect the O-N=O angle to be in the neighborhood of  $125^\circ$ ; Brockway, Beach, and Pauling (19) found an O-N=O angle of  $127 \pm 3^\circ$  for nitromethane. Due to the complete resonance of the equivalent structures, III-A and III-B, the nitro model will have  $C_{2v}$  symmetry and the N-H bond will be perpendicular to the least axis of inertia. Therefore, the N-H stretching vibration will be along the intermediate axis of inertia and the alternating dipole moment must lie on

this axis. From the selection rules for such a transition, given by Herzberg (20), we find that for transitions having  $\Delta J = 0$  the subscript  $\tau$  must change by  $\pm 2$  ( $\tau$  is the subscript on  $E_{\tau}$ , the exact energy levels of King, Hainier, and Cross (21) for the asymmetric top). This corresponds to  $\Delta K = \pm 1$  for the approximate symmetric top. Thus, we can have no  $Q_Q$  branch (no transitions having  $\Delta J = 0$ , and  $\Delta K = 0$ ). More precisely, from the exact energy levels,  $E_{\tau}$ , given by King, Hainier and Cross (21), and the selection rules for  $\tau$  we should find no absorption maxima near the band center for the N-H absorption band of the nitro model. The presence of the fairly strong  $Q_Q$  branch, as indicated in Fig. IV, is strong evidence against the nitro model.

Further evidence discrediting the nitro model is the experimental rotational constant,  $A_0 - \frac{1}{2}(B_0 + C_0) = 2.40 \text{ cm}^{-1}$ . We shall attempt to assume reasonable bond distances and calculate the O-N=O angle to give the correct rotational constant. Electron diffraction results of Brockway, Beach, and Pauling (19) for nitromethane give a normal C-N distance of  $1.46 \pm .02 \text{ \AA}$ , N-O distances of  $1.21 \pm .02 \text{ \AA}$  (similar to that in  $\text{NO}_2$  (22)), and an O-N=O angle of  $127 \pm 3^\circ$ . For the nitro model of nitrous acid, we chose the upper limit for the N-O distance,  $1.23 \text{ \AA}$ , and a slightly long N-H distance of  $1.02 \text{ \AA}$  ( $1.014$  in ammonia) and calculated rotational constants for different O-N=O angles. The results are given in Table V.

Table V.

Rotational Constants for Different Parameters in  
the Nitro Model of Nitrous Acid

$R_{N-H} \overset{O}{\parallel}$	$R_{N-O} \overset{O}{\parallel}$	$O-N=O$	$A_0 - \frac{1}{2}(B_0 + C_0) \text{ cm}^{-1}$
1.02	1.23	120°	2.51
1.02	1.23	118°	2.37
1.02	1.23	116°	2.25
1.02	1.23	114°	2.13
1.02	1.41	125°	2.40
		Observed	2.40

Slightly long N-O and N-H distances were chosen as they allow a larger O-N=O angle to agree with the observed rotational constant. However, even with these long distances, the O-N=O angle cannot be much greater than 118° and agree with the observed rotational constant. In order to have a nitro model with the expected 125° O-N=O angle and the observed rotational constant, the N-O distance would be about 1.41 Å, as tabulated in Table V. This is close to a normal N-O single bond distance, and thus very unlikely for a planar nitro group. Since there is no apparent reason for the O-N=O angle to be much less than 125° in a nitro group, the above facts substantiate our rejection of the planar nitro model.

A further argument against the planar nitro model is the observed rotational constant for the deuterium analogue, 1.95 cm.<sup>-1</sup> Thus the observed ratio of rotational constants,  $X_0(\text{HONO})/X_0(\text{DONO})$ , is 1.23. For the planar nitro model the calculated

ratio of these rotational constants is 1.43.

None of the above arguments can rule out a nonplanar nitro structure. However, a nonplanar nitro structure is very unlikely as it sacrifices the double bond, and we are left with three single bonds instead of two single bonds and a double bond.

Consequently we are left with the "cis" and "trans" forms of nitrous acid to explain the two hydrogen stretching vibrations. We expect a lower frequency for the cis form than for the trans form, due to intramolecular hydrogen bonding, as indicated by the dashed line in I-A and I-B of Figure VIII. Therefore, we have assigned the frequency  $3426 \text{ cm}^{-1}$  to the cis form and have labelled it  $\nu_1^c$ . In the following paragraphs we shall discuss the pros and cons of the cis model.

The resonance indicated in Figure VIII gives the terminal oxygen atom an appreciable negative charge, and increases the positive charge of the hydrogen atom. Therefore, the hydrogen atom is probably pulled strongly toward this nearby terminal oxygen atom, forming an intramolecular hydrogen bond. As a result of this hydrogen bond, the hydrogen atom would have less attraction for the oxygen atom to which it is bonded, and thus the strength of the O-H bond would be decreased.

The  $Q_Q$  maximum is compatible with this cis-HONO structure as the O-H bond is no longer necessarily perpendicular to the least axis of inertia.

We shall now assume bond distances and the H-O-N bond angle for cis-HONO and calculate the O-N=O angle to give the correct rotational constant. Using Badger's rule (23), from the frequency for the N=O vibration we find that the N=O distance should be 1.21 Å. From electron diffraction work, Rogowski (24) reports the O-N and O=N distances in methyl nitrite to be 1.37 ± .02 Å and 1.22 ± .02 Å respectively. The Schomaker-Stevenson (25) value for the N-O single bond distance is 1.43 Å. The resonance indicated in Figure VIII should decrease the distance somewhat, so 1.37 Å is a reasonable value. From the low frequency of the O-H stretching vibration, Badger's rule indicates that the O-H bond distance is 0.98 Å. We assume that the H-O-N bond angle is about 90°, as the hydrogen is probably pulled strongly toward the terminal oxygen. From the above considerations we assume that the most likely values of the parameters are:

$$\begin{aligned}
 r_{\text{N}=\text{O}} &= 1.22 \text{ \AA} \\
 r_{\text{N}-\text{O}} &= 1.37 \text{ \AA} \\
 r_{\text{O}-\text{H}} &= 0.98 \text{ \AA} \\
 \angle \text{H-O-N} &= 90^\circ
 \end{aligned}$$

Using these parameters an O-N=O angle of 113° is required to give the correct rotational constant, 2.40 cm<sup>-1</sup>. The rotational constants were calculated for several models, having slight variations in the parameters, in order to investigate the sensitivity of the rotational constant to variations in the parameters. In

Table VI are listed the results for various models.

Table VI.

Rotational Constant,  $A = \frac{1}{2}(B+C)$ ,  
for Various Models of cis-Nitrous Acid.

$r_{N=O}$	$r_{N-O}$	$r_{O-H}$	$\angle H-N-O$	$\angle O-N=O$	$X=A = \frac{1}{2}(B+C)$	
					HONO	DONO
1.22 $\overset{\circ}{\text{A}}$	1.37 $\overset{\circ}{\text{A}}$	.98 $\overset{\circ}{\text{A}}$	90 $^{\circ}$	113 $^{\circ}$	2.40 cm $^{-1}$	2.02 cm $^{-1}$
1.22	1.37	.98	90	115	2.54	
1.22	1.37	.98	90	117	2.68	
1.22	1.37	.98	90	112	2.33	
1.24	1.37	.98	90	113	2.38	2.01
1.22	1.45	.98	90	115	2.44	2.04
1.22	1.37	.96	90	113	2.42	
1.22	1.37	.98	105	117	2.57	
Observed Value					2.40	1.95

It is seen from Table VI that an increase of 1 $^{\circ}$  in the O-N=O angle leads to about the same change in the rotational constant as decreasing any one of the distances by .07  $\overset{\circ}{\text{A}}$ , or decreasing the H-O-N angle by 10 $^{\circ}$ . Thus the rotational constant is far more sensitive to the O-N=O angle than to the other parameters. We are confident that the bond distances assumed are not off by more than 0.05  $\overset{\circ}{\text{A}}$  and that the H-O-N angle is between 90 and 105 $^{\circ}$ . Thus we report the O-N=O angle as 113  $\pm$  2 $^{\circ}$ .

This angle of 113 $^{\circ}$  is indeed much lower than the 125 $^{\circ}$  expected for an O-N=O angle, but for this cis model the strong hydrogen bond probably decreases both the H-O-N angle and the O-N=O angle.

From the data of Table VI we find that for the cis model the calculated ratio  $X_o(\text{HONO})/X_o(\text{DONO})$  is about 1.19. This compares favorably with the observed ratio, 1.23.

Thus the  $Q_Q$  maxima of  $2\nu_1^c$  for HONO and DONO, as well as the ratio of rotational constants of HONO and DONO, rule out the nitro structure. However, both of these facts are compatible with the cis-HONO structure.

### C. Cis-trans Equilibrium and Intensity Relations

From the foregoing arguments we have decided that the band  $\nu_1^c$  at  $3426 \text{ cm}^{-1}$  arises from the O-H vibration of cis-HONO, while the band  $\nu_1^t$  at  $3590 \text{ cm}^{-1}$  arises from the O-H vibration of trans-HONO.

The spectrum of nitrous acid was taken at different temperatures, but between 10 and  $65^\circ\text{C}$  there was no appreciable change in the relative intensities of  $2\nu_1^c$  and  $2\nu_1^t$ . A change of greater than 10% in the cis-trans equilibrium constant would probably have been detected. At higher temperatures the equilibrium concentration of nitrous acid was too small to render the comparison significant. Due to the formation of the strong intramolecular hydrogen bond we might expect cis-HONO to have a lower energy than trans-HONO.

If we allow a maximum value of 10% for the change in equilibrium constant from 10 to  $65^\circ\text{C}$ , we can calculate the maximum energy difference of the cis and trans forms, assuming this heat of reaction is not appreciably different at the two temperatures.

For the reaction,



$$K_T = P_{\text{cis}}/P_{\text{trans}}$$

Integration of the van't Hoff equation assuming  $\Delta E$  is constant, gives

$$\ln (K_{T_2}/K_{T_1}) = -\frac{\Delta E}{R} \left\{ \frac{1}{T_2} - \frac{1}{T_1} \right\} .$$

If  $T_1 = 283^\circ\text{K}$  and  $T_2 = 338^\circ\text{K}$ , and  $K_{T_2}/K_{T_1} = 0.90$  then  $\Delta E = -330$  calories/mole. In order to calculate the equilibrium constant, we must know the entropy change,  $\Delta S$ , for the above reaction, as

$$K_T = e^{-\Delta E/RT} e^{\Delta S/R}$$

The trans form might be expected to have a higher entropy than the cis form as the oscillation of the hydrogen out of the plane is not hindered by a hydrogen bond. However, if the entropy were very appreciable in the trans form there would be a significant concentration of trans molecules in excited states of the low frequency torsional vibration, which would cause the absorption bands of the trans form to be not a single band but rather a band sequence containing members arising from transitions from the excited states. Since, however, the band  $2\nu_1^t$  has a sharp  $Q_Q$  branch and no observable satellite  $Q_Q$  branches, it appears that there is not a large percentage of trans molecules in an excited state at room temperature. Therefore, it is reasonable to assume that  $\Delta S$  for the reaction, trans  $\rightarrow$  cis, is very small.

If we assume  $\Delta S = 0$ ,  $K = e^{-\Delta E/RT}$ , with  $\Delta E = -330$  cal/mole,  $K_{298} = 1.74$ . Thus, the experimental evidence indicates that for the reaction,



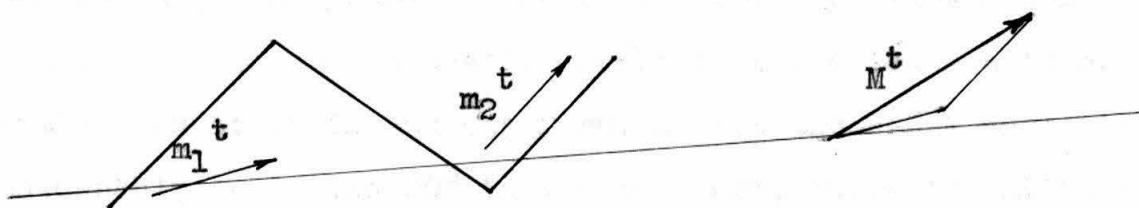
$$0 \leq -\Delta E \leq 330 \text{ calories/mole}$$

$$1 \leq K \leq 1.74$$

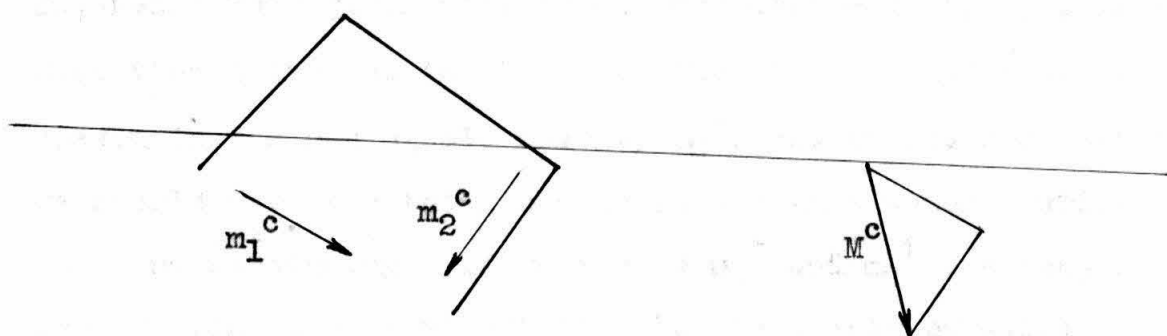
We are now confronted with two problems. First, since cis-HONO appears to form a strong hydrogen bond, why is the energy difference of cis and trans forms only 330 calories/mole? From the relation between the energy of hydrogen bonds and the frequency shifts of O-H bands presented by Badger (26), we should expect the energy of the hydrogen bond in cis-HONO to be between 6000 and 7000 calories per mole. A possible explanation of these observations may lie in the abnormally small O-N=O angle which suggests that the decrease in energy resulting from the formation of the hydrogen bond is largely compensated for by the energy required to distort the molecule.

The second problem is that the intensity of  $\nu_1^t$  is about three times as great as that of  $\nu_1^c$ , though we expect the cis form to predominate. This can be explained by a consideration of the changing electric moment during the O-H vibration in the two models. Fig. IX pictures schematically a possible representation of the changing electric moment.

There are two structural differences in the cis and trans models which cause the trans form to have a smaller angle between



Trans HONO



Cis HONO

Fig. IX. Schematic Representation of the Changing Electric Moment in Nitrous Acid.

the O-H bond and the least axis of inertia. First, the least axis of inertia is not parallel to the O - - - O axis but is instead tilted about  $2^\circ$  toward the hydrogen atom. Furthermore, the H-O-N angle is probably about  $105^\circ$  for the trans model, which makes the O-H bond more nearly parallel to the least axis of inertia than it is in the cis form, unless the H-O-N angle is considerably less than  $90^\circ$  in the cis form, which is unlikely.

From the above discussion we expect the O-H vibration in trans-HONO to have more parallel character than that in cis-HONO. More important than this, however, is the effect of the resonance indicated in Fig. VIII. As the hydrogen atom moves away from the oxygen atom resonance to structure II-B of Fig. VIII is favored. This gives rise to an increased moment,  $m_1^t$ , in the direction indicated in Fig. IX. When this is added to the increase in the O-H dipole moment,  $m_2^t$ , due to the bond stretching, we should have the total change in electric moment during the O-H bond stretching. If we assume  $m_1^t$  and  $m_2^t$  are roughly equivalent we find the resultant  $M^t$  which is nearly parallel to the least axis of inertia. If we assume similar effects of similar magnitude for the cis form, adding  $m_1^c$  and  $m_2^c$  gives  $M^c$  which is nearly perpendicular, as indicated in Fig. IX. The resultant  $M^t$  is much larger than  $M^c$ . Remembering that the intensity of absorption is proportional to the square of the changing electric moment we see that even though there is more cis-HONO than trans-HONO the O-H vibration for the trans form can give rise to much greater absorption.

Of course the above assumptions are pure conjecture but they are not unreasonable and do offer a likely explanation for the observed phenomenon. Actually the resonance effect may be less important for the cis form as the hydrogen atom is already about  $.02 \text{ \AA}$  farther away from the oxygen so the change in resonance during the O-H vibration is not as great.

#### D. Analysis of Normal Vibrations of HONO

In the preceding sections we have shown that there are two forms of nitrous acid in equilibrium, cis-HONO and trans-HONO. There is probably a little more cis than trans present at room temperature. There remains the problem of assigning the frequencies at  $1696 \text{ cm}^{-1}$ ,  $1270 \text{ cm}^{-1}$ ,  $856 \text{ cm}^{-1}$ , and  $794 \text{ cm}^{-1}$ . Since there are two forms of nitrous acid and one form is not in great predominance, we should expect to observe two sets of frequencies, not greatly different. There may be two bands near or at  $1696 \text{ cm}^{-1}$  - the envelope of absorption in this region is not distinct. The absorption at  $1696 \text{ cm}^{-1}$  is undoubtedly due to the N=O double bond stretching vibration. The band at  $1270 \text{ cm}^{-1}$  is probably due to an H-O-N -bending vibration, though its isotopic shift, to  $1019 \text{ cm}^{-1}$ , is less than expected. It is surprising that there are not two bands in this region, one due to cis-HONO and the other due to trans-HONO. However, there does appear to be a second, weaker band in the HONO spectrum at  $1314 \text{ cm}^{-1}$  (see Fig. IV). Either one form exhibits much stronger absorption than the other, or the frequencies in both forms are practically identical.

The two frequencies at  $856\text{ cm}^{-1}$  and  $794\text{ cm}^{-1}$  might be thought to arise from a similar normal mode of vibration in the two isomers of HONO. However, their great similarity in appearance and equal intensity of absorption (See Figure IV) suggest that they arise from two vibrational levels of the same species which have mixed their eigenfunctions and repelled each other through Fermi resonance. This suggestion is further substantiated by the spectrum of DONO in this region. Two bands appear, at  $816\text{ cm}^{-1}$  and  $739\text{ cm}^{-1}$  which are further apart than the two corresponding bands of HONO, and the band at  $816\text{ cm}^{-1}$  has twice the intensity of that at  $739\text{ cm}^{-1}$ . Thus it appears that there are two vibrational levels at approximately  $825\text{ cm}^{-1}$ , which repel each other through Fermi resonance, and one of them borrows intensity from the other. In DONO one of these levels is at  $816\text{ cm}^{-1}$  while the other is shifted to  $739\text{ cm}^{-1}$ ; or perhaps the levels lie in between these two frequencies, still somewhat repelling each other.

A comparison with the spectrum of formic acid may be of value. The strong perpendicular character of the O-H band in formic acid (10,11) indicates that formic acid is predominantly in the cis form. We might expect its spectrum to be similar to that of cis-HONO. The spectrum of formic acid monomer was observed in this laboratory in the region 2-15  $\mu$ . With an equivalent path length of formic acid monomer, sufficient to give an O-H band of similar intensity to that of cis-HONO in Fig. IV-d, the only strong band observed below  $1600\text{ cm}^{-1}$  is at  $1109\text{ cm}^{-1}$ . V. Z. Williams (11)

reports a strong band at  $1105\text{ cm}^{-1}$ . This band does not correspond to any of the bands observed in nitrous acid and may well arise from a C-H bending vibration of formic acid (compare with  $1167\text{ cm}^{-1}$  for the out of plane bending vibration of formaldehyde (30)). Thus, if cis-HONO has a spectrum similar to that of formic acid we are led to believe that the bands at  $856\text{ cm}^{-1}$ , and  $794\text{ cm}^{-1}$  are from the trans form. To be sure this is not a strong argument, but it does offer some support.

Furthermore, since the electric moment of nitrous acid is mainly determined by the distance of the positively charged hydrogen from the negatively charged terminal oxygen atom as well as by the amount of double-bond resonance, the trans form is expected to have a larger electric moment than the cis form. Therefore, the change in amount of resonance during the normal vibrations will cause a greater change in the electric moment of the trans form than of the cis form. Thus we might expect the trans form to show greater absorption than the cis form throughout the spectrum, as all the normal vibrations probably affect the amount of resonance somewhat.

Due to the above considerations we believe that the spectrum of the trans form of HONO exhibits the frequencies 3590, 1696, 1270, 856, and  $794\text{ cm}^{-1}$ . The first three are the O-H stretching, N = O stretching, and H-O-N bending respectively. For the bands at  $856\text{ cm}^{-1}$  and  $794\text{ cm}^{-1}$  there are three remaining vibrations to choose from: (a) the hydrogen oscillating out of the plane,

(b) the bending of the  $-O-N=O$  angle, and (c) the  $-O-N-$  single bond stretching. The out of the plane vibration should be pure, but the other two may be mixtures of  $-O-N=O$  bending and  $-O-N-$  stretching. If one of these bands did arise from the oscillation of the hydrogen atom out of the  $O-N=O$  plane, its isotopic mate in DONO should have approximately 0.77 times its frequency, according to the Teller-Redlich Product rule (31). The greatest possible shift observed is from  $856\text{ cm}^{-1}$  to  $739\text{ cm}^{-1}$ , which is a factor of about 0.86. Thus, it is very unlikely that any of the observed vibrations is the out of the plane vibration.

We conclude that the bands at  $856\text{ cm}^{-1}$  and  $794\text{ cm}^{-1}$  involve mainly the  $O-N=O$  bending and  $-O-N-$  stretching vibrations, repelling each other from about  $825\text{ cm}^{-1}$ . For the two bands at  $825\text{ cm}^{-1}$  there are three possibilities: (a) an  $-O-N=O$  bending vibration at  $825\text{ cm}^{-1}$  and an  $-O-N-$  stretching vibration at  $825\text{ cm}^{-1}$ ; (b) an  $O-N=O$  bending vibration at  $413\text{ cm}^{-1}$  and an  $-O-N-$  stretching vibration at  $825\text{ cm}^{-1}$ ; (c) the reverse of (b). In order to choose from these possibilities it was decided to attempt a normal coordinate treatment and try to choose a set of force constants to give the correct frequencies for HONO. Then, using these same force constants, the frequencies for DONO were calculated for comparison with the experimental observations. Since the trans form is favored as causing the observed absorption bands we have first made the normal coordinate treatment for a trans model.

To write out the secular equation the method of Wilson (32) was used. Following Wilson, if  $R_k$  represents an internal

coordinate, and  $X_i$  a cartesian coordinate, we can write

$$R_k = \sum_{i=1}^{3n} B_{ki} X_i \quad (k = 1, 2, \dots, 3n-6)$$

A matrix  $G$  is defined such that

$$G_{k\ell} = \sum_{i=1}^{3n} \frac{B_{ki} B_{\ell i}}{m_i} \quad (k, \ell = 1, 2, \dots, 3n-6)$$

The potential energy is given by

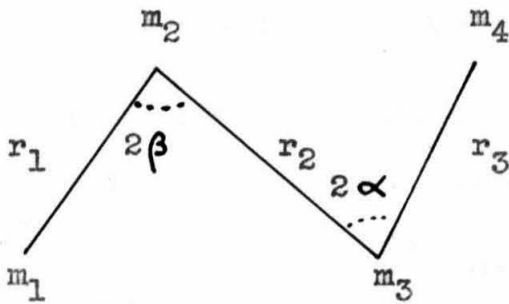
$$2V = \sum_{k, \ell=1}^{3n-6} F_{k\ell} R_k R_\ell \text{ in which } F_{k\ell} \text{ is a force constant.}$$

Wilson has shown that the secular equation may now be written out in algebraic form as

$$\sum_{S=0}^{3n-6} (-\lambda)^{3n-6-S} \sum_{k < \ell < \dots} \sum_{i < j < \dots} \begin{vmatrix} G_{ki} & G_{kj} & \dots \\ G_{\ell i} & G_{\ell j} & \dots \\ \dots & \dots & \dots \end{vmatrix} \begin{vmatrix} F_{ki} & F_{kj} & \dots \\ F_{\ell i} & F_{\ell j} & \dots \\ \dots & \dots & \dots \end{vmatrix} \quad (2)$$

where the sum is over all different sets of  $S$  letters  $k, \ell$ , etc., with  $k < \ell, \ell < m$ , etc., and over all different sets of  $S$  letters  $i < j < \dots$ , these to be chosen from the  $3n-6$  possible values.

For planar HONO the out of the plane vibration is of a different symmetry class than the other five, and so may be separated from the secular determinant. This leaves us with a fifth order secular equation. Using a model as in Figure X, we can set up the determinant  $G$ . Here our internal coordinates are;



$$\begin{aligned}
 R_1 &= \Delta r_1 \\
 R_2 &= \Delta r_3 \\
 R_3 &= r_1 r_2 \Delta(2\beta) \\
 R_4 &= \Delta r_2 \\
 R_5 &= r_2 r_3 \Delta(2\alpha)
 \end{aligned}$$

Figure X

$\frac{m_1 + m_2}{m_1 m_2}$	0	$\frac{-2r_1 s_\beta c_\beta}{m_2}$	$\frac{c_\beta^2 - s_\beta^2}{m_2}$	$\frac{-2r_3 s_\beta c_\beta}{m_2}$	
	$\frac{m_3 + m_4}{m_3 m_4}$	$\frac{-2r_1 s_\alpha c_\alpha}{m_3}$	$\frac{c_\alpha^2 - s_\alpha^2}{m_3}$	$\frac{-2r_3 s_\alpha c_\alpha}{m_3}$	
		$G_{33}$	$\frac{-2r_2 s_\beta c_\beta}{m_2}$	$G_{35}$	= G
			$\frac{m_2 + m_3}{m_2 m_3}$	$\frac{-2r_2 s_\alpha c_\alpha}{m_3}$	
				$G_{55}$	

G is a symmetrical determinant.

$$G_{33} = r_2^2 \left( \frac{m_1 + m_2}{m_1 m_2} \right) + r_1^2 \left( \frac{m_2 + m_3}{m_2 m_3} \right) + \frac{2r_1 r_2}{m_2} (s_\beta^2 - c_\beta^2)$$

$$G_{35} = \frac{r_1 r_3}{m_2} + \frac{r_2 r_3}{m_2} (s_\beta^2 - c_\beta^2) + \frac{r_1 r_3}{m_3} + \frac{r_1 r_2}{m_3} (s_\alpha^2 - c_\alpha^2)$$

$$G_{55} = r_2^2 \left( \frac{m_3 + m_4}{m_3 m_4} \right) + r_3^2 \left( \frac{m_2 + m_3}{m_2 m_3} \right) + \frac{2r_2 r_3}{m_3} (s_\alpha^2 - c_\alpha^2)$$

$$c_{\alpha} = \cos \alpha, s_{\alpha} = \sin \alpha, c_{\beta} = \cos \beta, s_{\beta} = \sin \beta.$$

We have chosen our internal coordinates in accordance with a valence force system. We must now evaluate one fifth-order, five fourth-order, ten third-order, and ten second-order determinants from the elements of matrix G. Therefore, at this point we must assume a model and set up a numerical matrix G to use in Equation (2). In discussing the cis-nitrous acid, an argument was presented for assuming an N=O distance of 1.22 Å, and an N-O distance of 1.37 Å. The O-N=O angle arrived at was 113°. For the trans model the O-N=O angle should probably be larger as there is no hydrogen bond to decrease this angle. Arbitrarily, we have chosen for the trans-model,  $r_1 = 0.96 \text{ \AA}$ ,  $r_2 = 1.37 \text{ \AA}$ ,  $r_3 = 1.22 \text{ \AA}$ ,  $2\beta = 100^\circ$  and  $2\alpha = 120^\circ$ . Also,  $m_1 = 1$ ,  $m_2 = m_4 = 16$ , and  $m_3 = 14$  (all in atomic weight units). We can now set up G in numerical form.

$$G = \begin{vmatrix} \dagger 1.062 & 0 & -.059 & -.011 & -0.75 \\ & \dagger .134 & -.060 & -.036 & -.076 \\ & & \dagger 2.119 & -.085 & \dagger .227 \\ & & & \dagger .134 & -.085 \\ & & & & \dagger .580 \end{vmatrix}$$

At this point we shall note that for cis-HONO with the same values of  $r_1$ ,  $r_2$ , etc., the only changes in the determinant G are the signs on  $G_{15}$ ,  $G_{23}$ ,  $G_{35}$ . We do not have enough information

to include interaction force constants so, in writing out the secular equation, we will assume  $F_{ki} = 0$ , if  $k \neq i$ . Using the above numerical matrix for G, we can then write out the secular equation.

$$\begin{aligned}
 & \lambda^5 - \lambda^4 (1.062F_{11} + 0.134F_{22} + 2.119F_{33} + 0.134F_{44} \\
 & + 0.580F_{55}) + \lambda^3 (0.1423F_{11}F_{22} + 2.248F_{11}F_{33} \\
 & + 0.1422F_{11}F_{44} + 0.609F_{11}F_{55} + 0.2803F_{22}F_{33} + 0.0166F_{22}F_{44} \\
 & + 0.0715F_{22}F_{55} + 0.2768F_{33}F_{44} + 1.177F_{33}F_{55} + 0.0705F_{44}F_{55}) \\
 & - \lambda^2 (0.2973F_{11}F_{22}F_{33} + 0.0177F_{11}F_{22}F_{44} + 0.0752F_{11}F_{22}F_{55} \\
 & + 0.2935F_{11}F_{33}F_{44} + 1.237F_{11}F_{33}F_{55} + 0.0741F_{11}F_{44}F_{55} + \\
 & + 0.0334F_{22}F_{33}F_{44} + 0.1451F_{22}F_{33}F_{55} + 0.00738F_{22}F_{44}F_{55} \\
 & + 0.1420F_{33}F_{44}F_{55}) + \lambda (0.0354F_{11}F_{22}F_{33}F_{44} + 0.1520F_{11}F_{22}F_{33}F_{55} \\
 & + 0.00774F_{11}F_{22}F_{44}F_{55} + 0.1490F_{11}F_{33}F_{44}F_{55} + 0.0147F_{22}F_{33}F_{44}F_{55}) \\
 & - 0.01535F_{11}F_{22}F_{33}F_{44}F_{55} = 0
 \end{aligned} \tag{3}$$

The units of  $F_{11}$ ,  $F_{22}$ , and  $F_{44}$  are dynes/cm. The units of  $F_{33}$  and  $F_{55}$  are  $(\text{\AA})^{-2}(\text{dynes/cm.})$ .  $\lambda$  is related to the frequency by the equation

$$6.023 \times 10^{23} \lambda = 4\pi^2 \bar{\nu}^2$$

where  $\bar{\nu}$  is in reciprocal seconds. This converts to

$$\nu_{\text{cm}^{-1}} = 4.12 \sqrt{\lambda}$$

Now it is necessary to choose appropriate force constants to give frequencies corresponding to the observed frequencies. In order to do this, a fifth order algebraic equation was set up by expanding the following equation:

$$\prod_{k=1}^5 (\lambda - \lambda_k) = 0 \quad (4)$$

where  $\lambda_k$  are the numerical values of  $\lambda$  corresponding to observed frequencies. In order to give the correct  $\lambda_k$ , the force constants in the secular Equation (3) must be chosen so as to give the same numerical coefficients of different powers of  $\lambda$  as appear in Equation (4). Actually the frequencies for infinitesimal vibrations should be used, but we do not have enough experimental data to determine the anharmonic constants. However, the observed frequencies are probably close to the zero-order frequencies in all cases except for the hydrogen stretching. We are somewhat better off if we use the  $\omega_1^0$  from the expression

$$v_1 \nu_1 = \omega_1^0 v_1 + X_{11}^0 v_1^2$$

where  $v_1 \nu_1$  is the observed frequency for the transition from  $v_1 = 0$  to  $v_1 = v_1$ , all other  $v_i$  remaining equal to zero (18).  $v_1$  is the vibrational quantum number for frequency  $\nu_1$ . Using this expression, from the experimental data we find for the O-H stretching vibration,  $\omega_1^0 = 3672 \text{ cm}^{-1}$  and for the O-D stretching

in DONO,  $\omega_1^0 = 2694 \text{ cm}^{-1}$ . Now we have three possibilities to investigate, (a), (b), or (c) in Table VII.

Table VII.

Possible Assignments of Observed Vibrational  
Frequencies for HONO and DONO

	HONO	DONO	HONO	DONO	HONO	DONO
$\omega_1^0$	3672 $\text{cm}^{-1}$	2694	3672	2694	3672	2694
$\nu_2$	1696	1690	1696	1690	1695	1690
$\nu_3$	1270	1019	1270	1019	1270	1019
$\nu_4$	825	816	825	816	825	739
$\nu_5$	825	739	413	370	413	408
	(a)		(b)		(c)	

Force constants were chosen to give results corresponding as well as possible to the frequencies of Table VII for HONO. Then the secular equation was set up for DONO in the form of Equation (3) with different numerical coefficients. This was arrived at from Equation (2) using the matrix G for DONO which is the same as for HONO except that  $G_{11} = 0.562$  instead of 1.062, and  $G_{33} = 1.192$  instead of 2.119. Then using the force constants giving the best results for HONO, the frequencies were calculated for DONO. Table VI gives the calculated results for three different sets of force constants along with the observed results.

Table VIII.

Comparison of Calculated Frequencies with Observed Frequencies. (a), (b), and (c) are Calculated Results Using Indicated Force Constants. (d) Gives Observed Frequencies

i	$F_{ii} \times 10^5$ dynes/cm	$\checkmark_{\text{HONO}} \text{ cm}^{-1}$	$\checkmark_{\text{DONO}} \text{ cm}^{-1}$	$\checkmark_{\text{HONO}/\text{DONO}}$
(a)				
1	7.5	3690	2700	1.37
2	11.7	1680	1660	1.01
3	0.44	1270	1037	1.227
4	3.3	827	744	1.112
5	0.26	419	415	1.01
(b)				
1	7.5	3670	2690	1.37
2	11.7	1690	1665	1.01
3	0.248	1290	1292	1.00
4	4.34	859	(700)*	1.23
5	1.31	802	(700)*	1.15
(c)				
1	7.5			
2	11.7			
3	0.44	1275	1040	1.23
4	1.1	427	444	0.96
5	0.78	837	730	1.15
(d) (observed)				
1		3672	2694	1.365
2		1696	1690	1.002
3		1270	1019	1.249
4		825	739	1.119
5		825	816	1.010

\* Solution is imaginary, but close to  $700 \text{ cm}^{-1}$ .

Case (a) in Table VIII agrees quite well with the observed results, (d) of Table VIII. Case (b) does not agree at all well with the observed results. This is unfortunate as for case (a) the strongest band in the spectrum of DONO (at  $816\text{ cm}^{-1}$ ) must be the first overtone of the O-N=O bending vibration. For case (c) this band at  $816\text{ cm}^{-1}$  must be from the first overtone of the -O-N- stretching vibration, which is even more unlikely as it requires a very low force constant for the -O-N- bond stretching. Many unsuccessful attempts were made to arrive at better solutions with the band at  $816\text{ cm}^{-1}$  in DONO attributed to a fundamental vibration. A large interaction constant for the interaction of the O-N=O bending with the -O-N- bond stretching was included. The results of including the interaction constant are given in Table IX.

Table IX.

Frequencies Calculated for HONO and DONO Including  
Interaction Constant  $F_{45}$

	$\nu_{\text{HONO}}$	$\nu_{\text{DONO}}$	$\nu_{\text{HONO}}/\nu_{\text{DONO}}$
$F_{33} = 0.40$	1273	$1130\text{ cm}^{-1}$	1.13
$F_{44} = 3.24$	$840\text{ cm}^{-1}$	$(715)^*\text{ cm}^{-1}$	1.18
$F_{55} = 1.07$	$315\text{ cm}^{-1}$	$(715)^*\text{ cm}^{-1}$	1.14
$F_{45} = 0.25$			

\* Imaginary solution -- near  $715\text{ cm}^{-1}$

An attempt was also made to include  $F_{34} \neq 0$  and  $F_{35} \neq 0$ . These attempts did not contribute to the situation.

In all cases of Table VI and Table VII, in going from HONO to DONO the frequencies around  $825 \text{ cm}^{-1}$  are decreased well below  $750 \text{ cm}^{-1}$ . The experimental results indicate that one frequency is shifted very little ( $825 \text{ cm}^{-1}$  to  $816 \text{ cm}^{-1}$ , or at most  $856$  to  $816 \text{ cm}^{-1}$ ). This is then probably the overtone of  $413 \text{ cm}^{-1}$  or arises from another species.

Indeed, it seems unreasonable to attribute the strongest band in the observed spectrum to an overtone vibration. However, extensive investigations failed to arrive at a suitable solution in which the DONO band at  $816 \text{ cm}^{-1}$  arises from a fundamental vibration. Assuming Fermi resonance occurs in DONO also and the bands at  $816$  and  $739 \text{ cm}^{-1}$  arise from vibrations around  $780 \text{ cm}^{-1}$ , we still could not find a suitable solution.

The normal coordinate treatment does not depend critically on choosing an exact model. Another model was treated, having an O-N=O angle eight degrees smaller, and similar results were obtained, except that a slightly higher force constant was necessary for the O-N=O bending. A cis-model was also treated using the same frequencies, except for the O-H frequency, and the results show only slight variations from the treatment of the trans form.

The calculated force constants are presented below, all in (dynes/cm.).

Coordinate	Force Constant, dynes/cm.
R(O-H)	$7.5 \times 10^5$
R(N=O)	$11.7 \times 10^5$
R(N-O)	$3.3 \times 10^5$
$\angle$ O-N=O	$0.26 r_2 r_3 \times 10^5 = .435 \times 10^5$
$\angle$ N-O-H	$0.44 r_1 r_2 \times 10^5 = 0.58 \times 10^5$

Since we did not use the frequencies for infinitesimal vibrations, the force constants should probably be a trifle higher. There is not much to compare these force constants with except for the O-H stretching and bending force constants in water ( $7.76 \times 10^5$  and  $0.69 \times 10^5$  respectively). The N=O stretching force constant is close to the C=O stretching force constant,  $12.1 \times 10^5$ . As expected it is higher than that of N=O in NO<sub>2</sub>,  $9.13 \times 10^5$ . The O-N=O bending force constant of  $0.44 \times 10^5$  is low compared to the O-N=O bending force constant of the nitrate ion,  $0.64 \times 10^5$  dynes/cm. The above force constants are quoted from tables in Herzberg's Infrared and Raman Spectra of Polyatomic Molecules, pages 170, 174, 178, and 193.

The excellent agreement of solution (a) of Table VIII with the observed spectra may be fortuitous. However, it is supported by the failure to find other suitable solutions. There is the possibility that the two bands at 856 and 794 cm<sup>-1</sup> arise from two difference species, cis-HONO and trans-HONO. However, a third band appears in this region in the DONO spectrum, at about 845 cm<sup>-1</sup> (see Fig. IV), which may arise from the other species.

An investigation of the spectra of HONO and DONO in the region of 25 microns would no doubt be of value in solving this problem.

E. Comparison of  $2 \sphericalangle_{\text{O-H}}$  of Formic Acid with  $2 \sphericalangle_{\text{O-H}}$  of cis-HONO.

The band  $2 \sphericalangle_{\text{O-H}}$  of formic acid is shown in Fig. XI. This is similar in appearance to  $2 \sphericalangle_{\text{O-H}}$  of cis-HONO shown in Fig. VI, except that cis-HONO has a much stronger  $Q_2$  branch indicating more parallel character, in agreement with smaller bond angles for cis-HONO than for formic acid.

For the spectrum of Fig. VI the pressure of nitrous acid is believed to be about 21 mm Hg, as calculated in Appendix II. If we assume slightly more than 50% of this nitrous acid is the cis form, the pressure of cis-HONO is about 12 mm Hg. The formic acid exhibiting the spectrum of Fig. XI was at a temperature of 120° and thus believed to be almost completely in the monomeric state. The pressure of formic acid was about 45 mm. The absorption in the formic acid spectrum at the maximum of the band is about 50%. The absorption for cis-HONO at the maximum is about 15%. Using these percentage absorptions and the pressures of 12 mm for cis-HONO and 45 mm for formic acid, from Beer's Law the absorption coefficient in the two cases is about the same. This is a very approximate use of Beer's Law, but it indicates that these two O-H bands exhibit a similar amount of absorption and thus lends support to our assignment of this band of nitrous acid to cis-HONO.

There is no indication of a dimer of nitrous acid, analogous to the dimer so prevalent in formic acid at room temperature. This may be because the pressure of cis-HONO is much lower than that of formic acid in the observed spectra.

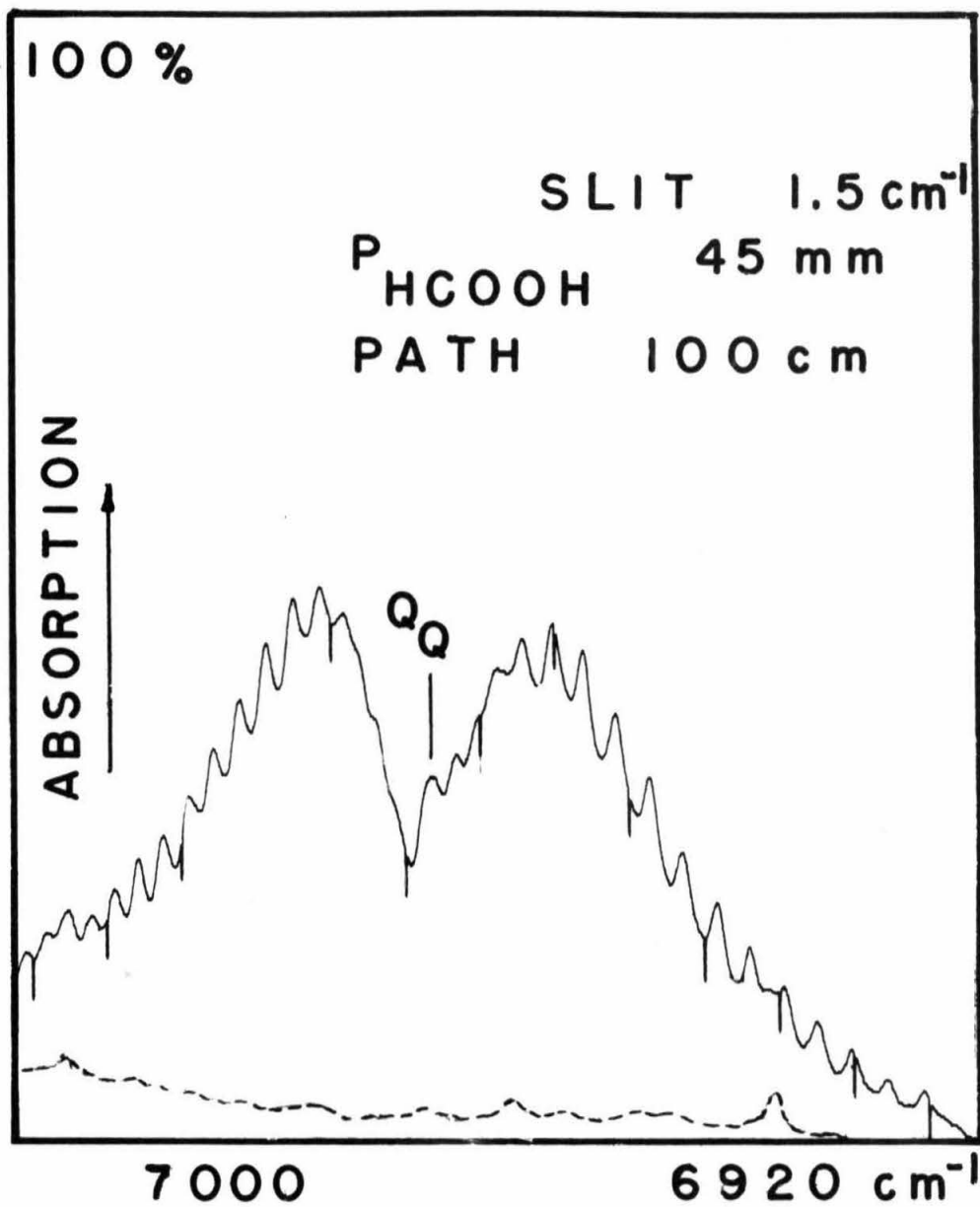


Fig. XI. Second harmonic of the O-H stretching vibration of formic acid.

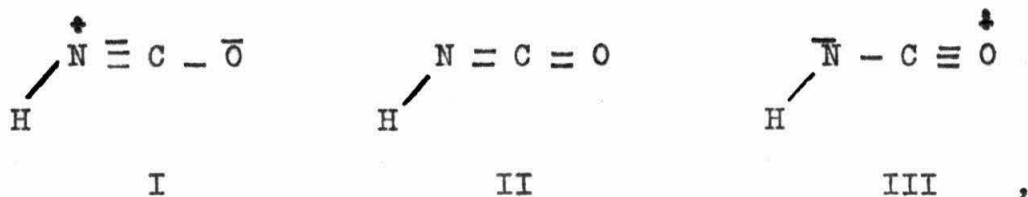
PART III  
INFRARED SPECTRA AND MOLECULAR STRUCTURE OF  
ISOCYANIC ACID, AND ISOTHIOCYANIC  
ACID

Introduction.

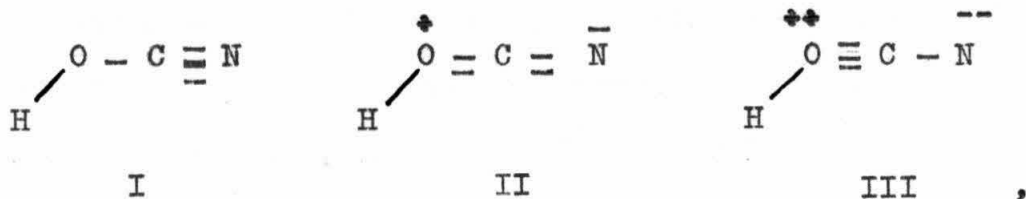
It is often stated that cyanic acid is a tautomeric mixture of HNCO and HOCN (33). However, there is apparently no chemical evidence which demands the existence of HOCN.

Herzberg and Verleger (34) observed the third harmonic of the hydrogen stretching frequency of cyanic acid in the photographic infrared at  $9700\text{ cm}^{-1}$ . They reported that the band was much more complicated than the analogous band of hydrazoic acid observed by Eyster (35). Due to the complicated structure of the band they concluded that the cyanic acid molecule is probably a strongly asymmetric top but that its smallest moment of inertia is quite small (as shown by the large extent of the band).

Eyster, Gillette, and Brockway (36) investigated the structure of HNCO by electron diffraction and reported a linear NCO group with N-C and C-O distances of about  $1.19\text{ \AA}$  each. They pointed out that these distances are compatible with resonant structures of HNCO, but not of HOCN. That is, in HNCO resonance is favorable among the three structures,



similar to the resonance in  $\text{CO}_2$ . For this structure we should expect N-C and C-O distances which are not very different. However, for HOCN, the resonant structures are



the third structure being very unstable due to the double charges. If we had equal resonance between structures I and II of HOCN, we should expect the O-C distance to be considerably longer than the C-N distance due to the large amount of single bond character in the C-O bond. The HNCN structure is expected to be more stable than the HOCN structure because of the increased possibility of resonance.

Goubeau (37) studied the Raman spectra of cyanates and of liquid cyanic acid. He observed three bands in liquid cyanic acid - a weak band at  $1204 \text{ cm}^{-1}$  and strong bands at  $1307 \text{ cm}^{-1}$  and  $3320 \text{ cm}^{-1}$ . He interpreted the weak band at  $1204 \text{ cm}^{-1}$  as the first overtone of one of the NCO bending vibrations of the molecule. The band at  $1307 \text{ cm}^{-1}$  was assigned to the symmetrical stretching of the O and N against the carbon atom, while  $3320 \text{ cm}^{-1}$  was assigned to the hydrogen stretching vibration. The antisymmetric NCO stretching vibration, expected to be around  $2200 \text{ cm}^{-1}$ , was not observed. Goubeau explained the absence of this band by the approximate symmetry of the molecule; that is, the N-H group apparently acts approximately like an oxygen atom, and thus the absorption bands of the NCO group resemble those of  $\text{CO}_2$ . For  $\text{CO}_2$  the antisymmetric vibration is inactive in the Raman spectrum. The strong band at  $1307 \text{ cm}^{-1}$  was presented as evidence

for the structure  $\text{H-N=C=O}$ , for if the structure were  $\text{H-O-C}\equiv\text{N}$  Goubeau expected to observe a  $\text{C}\equiv\text{N}$  frequency around  $2300\text{ cm}^{-1}$  and a  $\text{C-O}$  vibration around  $860\text{ cm}^{-1}$ , as he found in solutions of metallic cyanates. It should be pointed out that the frequency  $3320\text{ cm}^{-1}$ , though in the region of  $\text{N-H}$  frequencies, could also be attributed to a hydrogen bonded  $\text{O-H}$  frequency, which one would expect in liquid  $\text{HOCN}$ .

Goubeau and Gott (38) investigated the Raman spectrum of thiocyanic acid as the liquid, in solution in carbon tetrachloride, and in solution in carbon disulfide. For the liquid they reported, Raman shifts of 735, 980, and  $2120\text{ cm}^{-1}$  while in carbon tetrachloride solution they found 848, 2038, and  $3590\text{ cm}^{-1}$ , and in carbon disulfide solution they found 870, 2099, and  $3430\text{ cm}^{-1}$ . These results were inconclusive and appear inconsistent.

Beard and Dailey (39) calculated the structure of  $\text{HNCS}$  from the microwave spectra of  $\text{HNCS}$ ,  $\text{HNC}^{13}\text{S}$ ,  $\text{DNCS}$ , and  $\text{DNC}^{13}\text{S}$ . They reported that an  $\text{HSCN}$  model would not fit their data, and that  $\text{HSCN}$  could not be present at more than 5% of the concentration of  $\text{HNCS}$ . The configuration they reported for  $\text{HNCS}$ , in the ground vibrational level, and assuming a linear  $\text{NCS}$  group, is

$$\begin{aligned}r_{\text{C-S}} &= 1.57 \pm 0.01 \text{ \AA} \\r_{\text{N-C}} &= 1.21 \pm 0.01 \text{ \AA} \\r_{\text{N-H}} &= 1.2 \pm 0.1 \text{ \AA} \\\angle \text{HNC} &= 112^\circ \pm 10^\circ\end{aligned}$$

We should expect a much shorter N-H distance, around  $1.00 \text{ \AA}$ , and a larger HNC angle, around  $125^\circ$ , from normal bond distances and bond angles (40).

Prior to the present investigation the N-H bond distance and HNC bond angle of HNC<sup>O</sup> had not been determined. The N-H distance and HNC bond angle found by Beard and Dailey (39) for HNCS are quite anomalous. From an investigation of the infrared spectrum of HNC<sup>O</sup> and HNCS we have been able to assign the vibrational frequencies of HNC<sup>O</sup> and HNCS as well as to locate the "effective" position of the hydrogen atom with respect to the NCO group and NCS group respectively, in the ground vibrational state.

After a brief discussion of the experimental procedure for this investigation, the expected forms of the normal modes of vibration are presented schematically in Fig. XII. Following this the results of our investigation are presented and discussed. First the vibrational spectrum of isocyanic acid is treated, then the rotational fine structure found in several of the bands is analyzed to determine the H-N-C angle. Finally the vibrational spectrum of thiocyanic acid is treated, and the H-N-C angle is estimated from the rotational structure.

#### Experimental Procedure.

The spectrum of HNC<sup>O</sup> was observed under high dispersion from 1 to  $3.2 \mu$  and under low dispersion from  $1.8 \mu$  to  $15 \mu$ , using the previously described vacuum grating spectrograph for

the high dispersion work, and the Beckman IR-2 spectrograph for the low dispersion work. (See page 13 for a description of spectrographs). As in Section II, slit widths given are effective slit widths (see page 15).

The HNCO was prepared by heating cyanuric-acid to around 300°C and rapidly cooling to dry ice temperature, causing the colorless liquid HNCO to condense. The HNCO was then allowed to evaporate into the absorption cell at room temperature. The vapors slowly polymerize but can be kept in appreciable concentration in the monomeric state for several hours at room temperature.

HNCS was prepared by mixing  $H_3PO_4$  and KSCN at room temperature - as suggested by Beard and Dailey (39).

A mixture of about 80% DNCO and 20% HNCO was prepared from cyanuric acid which stood overnight with a slight excess of heavy water.

In studying the spectrum of HNCS in the region 2-15 $\mu$  it was found necessary to use rock salt windows as HNCS readily attacks silver chloride.

#### Normal Modes of Vibration of HNCO and HNCS.

The approximate normal modes of vibration of HNCO and HNCS are shown schematically in Fig. XII. There is only one element of symmetry, the plane of the molecule. There will be five normal modes of vibration taking place in the plane of the molecule, of symmetry class A', and one in which the atoms move out

of the plane, of symmetry class A''. The five frequencies of class A' are numbered 1 through 5 in order of their frequencies as assigned in the next section,  $\nu_1$  being the highest frequency and  $\nu_5$  the lowest. The order is the same for HNC0 and HNCS.

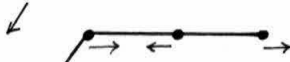
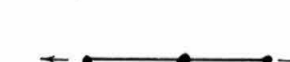
		Symmetry	
	$\nu_1$	Hydrogen stretching	A'
	$\nu_2$	Antisymmetric stretching	A'
	$\nu_3$	Symmetric stretching	A'
	$\nu_4$	Hydrogen bending	A'
	$\nu_5$	CNO bending	A'
	$\nu_6$	CNO bending	A''

Figure XII

Normal Modes of Vibration of HNC0 and HNCS

Presentation and Discussion of Results.

A. Vibrational Frequencies of HNC0 and DNCO

In Fig. XIII are shown the observed spectra of HNC0 and DNCO from 2-15  $\mu$ , under low dispersion.  $\nu_1$  is the sharp band of medium strength at 3534  $\text{cm}^{-1}$ . The strong band at 2280  $\text{cm}^{-1}$  is without a doubt the antisymmetric stretching vibration,  $\nu_2$ . Apparently the symmetric stretching vibration,  $\nu_3$ , is very

Fig. XIII. Absorption spectra of  
HNCO and DNCO from 2-15 microns.



weak and shows up only with considerable pressure. We must assign the weak band at  $1340\text{ cm}^{-1}$  to  $\nu_3$ , as it is expected to be close to  $1307\text{ cm}^{-1}$ , as found by Goubeau (37). If the HNC O molecule approaches  $\text{CO}_2$  in its normal modes  $\nu_3$  should be strong in the Raman and weak in the infrared, while  $\nu_2$  should be weak in the Raman and strong in the infrared. Thus since Goubeau did not find  $\nu_2$  in the Raman spectrum of HNC O we are not surprised to find  $\nu_3$  very weak in the infrared.

The longer wavelength spectrum is not very clear. There is only weak absorption out to 10 microns but from 10 to 15 microns there is much absorption. With the aid of combination bands in the high dispersion spectrum we have attributed the absorption in the region 10 - 15 microns mainly to the hydrogen bending vibration,  $\nu_4$ . The several narrow peaks are believed to be the  $P_{Q_K}$  and  $R_{Q_K}$  maxima of the perpendicular structure of this band.

The complete spectra of HNC O and DNC O between  $1\ \mu$  and  $2.5\ \mu$  are not shown here. Several of the HNC O bands are shown in Figs. XIV, XV, XVI, and XVII. In Table X are listed the observed frequencies for HNC O and DNC O, together with estimated relative intensities of absorption for HNC O. The assignments for  $\nu_4$ ,  $\nu_5$ , and  $\nu_6$  were made by noticing the trio of bands on the short wavelength side of  $\nu_1$  duplicated by a trio of bands on the short wavelength side of  $2\nu_1$ . Thus,

Fig. XIV. Absorption spectrum of  
the second harmonic of the N-H  
stretching vibration of HNCO.

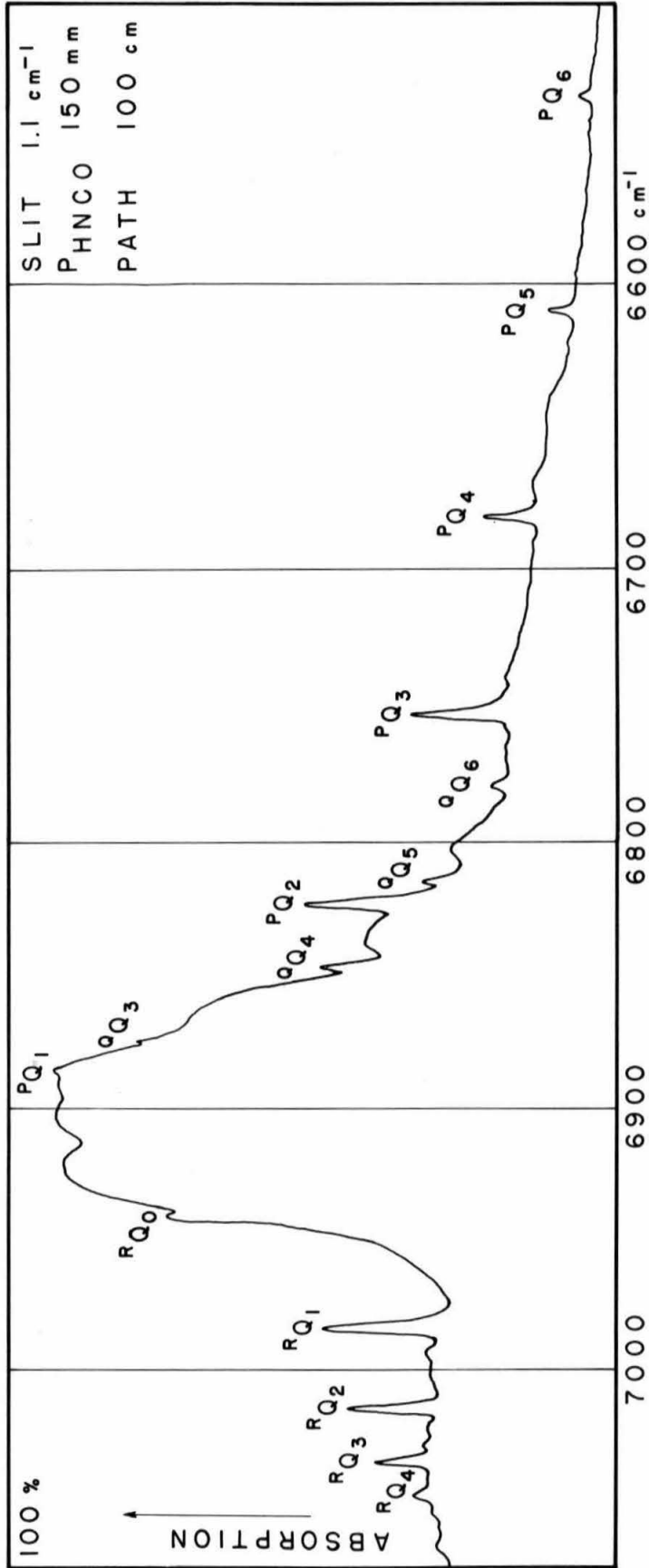


Fig. XV. Absorption spectrum of  
the fundamental of the N-H stretch-  
ing vibration of HNCO.

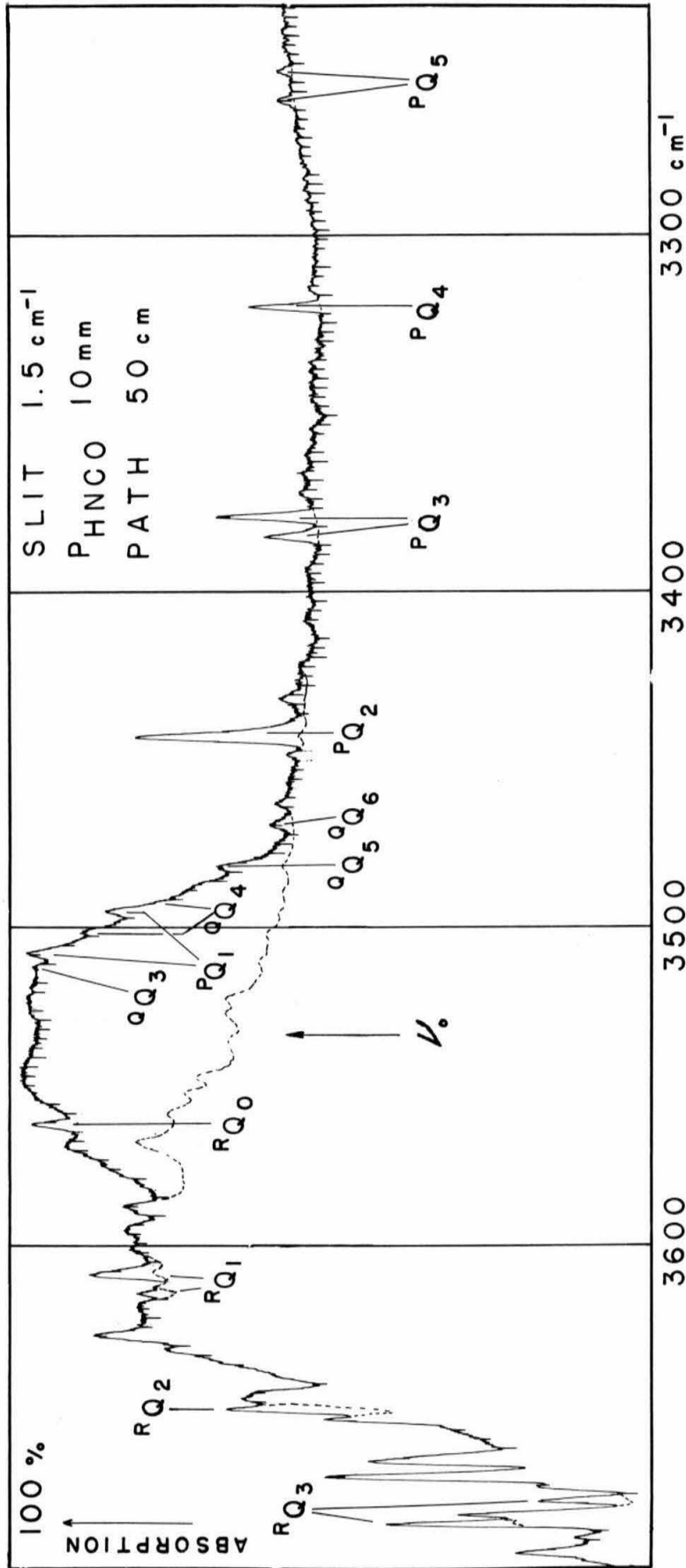


Fig. XVI. Absorption spectrum of  
HNCO between 4000 and 4800  $\text{cm}^{-1}$ .

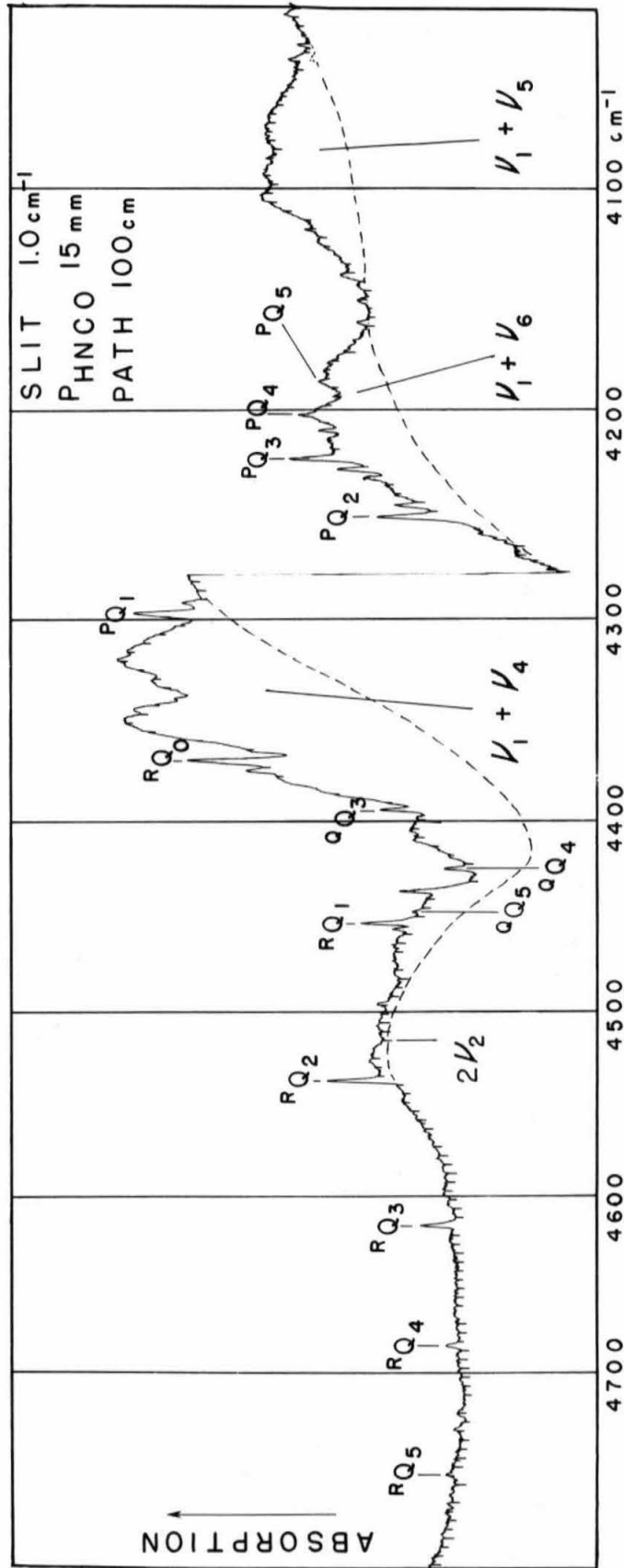


Fig. VII. Absorption spectrum of  
the perturbed band of HNC0 at  
5790 cm<sup>-1</sup>.

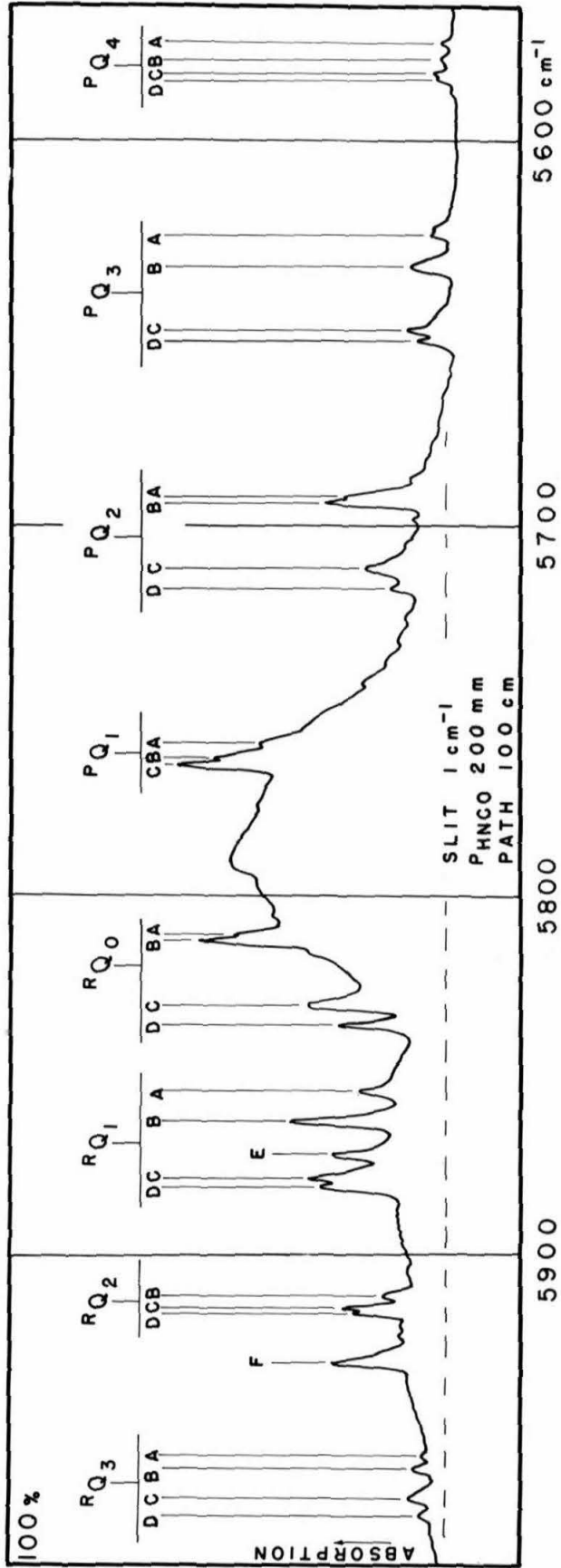


Table X.

Observed Vibrational Frequencies of HNCO and DNCO

Assignment	Frequency, $\text{cm}^{-1}$		Relative intensities for HNCO
	HNCO	DNCO	
$\nu_6$ ( $\text{N}\overset{\downarrow}{\text{C}}\overset{\downarrow}{\text{O}}$ , $A''$ )	(651)*	(622)*	
$\nu_5$ ( $\text{N}\overset{\downarrow}{\text{C}}\overset{\downarrow}{\text{O}}$ , $A'$ )	(549)*	(470)*	
$\nu_4$ ( $\text{H}\overset{\downarrow}{\text{N}}\overset{\downarrow}{\text{C}}$ )	779	?	
$\nu_3 - \nu_5$ (?)	790 $\pm$ 1	751 $\pm$ 1	30
$2\nu_5$ (?)	1045 $\pm$ 10		
$\nu_5 + \nu_6$ (?)	1150 $\pm$ 10		
$\nu_3$ ( $\leftarrow \text{NCO} \rightarrow$ )	1340 $\pm$ 5	1305 $\pm$ 5	3.0
$3\nu_6$	1895 $\pm$ 5	1737 $\pm$ 5	0.5
$\nu_2$ ( $\rightarrow \leftarrow \text{NCO} \rightarrow$ )	2280 $\pm$ 5	2255 $\pm$ 5	100
$2\nu_3$	2620 $\pm$ 10		.05
	3000 $\pm$ 10	3003 $\pm$ 10	0.1
$\nu_2 + \nu_4$ (?)	3105 $\pm$ 10	2880 $\pm$ 10	0.4
$\nu_1$ (H-N, D-N)	3534 $\pm$ 1	2640 $\pm$ 10	30
$\nu_1 + \nu_5$	4083 $\pm$ 5	3110	0.2
$\nu_1 + \nu_6$	4183 $\pm$ 5	3262 $\pm$ 10	0.2
$\nu_1 + \nu_4$	4327 $\pm$ 1		1.0
$2\nu_2$	4516 $\pm$ 2	4459 $\pm$ 2	.02
$\nu_1 + \nu_3$	4866 $\pm$ 2	3920 $\pm$ 2	.05
$\nu_1 + \nu_2$	5795 $\pm$ 5**	4859 $\pm$ 5	.08
$2\nu_1$	6916 $\pm$ 1	5193 $\pm$ 2	0.80
$2\nu_1 + \nu_5$	7465 $\pm$ 5	5653 $\pm$ 5	.004
$2\nu_1 + \nu_6$	7570 $\pm$ 5		.004
$2\nu_1 + \nu_4$	7724 $\pm$ 5		.008
$2\nu_1 + \nu_3 - \nu_5$		5940 $\pm$ 5	

\* These frequencies were not observed directly. Values arrived at from combination frequencies.

\*\* Perturbed by at least two other levels.

$$4327 - 3534 = 793 ; 7723 - 6916 = 807$$

$$4185 - 3534 = 651 ; 7570 - 6916 = 654$$

$$4083 - 3534 = 549 ; 7465 - 6916 = 549$$

The agreement in these differences is striking. In a following section on the hydrogen bending vibration a value of  $779 \text{ cm}^{-1}$  is calculated for  $\nu_4$  from the rotational structure of the band at  $800 \text{ cm}^{-1}$ . So we have made the assignments,

$$\nu_4 = 779 \text{ cm}^{-1}, \nu_5 = 549 \text{ cm}^{-1}, \text{ and } \nu_6 = 651 \text{ cm}^{-1}.$$

$779 \text{ cm}^{-1}$  is indeed quite low for a hydrogen bending frequency. This in itself suggests a large HNC angle - as in HCN the hydrogen bending frequency is  $712 \text{ cm}^{-1}$  (41).

$650 \text{ cm}^{-1}$  was assigned to  $\nu_6$  as this is close to the bending frequency in  $\text{CO}_2$ ,  $667 \text{ cm}^{-1}$ .  $\nu_6$  is the out of the plane vibration and thus depends only on the distortion of the linear NCO group.  $\nu_5$ , however, is of class  $A'$  and can no doubt interact strongly with the nearby hydrogen bending vibration. Thus, it can be pushed down somewhat to  $549 \text{ cm}^{-1}$ .

The peak at  $790 \text{ cm}^{-1}$  is not easily explained as part of the hydrogen bending vibration. It may be a difference band,  $\nu_3 - \nu_5$ , corresponding to a similar band found at  $721 \text{ cm}^{-1}$  in the spectrum of  $\text{CO}_2$  by Barker and Martin (42).

The spectrum of DNCO is not particularly enlightening. The high dispersion spectrum from 1.5 microns to 2.7 microns is not shown here, but the observed frequencies are listed in

Table X. The low dispersion spectrum, from 2 - 15 microns, is shown in Fig. XIII, curve A. The amount of HNCO contaminating this spectrum is about the same as the amount of HNCO in the spectrum of curve B, as evidenced by the similarity in intensities of the N-H bands. The long wavelength spectrum, from 10 to 15 microns is not very different in the two spectra, A and B of Fig. XIII, suggesting that most of the absorption in this region arises from HNCO even for curve A which is the spectrum of a mixture of about 80% DNCO, as estimated by the intensities of the N-D and N-H bands. However, there is a band at  $751\text{ cm}^{-1}$  in DNCO. It is unlikely that this is the deuterium bending frequency as it is not strong and furthermore, we should expect to find it at a much lower frequency, being shifted considerably from  $780\text{ cm}^{-1}$ . Perhaps it is the difference band  $\nu_3 - \nu_5$ .

The evidence of a band at  $470\text{ cm}^{-1}$  suggests that the NCO bending vibration at  $549\text{ cm}^{-1}$  in HNCO does interact with the hydrogen bending vibration, and therefore is considerably shifted in DNCO.

#### B. Rotational Structure of the First Overtone of the N-H Stretching Vibration

The high dispersion spectrum of the first overtone of the N-H stretching vibration in HNCO is shown in Fig. XIV. The band center is at  $6915.7 \pm 0.3\text{ cm}^{-1}$ .

The HNCO molecule is very nearly a symmetric top and the top axis is very nearly parallel to the linear NCO group. The

selection rules for the infrared vibration-rotation spectra of a symmetric top molecule are given by Herzberg(43).

(a) Parallel band - If the change in electric moment of the vibrational transition is parallel to the top axis, the change in rotational quantum numbers must be;

$$\begin{array}{lll} \Delta K = 0 & \Delta J = 0, \pm 1 & \text{if } K \neq 0 \\ \Delta K = 0 & \Delta J = \pm 1 & \text{if } K = 0 \end{array}$$

J is the quantum number of the total angular momentum and K is the quantum number of the angular momentum about the top axis.

(b) Perpendicular band - If the change in electric moment of the vibrational transition is perpendicular to the top axis,  $\Delta K = \pm 1, \Delta J = 0, \pm 1$ .

In HNC0, since the HNC bond angle is probably less than  $180^\circ$  and greater than  $90^\circ$ , the stretching of the N-H bond should give rise to a hybrid band having both parallel and perpendicular components. The strong absorption near the center of the band of Fig. XIV arises mainly from the parallel component for which  $K = 0, \Delta K = 0, \Delta J = \pm 1$ . Thus there should be an absorption minimum at the center of the band corresponding to the forbidden transition having  $K = 0, \Delta K = 0, \Delta J = 0$ . This minimum, however, is partially obscured by the parallel R branch for which  $K = 1, \Delta K = 0, \Delta J = + 1$ . The parallel branches for higher K values are displaced to the low frequency side of the band center because of the difference in rotational constants in the upper and lower vibrational states. This will be evident from

Equation (7) for the frequencies of the  $Q_{Q,K}$  maxima, to be discussed below. The sharp  $Q_{Q,K}$  maxima arise from transitions for different K values having  $\Delta K = 0$ ,  $\Delta J = 0$ .

The  $P_{Q,K}$  and  $R_{Q,K}$  maxima arise from the perpendicular component of the changing electric moment, for which  $\Delta J = 0$  and  $\Delta K = \pm 1$ . Each  $Q_{Q,K}$ ,  $P_{Q,K}$ , and  $R_{Q,K}$  maximum is the observed maximum of an envelope of unresolved lines of many different J values. For  $Q_{Q,K}$  and  $P_{Q,K}$  maxima,  $J \geq K$ . For  $R_{Q,K}$  maxima,  $J \geq K \pm 1$ .

The perpendicular branches involving transitions for which  $\Delta J = \pm 1$  and  $\Delta K = \pm 1$  are too broad and too weak to form observed maxima.

The measured frequencies of the observed vibration-rotation maxima of Fig. XIV are listed in Table XI.

Table XI.

Frequencies Measured from Fig. XIV for the First Overtone of the N-H Vibration in HNC0. ( $\pm 0.10 \text{ cm}^{-1}$ )

$K''$	R $Q_{Q,K}$	P $Q_{Q,K}$	$Q_{Q,K}$
0	6940.74 $\text{cm}^{-1}$		
1	6983.40	6885.18	
2	7015.16	6822.19	
3	7036.32	6753.03	6873.56
4	7049.51	6681.47	6845.86
5		6608.27	6813.89
6		6534.67	6779.24
7		6463.26	

$K'' =$  Quantum number for angular momentum about the figure axis in the lower vibrational state.

We may express the total energy of vibration and rotation by

$$T = G(v_1, v_2, \dots) + F(J, K, v_1, v_2, \dots).$$

Slawsky and Dennison (44) showed that the rotational energy of a non-rigid symmetric top of the ammonia type,  $C_{3v}$ , can be represented by

$$F(J, K) = BJ(J+1) + (A-B)K^2 - D_J J^2 (J+1)^2 - D_{JK} J(J+1)K^2 - D_K K^4 \quad (5)$$

$$B = \frac{h}{8\pi^2 c I_B}, \quad A = \frac{h}{8\pi^2 c I_A}$$

$I_A$  = moment of inertia about the figure axis,

$I_B$  = moment of inertia about the other principal axes.

HNCO is very nearly a prolate symmetric top and we shall attempt to fit its vibration-rotation spectrum with a rotational term similar to Equation (5). However, we shall use the notation adopted by Zumwalt and Giguere (45) in discussing hydrogen peroxide, and by Eyster (35) in discussing hydrazoic acid, and write the more general relation:

$$G(v_1, v_2, \dots) + F(J, K, v_1, v_2, \dots) = \sum_{i,j=0}^{\infty} X_{ij}^{(v)} \{J(J+1)\}^i K^{2j} \quad (6)$$

$v_1, v_2, \dots$  are the vibrational quantum numbers of the vibrational level.

The superscript (v) represents the vibrational level

$(v_1, v_2, \dots)$ .

$$X_{00}^{(v)} = G(v_1, v_2, \dots)$$

$$X_{01}^{(v)} = A_v - \frac{1}{2}(B_v + C_v), \quad X_{10}^{(v)} = \frac{1}{2}(B_v + C_v)$$

$$A_v = g\left(\frac{1}{I_A}\right)_v, \quad B_v = g\left(\frac{1}{I_B}\right)_v, \quad C_v = g\left(\frac{1}{I_C}\right)_v$$

$$g = \frac{h}{8\pi^2 c}$$

$I_A$ ,  $I_B$ , and  $I_C$  are the three principal moments of inertia.

$A_v \gg B_v > C_v$  for a spindle molecule as HNC0.

$\left(\frac{1}{I}\right)_v =$  time average of  $\frac{1}{I}$  in vibration state  $v$ .

From Equation (6), for the  ${}^R Q_K$ ,  ${}^P Q_K$ , and  ${}^Q Q_K$  maxima observed we may write for the absorption frequencies:

$${}^R Q_K: \nu = \sum_{i,j=0}^{\infty} \left\{ X_{ij}^{(v)} (K+1)^{2j} - X_{ij}^0 K^{2j} \right\} \left\{ J_R^{(K)} (J_R^{(K)} + 1) \right\}^i$$

$${}^P Q_K: \nu = \sum_{i,j=0}^{\infty} \left\{ X_{ij}^{(v)} (K-1)^{2j} - X_{ij}^0 K^{2j} \right\} \left\{ J_P^{(K)} (J_P^{(K)} + 1) \right\}^i \quad (7)$$

$${}^Q Q_K: \nu = \sum_{i,j=0}^{\infty} (X_{ij}^{(v)} - X_{ij}^0) K^{2j} \left\{ J_Q^{(K)} (J_Q^{(K)} + 1) \right\}^i$$

$J_R^{(K)}$ ,  $J_P^{(K)}$ , and  $J_Q^{(K)}$  are the  $J$  values of observed maximum

absorption in the  ${}^R Q_K$ ,  ${}^P Q_K$ , and  ${}^Q Q_K$  maxima respectively. These values depend on the matrix elements of the transition electric moment, on the spacing between lines of different J, and on the resolution of the spectrometer.

For hydrazoic acid (35) Eyster was able to represent the energy levels quite well by neglecting differences between  $J_R^{(K)}$ ,  $J_P^{(K)}$ ,  $J_Q^{(K)}$ ,  $J_R^{(K+1)}$ , etc., and also by neglecting any cross term coefficients,  $X_{ij}^{(v)}$ , where both i and j are unequal to zero. Furthermore, he was able to neglect coefficients having  $j > 2$ . Neglecting these small quantities Eyster was able to determine  $X_{01}^0$  and  $X_{02}^0$  from the combinations

$$\Delta F''(K) = {}^Q Q_K - {}^P Q_{K+1} = {}^R Q_K - {}^Q Q_{K+1} \quad (8)$$

$$\Delta_2 F''(K) = {}^R Q_{K-1} - {}^P Q_{K+1}$$

In the absorption band of Fig. XIV, the  ${}^P Q_K$  and  ${}^R Q_K$  maxima are very widely spaced indicating that  $X_{01}^0$  is very large. Also, these maxima are quite narrow indicating that the terms in Equation (7) with  $i \neq 0$  are very small, otherwise the lines of different J value would broaden the maxima more. Therefore, we shall attempt to find  $X_{01}^0$  and  $X_{02}^0$  from the combinations  $F''(K)$  making the same approximations Eyster made (35). Thus, we are for the present neglecting differences in  $J_R^{(K)}$ ,  $J_P^{(K)}$ ,  $J_Q^{(K)}$ , etc., and neglecting  $X_{ij}^0$  having  $j > 2$ . From Equations (7) we arrive at

$$\Delta_2 F''(K) = Q_{K-1}^R - Q_{K+1}^P = x_{01}^0 \left\{ (K+1)^2 - (K-1)^2 \right\} + x_{02}^0 \left\{ (K+1)^4 - (K-1)^4 \right\}$$

$$\text{Define } f''_K = \frac{\Delta_2 F''(K)}{4K} = x_{01}^0 + 2x_{02}^0 (K^2 + 1) \quad (9)$$

Using the data of Table XI we have tabulated these combinations in Table XII with the calculated values of  $x_{02}^0$ .

Table XII.

Combinations from Table XI for Determining  $x_{02}^0$ .

K	$\Delta_2 F''(K)$	$f''_K$	$x_{02}^0$
1	118.55	29.64	-0.140 -0.99 -0.076 -0.056
2	230.37	28.80	
3	333.69	27.81	
4	428.00	26.75	
5	514.84	25.74	

The values given for  $x_{02}^0$  are those calculated from Equation (9) for the two indicated adjacent K states. Obviously Equation (9) is highly inadequate, and it is necessary to include coefficients  $x_{0j}^0$  having  $j > 2$ .

In Appendix IV it is shown that the centrifugal stretching of HNC0 should give rise to a power series in  $K^2$  with appreciable coefficients, more of which must be included as we consider higher and higher K levels. Therefore, we must write for

$$\Delta_2 F''(K) = Q_{K-1}^R - Q_{K+1}^P = \sum_{j=0}^{\infty} x_{0j}^0 \left\{ (K+1)^{2j} - (K-1)^{2j} \right\} \quad (10)$$

In Table XII we have  $\Delta_2 F''(K)$  tabulated out to  $K=5$ . Therefore, we can solve for the first five coefficients,  $X_{0j}^0$ , neglecting all  $X_{0j}^0$  having  $j > 5$ . The coefficients  $X_{0j}^0$  for  $j > 5$  will be very small and not important for small  $K$ . These coefficients,  $X_{0j}^0$ , which we determine will be more and more accurate as  $j$  gets smaller, so the value for  $X_{01}^0$  and  $X_{02}^0$  are believed to be quite accurate. The calculations yield:

$$\begin{aligned} X_{01}^0 &= 30.40 \text{ cm}^{-1} & X_{02}^0 &= -.2236 \text{ cm}^{-1} \\ X_{03}^0 &= 9.05 \times 10^{-3} \text{ cm}^{-1} & X_{04}^0 &= -2.6 \times 10^{-4} \\ X_{05}^0 &= 3.0 \times 10^{-6} \text{ cm}^{-1} & & \end{aligned}$$

In arriving at the above coefficients we have neglected differences in  $J_R^{(K)}$ ,  $J_P^{(K)}$ , and  $J_Q^{(K)}$  and we have also neglected  $X_{ij}^0$  having both  $i \neq 0$  and  $j \neq 0$ . We wish now to attempt to learn the magnitude of these neglected terms and make corrections for them if necessary.

It was found that an investigation of the other combination of Equation (8),  $\Delta F''(K)$ , helped to make the corrections discussed immediately above. From Equation (8),  $\Delta F''(K) = \frac{Q_R}{K} - \frac{Q_P}{K+1} = \frac{Q_R}{K} - \frac{Q_{K+1}}{K+1}$ . These values may be obtained from Table XI and are listed in Table XIII. The data is meager, but for  $K=3$  and  $K=4$  we have values for both combinations in Table III. Unfortunately they do not agree and their difference,  $\Delta_K$ , is much greater than can be accounted for by experimental error. If we go back to the general Equation (7) we note that the reason for this is, no doubt, that  $J_R^{(K)}$ ,  $J_P^{(K)}$ , and  $J_Q^{(K)}$  are by no means the same. At this point

Table XIII

$\Delta F''(K)$  for the N-H Stretching Vibration

K	$\overset{Q}{Q}_K - \overset{P}{Q}_{K+1}$	$\overset{R}{Q}_K - \overset{Q}{Q}_{K+1}$	$\Delta K$
1			
2		141.60 $\text{cm}^{-1}$	
3	192.09 $\text{cm}^{-1}$	190.46	1.63 $\text{cm}^{-1}$
4	237.59	235.62	1.97
5	279.22		
6	315.98		

we shall introduce a simpler notation:

$$\alpha_K = J_R^{(K)} (J_R^{(K)} + 1)$$

$$\beta_K = J_P^{(K)} (J_P^{(K)} + 1)$$

$$\gamma_K = J_Q^{(K)} (J_Q^{(K)} + 1)$$

Now, from Equations (7):

$$\begin{aligned} \overset{Q}{Q}_K - \overset{P}{Q}_{K+1} &= \sum_{i,j=0}^{\infty} X_{ij}^{(v)} K^{2j} \{ \gamma_K^i - \beta_{K+1}^i \} \\ &\quad + X_{ij}^0 (K+1)^{2j} \beta_{K+1}^i - X_{ij}^0 K^{2j} \gamma_K^i \end{aligned}$$

$$\begin{aligned} \overset{R}{Q}_K - \overset{Q}{Q}_{K+1} &= \sum_{i,j=0}^{\infty} X_{ij}^{(v)} (K+1)^{2j} \{ \alpha_K^i - \gamma_{K+1}^i \} \\ &\quad + X_{ij}^0 (K+1)^{2j} \gamma_{K+1}^i - X_{ij}^0 K^{2j} \alpha_K^i \end{aligned}$$

Then, letting  $\Delta_K = \overset{Q}{Q}_K - \overset{P}{Q}_{K+1} - \overset{R}{Q}_K + \overset{Q}{Q}_{K+1}$

$$\Delta_K = \sum_{i,j=0}^{\infty} X_{ij}^{(V)} K^{2j} \{ \gamma_K^i - \beta_{K+1}^i \} + X_{ij}^{(V)} (K+1)^{2j} \{ \gamma_{K+1}^i - \alpha_K^i \} \\ + X_{ij}^0 K^{2j} \{ \alpha_K^i - \gamma_K^i \} + X_{ij}^0 (K+1)^{2j} \{ \beta_{K+1}^i - \gamma_{K+1}^i \}$$

First we notice that all terms having  $i = 0$  are identically zero.

Also it is obvious that  $\Delta_K = 0$  if  $\gamma_K = \beta_{K+1} = \gamma_{K+1} = \alpha_K$ .

All terms having both  $i > 0$  and  $(i + j) > 2$  are no doubt negligible compared to the others. Thus we can simplify  $\Delta_K$ ,

$$\Delta_K = \{ X_{10}^{(V)} - X_{10}^0 + (X_{11}^{(V)} - X_{11}^0) K^2 \} \{ \gamma_K + \gamma_{K+1} - \beta_{K+1} - \alpha_K \} \\ + X_{11}^{(V)} (2K+1) \{ \gamma_K - \alpha_K \} + X_{11}^0 (2K+1) \{ \beta_{K+1} - \gamma_{K+1} \}$$

(11)

$$+ \{ X_{20}^{(V)} - X_{20}^0 \} \{ \gamma_K^2 + \gamma_{K+1}^2 - \beta_{K+1}^2 - \alpha_K^2 \}$$

In determining  $X_{01}^0$  we used Equation (10) which was derived from Equations (7) by neglecting differences in  $J_R^{(K-1)}$  and  $J_P^{(K+1)}$ . A more exact expression is,

$$\Delta_2^{F''(K)} = \sum_{j=0}^{\infty} X_{0j}^0 \left\{ (K+1)^{2j} - (K-1)^{2j} \right\} + \delta_K'' \quad (12)$$

$$\begin{aligned} \delta_K'' = & \left\{ X_{10}^{(v)} - X_{10}^0 + (X_{11}^{(v)} - X_{11}^0) K^2 \right\} \left\{ \alpha_{K-1} - \beta_{K+1} \right\} \\ & + X_{11}^0 (2K) \left\{ \beta_{K+1} + \alpha_{K-1} \right\} + X_{11}^0 \left\{ \beta_{K+1} - \alpha_{K-1} \right\} \\ & + \left\{ X_{20}^{(v)} - X_{20}^0 \right\} \left\{ \alpha_{K-1}^2 - \beta_{K+1}^2 \right\} \end{aligned} \quad (13)$$

In writing the above expression for  $\delta_K''$  we have neglected all terms having both  $i > 0$  and  $(i+j) > 2$ .

In Equations (11) and (13) we have expressions for  $\Delta_K$  and  $\delta_K''$ . In Appendix V approximate values of  $\alpha_K$  and  $\beta_K$  are calculated. In Appendix VI an approximate value of  $X_{10}^{(2)} - X_{10}^0$  is calculated from  $X_{01}^0$  and  $X_{01}^{(2)}$ , the superscript (2) designating the second excited state of the N-H vibration of HNC0. In Appendix VII an approximate value of  $X_{11}^0$  is calculated. From the data of Appendices V, VI, and VII, and the data of Table XIII for  $\Delta_K$ ,

an approximate relation for  $\delta_K''$  as a function of K is calculated in Appendix VIII. It is shown in Appendix VIII that  $\delta_K'' < 0.10 (4K) \text{ cm}^{-1}$ . Since  $\delta_K''$  is approximately proportional to  $4K$ , we have merely to subtract it from the previously calculated value of  $X_{01}^0$ , which is the coefficient of  $4K$  in the expression for  $\Delta_2 F''(K)$ , Equation (11). Therefore we report  $X_{01}^0 = 30.30 \pm 0.10 \text{ cm}^{-1}$ .

To determine  $X_{01}^{(2)}$ , by which we mean the rotational constant  $X_{01}$  in the second excited vibrational level of the N-H stretching vibration, we employ another combination,

$$\Delta_2 F'(K) = \frac{R}{K} - \frac{P}{K} = \sum_{j=0}^{\infty} X_{0j}^{(v)} \{ (K+1)^{2j} - (K-1)^{2j} \} + \delta_K' \quad (14)$$

$$\delta_K' = \{ X_{10}^{(v)} - X_{10}^0 + (X_{11}^{(v)} - X_{11}^0) K^2 \} \{ \alpha_K - \beta_K \} \\ + X_{11}^{(v)} (2K) \{ \alpha_K + \beta_K \} + X_{11}^{(v)} \{ \alpha_K - \beta_K \}$$

The largest term in  $\delta_K'$  involves  $X_{11}^{(v)}$ . The largest term in  $\delta_K''$  involves  $X_{11}^0$  (see Equation (13)).  $X_{11}^{(v)}$  is approximately proportional to  $\sqrt{X_{02}^{(v)} X_{20}^{(v)}}$  (see Appendix VII). Both  $X_{02}^{(v)}$  and  $X_{20}^{(v)}$  will be smaller than  $X_{02}^0$  and  $X_{20}^0$  respectively, as in the excited state both moments of inertia will be increased and thus the

angular velocity will be decreased. Therefore  $\delta'_K < \delta''_K$ . Since  $\delta''_K < 0.10(4K)\text{cm}^{-1}$  we shall say, somewhat arbitrarily, that  $\delta'_K < 0.06(4K)$ .

From Table XI four combinations,  $\Delta_2^{F'}(K)$ , have been calculated and are listed in Table XIV.

Table XIV

$\Delta_2^{F'}(K)$  for  $2\nu_{\text{N-H}}$

K	$\Delta_2^{F'}(K)\text{cm}^{-1}$	$\Delta_2^{F'}(K)/4K$
1	98.22	24.555
2	192.97	24.18
3	283.29	23.61
4	368.04	23.00

From Table XIV and Equation (14) we have calculated that

$$X_{01}^{(2)} = 24.75 \text{ cm}^{-1}, X_{02}^{(2)} = -.065 \text{ cm}^{-1}$$

$$X_{03}^{(2)} = +5.6 \times 10^{-5} \quad X_{04}^{(2)} = +1.4 \times 10^{-5}$$

The last two coefficients are probably not very accurate since we have neglected the higher coefficients. In fact  $X_{04}^{(2)}$  should be negative if it were possible to include all terms in the series. However, it is believed that the value for  $X_{01}^{(2)}$  is quite accurate, within  $0.10 \text{ cm}^{-1}$ . Thus, in going from the ground vibrational state to the second excited state of the N-H vibration,  $X_{01}$  has changed by  $5.55 \text{ cm}^{-1}$ , or 18.3%.

From Table XI and Equations (7) it is found that  $\nu_0 = 6915.7 \pm 0.3 \text{ cm}^{-1}$  for the band center of the second harmonic of the N-H stretching vibration.

In Appendix IV, the theoretical values of  $X_{O_2}^0, X_{O_3}^0$ , etc., are considerably smaller than those found experimentally. The probable reasons for these discrepancies are discussed at the end of Appendix IV.

A rough check on the above values of  $X_{O_j}^0$  and  $X_{O_j}^{(2)}$  can be had from the  $Q_{Q_K}$  maxima. Assuming  $(X_{ij}^{(v)} - K_{ij}^0)$  is negligible for  $i > 0$ , from Equations (7)  $Q_{Q_K} = \nu_0 + \sum_{j=1}^{\infty} \{X_{O_j}^{(v)} - X_{O_j}^0\} K^{2j}$ . Using the values of  $X_{O_j}^0$  and  $X_{O_j}^{(v)}$  and  $\nu_0$  found above it is found that  $Q_{Q_3} = 6873.8$ . The experimental value for  $Q_{Q_3}$ , from Table XI, is 6873.56. The agreement is quite good considering the approximations involved. For higher K values the agreement is less satisfactory as the coefficients of powers of K higher than ten become important, and we do not know these coefficients.

### C. Molecular Structure Of HNC<sup>o</sup>

As mentioned previously Eyster, Gillette, and Brockway (36) made an electron diffraction investigation of HNC<sup>o</sup>. They reported two possible structures for the linear NCO group,

(a)	N-C	1.21 Å	(b)	N-C	1.18 Å
	C-O	1.18 Å		C-O	1.20 Å
	N-O	2.39 Å		N-O	2.38 Å

For CH<sub>3</sub>NCO they reported the distances N-C = 1.19<sub>±</sub>.03 Å and C-O = 1.18<sub>±</sub>.03 Å. These results favor structure (a) for HNC<sup>o</sup>, which is also favored by the fact that nitrogen usually has a larger atomic radius than oxygen, and the N-C and C-O bonds should be similar in character (essentially double bonds).

Therefore, we have assumed the N-C and C-O distances labelled (a) above.

The N-H distance and HNC angle cannot both be determined from the rotational constant  $A_0$ . One must be known to determine the other as we have not been able to determine  $A^0$  for DNCO. The N-H stretching frequency is higher than that in ammonia, indicating a shorter N-H bond. Through the use of Badger's rule (23) we have assigned a distance of  $0.99 \text{ \AA}$  for the N-H bond.

Schulman and Shoolery (47), in this laboratory, have found the rotational constant  $\frac{1}{2}(B_0 + C_0)$  from the microwave spectrum of HNCO. They report  $\frac{1}{2}(B_0 + C_0) = 0.367 \text{ cm}^{-1}$ . In the preceding section we have shown that  $A_0 - \frac{1}{2}(B_0 + C_0) = 30.30 \pm 0.1 \text{ cm}^{-1}$ . Therefore  $A_0 = 30.67 \pm 0.1 \text{ cm}^{-1}$ . From this value for  $A_0$  we have calculated that  $(I_A)_0 = 0.9125 \times 10^{-40} \text{ gm cm}^2$ .  $(I_A)_0$  is the effective least moment of inertia in the ground state.

By making the approximation that the least axis of inertia is parallel to the NCO group, from the above value for  $(I_A)_0$  we calculated an HNC angle of  $130^\circ 44'$ . Actually the least axis of inertia will be slightly tilted toward the hydrogen atom, requiring a smaller HNC angle to give the experimental moment of inertia,  $(I_A)_0$ . In Appendix IX we have assumed an HNC angle of  $129^\circ$  and calculated the value of  $I_A$  as a function of small changes in this angle.  $I_A$  is now the moment of inertia about the true least axis of inertia. As above we have also assumed  $r_{N-C} = 1.21 \text{ \AA}$ ,  $r_{C-O} = 1.18 \text{ \AA}$ , and  $r_{N-H} = 0.99 \text{ \AA}$ . The results of the calculations

of Appendix IX show that

$$(I_A)_{\Theta=0} = 0.8946 \times 10^{-40} \text{ gm cm}^2$$

$\Theta$  is the value of  $(\alpha - 129^\circ)$ , where  $\alpha$  is the HNC angle. It is also shown in Appendix IX that

$$\left(\frac{d I_A}{d \Theta}\right)_{\Theta=0} = -1.506 \times 10^{-40} \text{ gm cm}^2/\text{radian}$$

We wish to calculate  $\Theta$  to agree with the experimental value

$$(I_A)_0 = 0.9125 \times 10^{-40}. \quad (I_A)_0 - (I_A)_{\Theta=0} = \left(\frac{d I_A}{d \Theta}\right)_{\Theta=0} \Theta = 0.0179 \times 10^{-40} \text{ gm cm}^2$$

From this we find that  $\Theta = -0.0119$  radians  $= -41'$ . Therefore  $\alpha = 129^\circ + \Theta = 128^\circ 19'$ .

An error of  $0.01 \text{ \AA}$  in  $r_{\text{N-H}}$  leads to an error of  $40'$  in  $\alpha$ . An error of  $0.10 \text{ cm}^{-1}$  in  $A_0$  leads to an error of only  $7'$  in  $\alpha$ . It is believed that  $r_{\text{N-H}} = 0.99 \pm 0.01 \text{ \AA}$ , thus we have determined an effective HNC angle of  $128^\circ 19' \pm 40'$  for the ground vibrational state.

#### D. Rotational Structure of the N-H Fundamental Absorption Band

The fundamental of the hydrogen stretching vibration was also observed under high dispersion. Its spectrum is shown in Fig. 15. The  $\begin{matrix} R \\ Q \\ K \end{matrix}$  maxima are superimposed on the strong water band at 2.75 microns. Moreover, apparently two of the K levels in the first excited level of the hydrogen stretching vibration are perturbed by another close-lying level, possibly  $(\nu_2 + \nu_3)$ .

The frequencies of the  $Q_K^R$ ,  $Q_K^P$ , and  $Q_K^Q$  maxima are tabulated in Table XV.

Table XV.

Observed Maxima in the N-H Fundamental of HNC0

K	$Q_K^R$	$Q_K^P$	$Q_K^Q$
0	3560.94		
1	3614.51* 3608.96	3507.46* 3494.72	
2	3652.91	3442.25	
3	3691.36* 3683.84	3384.29* 3378.42	3511.45
4	3716.82	3319.60	3500.62* (3494.72)
5		3263.58* 3255.32	3480.84
6			3468.04

\* These levels are apparently doubled by perturbations from other levels.

The usual combinations for the ground state are tabulated in Table XVI, and the data of Tables XII and XIII from  $2 \nu_{N-H}$  are included for comparison.

Table XVI

Combinations from  $\checkmark_{N-H}$  and  $2\checkmark_{N-H}$  of HNC0 for Rotational Levels in the Ground Vibrational State

K	$\begin{array}{c} R \quad P \\ \text{Q} \quad - \quad \text{Q} \\ K-1 \quad K+1 \\ \checkmark_{N-H} \quad 2\checkmark_{N-H} \end{array}$		$\begin{array}{c} R \quad \text{Q} \quad \text{Q} \\ \text{Q} \quad - \quad \text{Q} \\ K-1 \quad K \\ \checkmark_{N-H} \quad 2\checkmark_{N-H} \end{array}$		$\begin{array}{c} \text{Q} \quad \text{Q} \quad P \\ \text{Q} \quad - \quad \text{Q} \\ K-1 \quad K \\ \checkmark_{N-H} \quad 2\checkmark_{N-H} \end{array}$	
	1	118.69cm <sup>-1</sup>	118.55			
2	230.22* 230.54	230.37				
3	333.31	333.69	141.46	141.60		
4	427.78* 428.52	428.00	190.74* (189.12)	190.46	191.85	192.09
5			235.98	235.62	237.04* (239.40)	237.59
6						279.22

\* These combinations result from levels which are apparently doubled by perturbation from other levels.

Considering the fact that a much wider slit was used for  $\checkmark_{N-H}$  than for  $2\checkmark_{N-H}$  the agreement is quite good, with the exception of the values in parentheses. These values in error both involve  $\text{Q}_{\text{Q}_4} = 3494.72 \text{ cm}^{-1}$  and thus it is believed that the assignment of  $\text{Q}_{\text{Q}_4}$  may be in error. The high intensity of the band at  $3494.72 \text{ cm}^{-1}$  suggests that it is more than a  $\text{Q}_{\text{Q}_K}$  branch. A probable explanation is that the  $\text{P}_{\text{Q}_1}$  band is split up by a perturbing level into two maxima, one at  $3507.46 \text{ cm}^{-1}$  and the other at

3494.72, obscuring the other component of the  $Q_4$  transition.

Due to the perturbations of the upper state we were not able to calculate the correct rotational constants of this first excited level of the N-H vibration. Since  $X_{01}^0 = 30.30 \text{ cm}^{-1}$  and  $X_{01}^{(2)} = 24.75 \text{ cm}^{-1}$  we would expect  $X_{01}^{(1)}$  to be halfway between these two, so probably  $X_{01}^{(1)} = 27.5 \text{ cm}^{-1}$ . (So far in this thesis the superscript on  $X_{01}$  has designated the vibrational quantum number of the N-H vibration, all other vibrational modes being unexcited).

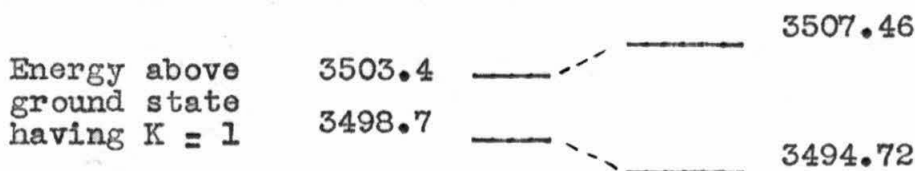
We can determine an approximate value of  $\nu_0$  from  $R_{Q_1}$ , assuming  $X_{01}^{(1)} = 27.5 \text{ cm}^{-1}$  and  $X_{02}^{(1)} = -0.1 \text{ cm}^{-1}$  (between  $X_{02}^0$  and  $X_{02}^{(2)}$ ).

$$\nu_0 = R_{Q_1} - X_{01}^{(1)} + X_{02}^{(1)} = 3533.5 \pm 0.5 \text{ cm}^{-1}$$

Using this value of  $\nu_0$  we can solve for the expected frequency of  $P_{Q_1}$ .

$$P_{Q_1} = \nu_0 - X_{01}^0 + X_{02}^0 = 3503.4$$

This value for  $P_{Q_1}$  substantiates our argument that  $P_{Q_1}$  may be split up, by perturbation from another level, into levels at 3507.46 and 3494.72, as pictured below



The level at 3498.7 represents the perturbing level.

E. Rotational Structure of the Combination Band,

$\nu_1 + \nu_4$ , of HNC0

The high dispersion spectrum of the combination band,  $\nu_1 + \nu_4$  of HNC0 is shown in Fig. XVI. There are several maxima which have not been identified, some arising from the combination band, ( $\nu_1 + \nu_6$ ), and others perhaps from a level lying close to ( $\nu_1 + \nu_4$ ), as ( $\nu_1 + \nu_3 - \nu_5$ ) for example. The rotational lines of the combination band ( $\nu_1 + \nu_4$ ) have been identified and are listed in Table XVII.

Table XVII

Observed Maxima for the Band  $\nu_1 + \nu_4$

K	R $Q_K$	P $Q_K$	$Q_{K-1} - Q_K$
0	4369.37		
1	4452.89	4296.97	
2	4536.18	4250.87	
3	4615.78	4223.19	4394.02
4	4683.12	4202.55	4424.47
5	4757.83	4187.29	4446.97

From the data of Table XVII the usual combinations for the ground state are given in Table XVIII.

Table XVIII.

Combinations for the Band  $\nu_1 + \nu_4$ , for the ground state.

K	R $Q_{K-1} - P_{K+1}$	R $Q_{K-1} - Q_K$	$Q_{K-1} - P_{K+1}$
1	118.50 cm <sup>-1</sup>		
2	229.70		
3	333.63	142.16	
4	428.49	191.31	191.47
5		236.15	237.18

These combinations agree well with those from  $2\nu_{N-H}$ .

In Table XIX are listed combinations from which the rotational constants in the upper state have been calculated. We have used the symbol  $X_{Oj}^{(2)}$  for the rotational constants of the second excited level of the N-H vibration. For this combination band we shall use the symbol  $X_{Oj}^{(11)}$  for the rotational constants of the upper level.

Table XIX

Combinations for the Band  $\nu_1 + \nu_4$ , for the Upper Level

K	R	P	R	Q	Q	Q	P
	$Q_K$	$-Q_K$	$Q_K$	$-Q_K$	$Q_K$	$Q_{K+1}$	$-Q_{K+1}$
1	155.92						
2	285.31						170.83
3	392.59		221.76				221.92
4	480.57		258.65				259.68
5	570.54		310.83				

From Equations (7) it is seen that the second and third columns in Table XIX should agree, in the approximation that we neglect the differences in  $J_R^{(K)}$ ,  $J_P^{(K)}$ , and  $J_Q^{(K)}$ . The agreement is fair.

From the second column of Table XIX, using Equation (10), we have calculated the rotational constants of the upper level of  $(\nu_1 + \nu_4)$ . The results are presented below, together with the values of  $X_{Oj}^0$ .

$$\begin{aligned}
 X_{O1}^{(11)} &= 42.63 \text{ cm}^{-1} & , & & X_{O1}^0 &= 30.30 \text{ cm}^{-1} \\
 X_{O2}^{(11)} &= -1.14 & , & & X_{O2}^0 &= -.224
 \end{aligned}$$

$$\begin{aligned} X_{03}^{(11)} &= 6.6 \times 10^{-2} \quad , \quad X_{03}^0 = 9 \times 10^{-3} \\ X_{04}^{(11)} &= -2.1 \times 10^{-3} \quad , \quad X_{04}^0 = -2.6 \times 10^{-4} \\ X_{05}^{(11)} &= 2.5 \times 10^{-5} \quad , \quad X_{05}^0 = 3 \times 10^{-6} \end{aligned}$$

The transition  $R_{Q_1}$  has less intensity than  $R_{Q_2}$ , whereas it should have more than  $R_{Q_2}$  (See Fig. XVI). This suggests that it has perhaps been perturbed by a nearby level, and thus lost intensity. If the perturbation is small it will not have much effect on the validity of the above rotational constants,  $X_{0j}^{(11)}$ . However these rotational constants are unusually large, and a check on their validity is desirable.

We can determine the value of  $\nu_0$  for this transition from the value of  $P_{Q_1}$ . From Equation (7), if we neglect

$$(X_{10}^{(v)} - X_{10}^0) \text{ and } X_{11},$$

$$P_{Q_1} = \nu_0 * \sum_{j=1}^{\infty} X_{0j}^0.$$

The values of  $X_{0j}^0$  are given above and believed to be quite accurate. The value for  $P_{Q_1}$  is given in Table XVII. From these we calculate that  $\nu_0 = 4327.1 \text{ cm}^{-1}$ .

From Equations (7), neglecting  $(X_{10}^{(v)} - X_{10}^0)$  and  $X_{11}^{(v)}$ ,

$$R_{Q_0} = \nu_0 * \sum_{j=1}^{\infty} X_{0j}^{(11)}.$$

Using the values for  $X_{0j}^{(11)}$  listed above, and the value of  $R_{Q_0}$

from Table XVII,  $\nu_0 = 4327.8$ . The difference of  $\nu_0$  calculated from  $P_{01}$  and  $\nu_0$  calculated from  $R_{00}$  is probably partly due to the neglect of  $X_{11}^0$  and  $X_{11}^{(11)}$ , which come in with different signs in the two cases. This calculation substantiates our calculation of  $42.6 \text{ cm}^{-1}$  for  $X_{01}^{(11)}$ . Thus the perturbation of the upper level of  $R_{01}$  does not greatly affect the calculation of  $X_{01}^{(11)}$ , but we should allow for an error of about  $0.5 \text{ cm}^{-1}$ .

From the above calculations we report  $X_{01}^{(11)} = 42.6 \pm 0.5 \text{ cm}^{-1}$ , and  $\nu_0 = 4327.5 \pm 0.5 \text{ cm}^{-1}$  for the combination band ( $\nu_1 + \nu_4$ ).

The above results indicate that there is a large increase in  $X_{01}$  when the hydrogen bending vibration is excited. This is to be expected as, even if it performed harmonic oscillations about the equilibrium position,  $X_{01}^{(11)}$  would be considerably larger than  $X_{01}^0$ . The anharmonicity of the vibration would be expected to increase  $X_{01}^{(11)}$  even more. The magnitude of  $X_{01}^{(11)}$  serves to substantiate the assignment of ( $\nu_1 + \nu_4$ ), as no other vibration than one involving  $\nu_4$  could have such a large effect.

#### F. Calculation of $X_{01}$ for Hydrogen Bending Vibration.

It is generally possible to represent the rotational constant as a linear function of the vibrational quantum numbers, as

$$X_{01}^{(v)} = X_{01}^{(e)} + \sum_{i=1}^6 \alpha_i (v_i + \frac{1}{2})$$

where  $X_{01}^{(e)}$  is the rotation constant for infinitesimal vibrations.

We have calculated values for  $X_{01}^0$ ,  $X_{01}^{(2)}$ , and  $X_{01}^{(11)}$  - for the

ground state, the second excited level of the N-H bending vibration, and the upper level of ( $\nu_1 + \nu_4$ ) respectively. Thus we have the relations

$$X_{01}^{(e)} + \frac{1}{2}(\alpha_1 + \alpha_2 + \alpha_3 + \alpha_4 + \alpha_5 + \alpha_6) = 30.30 \text{ cm}^{-1}$$

$$X_{01}^{(e)} + \frac{5}{2}\alpha_1 + \frac{1}{2}(\alpha_2 + \alpha_3 + \alpha_4 + \alpha_5 + \alpha_6) = 24.75$$

$$X_{01}^{(e)} + \frac{3}{2}\alpha_1 + \frac{3}{2}\alpha_4 + \frac{1}{2}(\alpha_2 + \alpha_3 + \alpha_5 + \alpha_6) = 42.6$$

From these equations we find that  $\alpha_1 = -2.78 \text{ cm}^{-1}$ , and  $\alpha_4 = +15.0 \text{ cm}^{-1}$ . Therefore,  $X_{01}^{(01)} = 30.30 + \alpha_4 = 45.30 \text{ cm}^{-1}$ .  $X_{01}^{(01)}$  is to represent the rotational constant in the first excited level of the HNC bending vibration.

In Table XX are given some possible assignments for the sharp maxima of absorption in the HNC bending band,  $\nu_4$ , of Fig. XIII.

Table XX

Observed Maxima in  $\nu_4$  at  $800 \text{ cm}^{-1}$

K	R	P	R	P	R	P
	Q K	Q K	Q K-1	Q K+1	Q K	Q K
0	831 $\text{cm}^{-1}$					
1	931	749		117		182
2		714		230		
3		701				

From the figure in the last column, neglecting centrifugal stretching,  $X_{01}^{(01)}$  is calculated as  $45.5 \text{ cm}^{-1}$ . The agreement with the above predicted value is fortuitous. It will actually

be larger as we certainly are not justified in neglecting the centrifugal stretching. However, the fact that the value is close is gratifying.

We have calculated  $\nu_0$  from

$$P_{Q_1} = \nu_0 + X_{O1}^0 + X_{O2}^0 + \dots, \text{ giving}$$

$$\nu_0 = 779.2 \text{ cm}^{-1}.$$

G. Perturbations in the Upper Level of the Band at  $5790 \text{ cm}^{-1}$ , ( $\nu_1 + \nu_2$ ).

In Fig. XVII is shown the spectrum of the band at  $5790 \text{ cm}^{-1}$ . The most likely band of sufficient intensity to give the observed absorption in this region is the combination frequency, ( $\nu_1 + \nu_2$ ). This band at  $5790 \text{ cm}^{-1}$  is apparently perturbed by one or more additional levels. However, we shall refer to it as ( $\nu_1 + \nu_2$ ).

It was found possible to assign the frequencies as indicated in Fig. XVII. Each  $R_{Q_K}$  and  $P_{Q_K}$  transition is split up into four maxima. In Table XXI are listed the frequencies of the transitions. In Table XXII the combinations  $\Delta_2 F''(K) = R_{Q_{K-1}} - P_{Q_{K+1}}$  are listed for each of the four maxima. The values of  $\Delta_2 F''(K)$  for  $2\nu_{N-H}$ , from Table XII, are included for comparison.

Table XXI

Frequencies of the Vibration-Rotation Transitions of ( $\nu_1 + \nu_2$ )

	K	A cm <sup>-1</sup>	B cm <sup>-1</sup>	C cm <sup>-1</sup>	D cm <sup>-1</sup>
R Q <sub>K</sub>	3	5957.70	5962.00	5970.40	5975.54
	2		5912.02	5915.34	5916.88
	1	5853.70	5862.46	5878.11	5881.11
	0	5810.78	5812.26	5829.85	5835.26
P Q <sub>K</sub>	1	5757.72	5761.63	5763.66	
	2	5692.39	5693.82	5711.48	5716.70
	3	5623.44	5631.74	5647.99	5650.74
	4	5574.14	5578.30	5581.85	5582.94

Table XXII

Combinations  $\Delta_2 F''(K) = \begin{matrix} R \\ Q_{K-1} \end{matrix} - \begin{matrix} P \\ Q_{K+1} \end{matrix}$  for ( $\nu_1 + \nu_2$ )

K	A	B	C	D	$2\nu_{N-H}$
1	118.39	118.44	118.37	118.56	118.55
2	230.26	230.72	230.12	230.37	230.37
3		333.72	333.49	333.94	333.69

The results of the comparison with the ground state of  $2 \nu_{\text{N-H}}$  are quite favorable as shown in Table XXII, indicating that we have made the correct assignments, and that this transition at  $5790 \text{ cm}^{-1}$  arises from the

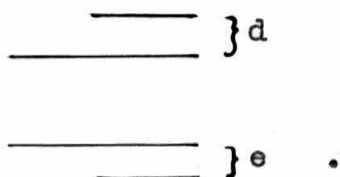
ground state of HNC0, having		6236.03 $\text{cm}^{-1}$
the rotational constants cal-	4	6230.92
culated in the section on		6222.52
		6218.22
$2 \nu_{\text{N-H}}$ . From these rota-		6035.45
tional constants and the	3	6034.14
data of Table XXI, we have		6030.70
constructed the energy		6026.53
level diagram for the upper	2	5911.26
state of $(\nu_1 + \nu_2)$ in Fig.		5908.38
XVIII. The energies given		5892.43
are the respective energies	1	5883.90
above the ground vibrational		5835.25
state with $K = 0$ .	0	5829.96
		5812.31
		5810.86
	0	5793.81
		5791.78
		5787.80
	K'	

Fig. XVIII

Energy above rotationless ground state for the upper level of the band at  $5790 \text{ cm}^{-1}$  (not to scale).

These quadruple levels could arise from Coriolis perturbations or from Fermi perturbations. The frequency shift due to a Coriolis perturbation is proportional to  $J(J + 1)$ . Since each  $R_{Q_K}$  and  $P_{Q_K}$  transition involves many different  $J$  values, a Coriolis perturbation would cause the resulting levels to be considerably spread out. The maxima of Fig. XVII are relatively sharp, so it is more likely that the perturbations in this band are Fermi perturbations, which do not increase with  $J$ .

Each  $R_{Q_K}$  and  $P_{Q_K}$  "group" of Fig. XVII gives a similar pattern - two strong bands within two weaker bands, as



The spacing is unsymmetrical, that is  $d \neq e$ . If the spacing were symmetrical, this pattern could be obtained if two levels interacted and the  $+$  and  $-K$  levels interacted differently.

It is shown in Appendix XI that three close-lying, interacting levels can give rise to the unsymmetrical pattern shown above. This is presented as a possible cause of the appearance of the band at  $5790 \text{ cm}^{-1}$ .

There are several combination levels having frequencies close to  $5800 \text{ cm}^{-1}$ . Four examples, all of the same symmetry,  $A'$ , are

$$\begin{aligned} \nu_1 + \nu_2 &= 5814 \text{ cm}^{-1} \\ \nu_2 + \nu_3 + 4\nu_5 &= 5820 \\ 2\nu_2 + 2\nu_6 &= 5816 \\ 2\nu_2 + \nu_3 &= 5856 \end{aligned}$$

Where these levels should fall exactly is not known as the anharmonic constants in the potential energy expression are unknown. Several other combinations can be made to give similar frequencies, but the fact that there are at least three levels near  $5800 \text{ cm}^{-1}$  is sufficient to offer a possible explanation of the structure of the band ( $\nu_1 + \nu_2$ ), as shown in Appendix XI.

#### H. Vibrational Frequencies of Isothiocyanic Acid

The spectrum of HNCS was mapped from 2-15 microns with the Beckman IR-2 spectrometer. This spectrum is shown in Fig. XIX. The spectrum of HNCS was also observed under high dispersion from 1-2.7 microns. The bands in this latter region are not shown here, with the exception of  $2\nu_1$  in Fig. XX. However, all of the observed frequencies attributed to HNCS are listed in Table XXIII. The frequencies  $\nu_4$ ,  $\nu_5$ , and  $\nu_6$  were not observed. Instead they were calculated from the observed bands assigned to  $2\nu_5$ ,  $\nu_5 + \nu_6$ ,  $2\nu_6$ ,  $\nu_1 + \nu_5$ ,  $\nu_1 + \nu_6$ ,  $2\nu_1 + \nu_5$ ,  $2\nu_1 + \nu_6$ ,  $\nu_2 + \nu_4$ ,  $\nu_1 + \nu_4$ , and  $2\nu_1 + \nu_4$ . These combinations are quite consistent with the observed frequencies of Table XXIII.

Fig. XIX. Absorption spectrum of  
a 50 cm path of HNC<sub>s</sub> from 2-15  
microns. The pressure was not  
known.

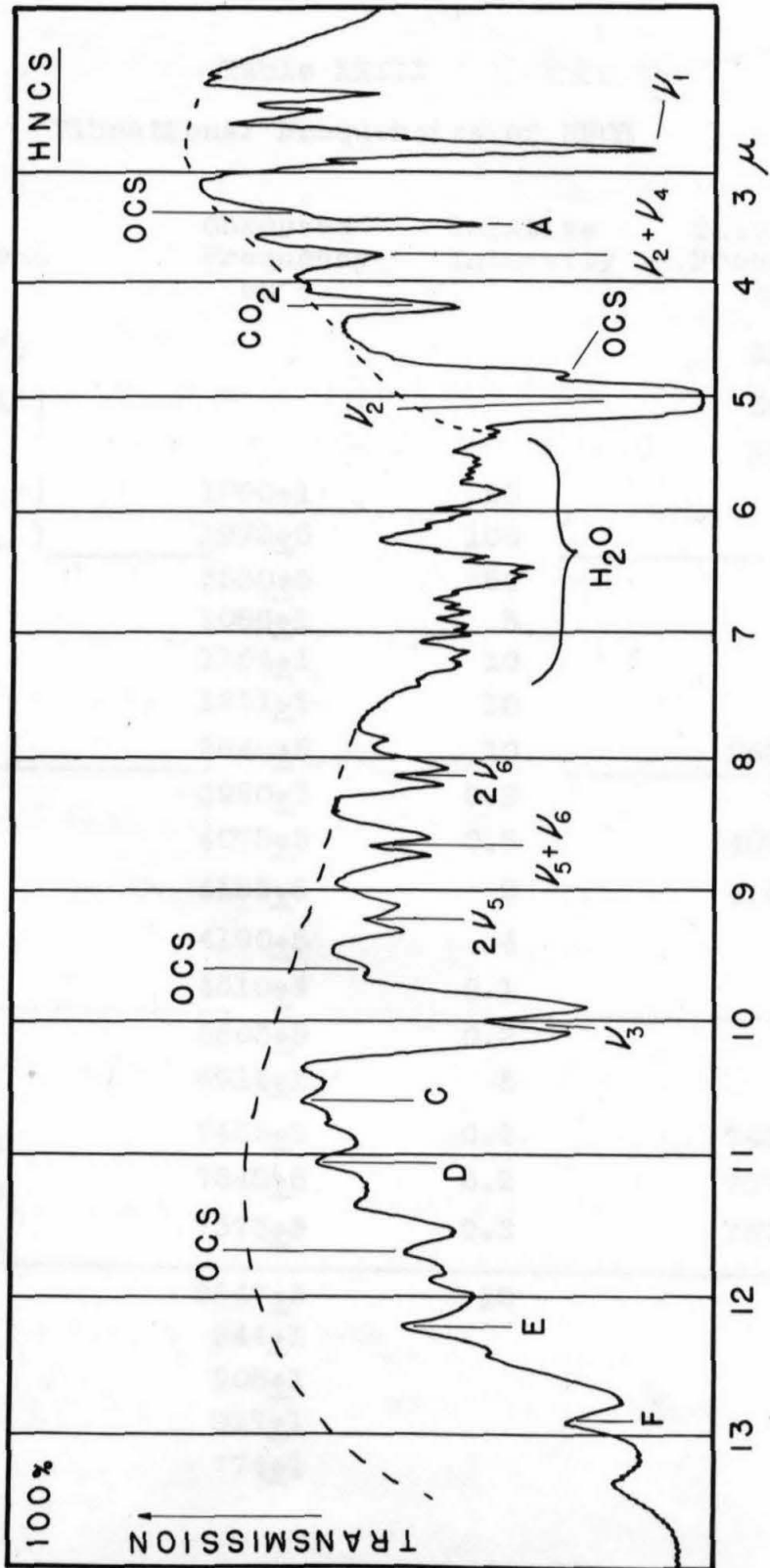


Table XXIII

Vibrational Frequencies of HNCS

Assignment	Observed Frequency cm <sup>-1</sup>	Relative Intensity	Calculated Frequency cm <sup>-1</sup>
$\nu_6(\text{NCS}, A'')$			616 cm <sup>-1</sup>
$\nu_5(\text{NCS}, A')$			543
$\nu_4(\text{HNCS})$			660
$\nu_3(\leftarrow \text{NCS} \rightarrow)$	1000 $\pm$ 1	25	
$\nu_2(\leftarrow \text{NCS} \leftarrow)$	1972 $\pm$ 5	100	
$\nu_1(\text{N-H})$	3530 $\pm$ 5	50	
$2\nu_5$	1086 $\pm$ 1	5	
$\nu_5 + \nu_6$	1154 $\pm$ 1	10	
$2\nu_6$	1231 $\pm$ 1	10	
$\nu_2 + \nu_4$	2640 $\pm$ 5	10	2632
$2\nu_2$	3950 $\pm$ 5	0.2	
$\nu_1 + \nu_5$	4075 $\pm$ 5	0.5	4073
$\nu_1 + \nu_6$	4155 $\pm$ 5	2	4146
$\nu_1 + \nu_4$	4190 $\pm$ 5	4	
$\nu_1 + \nu_3$	4510 $\pm$ 5	0.1	
$\nu_1 + \nu_2$	5503 $\pm$ 5	0.2	
$2\nu_1$	6914 $\pm$ 1	5	
$2\nu_1 + \nu_5$	7455 $\pm$ 5	0.1	7457
$2\nu_1 + \nu_6$	7545 $\pm$ 5	0.2	7530
$2\nu_1 + \nu_4$	7573 $\pm$ 5	0.2	7574
A	2847 $\pm$ 5	10	
C	944 $\pm$ 1		
D	905 $\pm$ 1		
E	817 $\pm$ 1		
F	774 $\pm$ 1		

In Fig. XX is shown the spectrum of  $2 \nu_1$  of HNCS. This band is similar to  $2 \nu_1$  of HNC0 (Fig. XIV) except that there are no sharp  $Q_{KQ}$  maxima in the parallel component of the band. The sharp minima, labelled 1, 2, 3, and 4 in Fig. XX, divide  $P_K$  and  $R_K$  branches. A  $\Sigma-\Sigma$  parallel band of a linear molecule shows P and R branches ( $\Delta J = \pm 1$ ) but no Q branch. Thus the parallel components of the band  $2 \nu_1$  have the appearance of parallel bands of linear molecules. Furthermore, all of the HNCS bands past eight microns consist of P and R branches with a minimum of absorption at the band center, similar to parallel bands of linear molecules. This suggests that HNCS is more nearly linear than HNC0. The rotational structure of the band  $2 \nu_1$  in Fig. XX is analyzed in the next section, and it is shown that HNCS is indeed more nearly linear than HNC0.

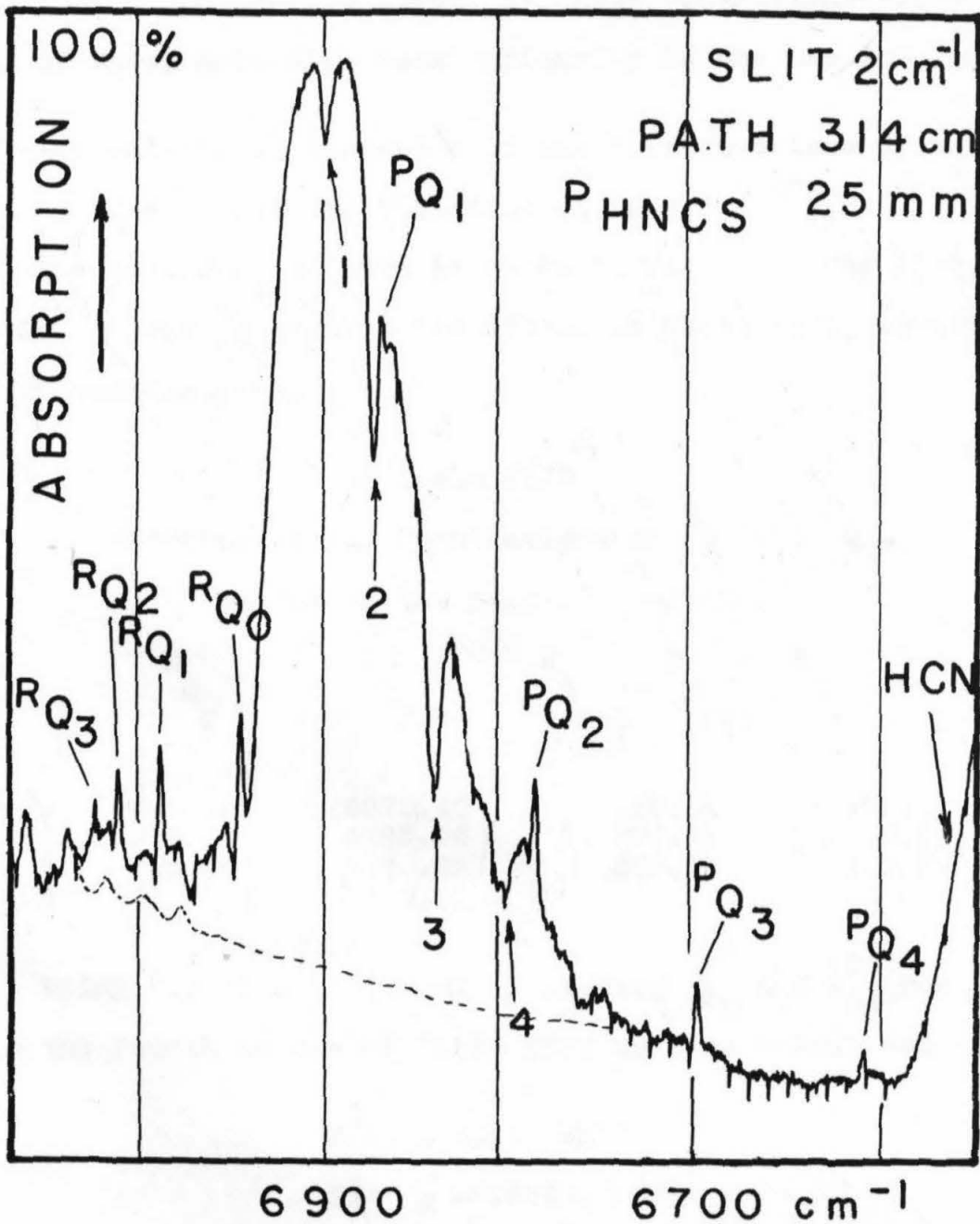
The bands A, B, C, D, and E in Fig. XIX have not been assigned. E and F are perhaps  $P_K$  and  $R_K$  branches of the hydrogen bending vibration at  $660 \text{ cm}^{-1}$ . A might be an H-S frequency of  $\text{H-S-C}\equiv\text{N}$ , while C and D may also arise from  $\text{H-S-C}\equiv\text{N}$  vibrations. However, the evidence is insufficient to establish the presence of HSCN.

It is remarkable that the N-H frequencies in HNCS and HNC0 are so nearly identical, as shown below

	HNCS	HNC0
$\nu_{\text{N-H}}$	3530 $\pm$ 5	3534 $\pm$ 1
$2 \nu_{\text{N-H}}$	6914 $\pm$ 1	6916 $\pm$ 1



Fig. XX. Absorption spectrum of  
the second harmonic of the N-H  
stretching vibration of HNCS.



This comparison in itself is quite convincing evidence that both of these molecules exist primarily in the iso form.

I. Rotational Structure of the First Overtone of the N-H Stretching Vibration of HNCS

The band  $2\nu_1$  of HNCS is shown in Fig. XX. The frequencies of the  $R_{Q_K}$  and  $P_{Q_K}$  maxima are listed in Table XXIV, together with useful combinations.

Table XXIV  
Frequencies and Combinations of  $R_{Q_K}$  and  $P_{Q_K}$   
Maxima of the Band  $2\nu_1$  of HNCS

K	$R_{Q_K}$	$P_{Q_K}$	$R_{Q_{K-1}}$	$P_{Q_{K+1}}$	$R_{Q_K} - P_{Q_K}$
0	6946.57				
1	6992.57	6870.40		160.61	122.17
2	7016.31	6785.96		294.29	230.35
3	7030.67	6698.28		405.70	332.39
4		6610.61			

Using Equation (12), but neglecting  $\delta_K''$  and  $X_{0j}^0$  for  $j > 3$ , from the fourth column of Table XXIV we have calculated that

$$\begin{aligned} X_{01}^0 &= 43.13 \text{ cm}^{-1} \\ X_{02}^0 &= -0.832 \\ X_{03}^0 &= 2.18 \times 10^{-2} \end{aligned}$$

Similarly, using Equation (14), we calculate that

$$\begin{aligned} X_{01}^{(2)} &= 32.22 \text{ cm}^{-1} \\ X_{02}^{(2)} &= -0.481 \\ X_{03}^{(2)} &= 1.52 \times 10^{-2} \end{aligned}$$

The superscript (2) signifies that the second level of the N-H stretching vibration is excited, all other levels being unexcited.

If we neglect  $X_{O_3}^0$  and  $X_{O_3}^{(2)}$ , we calculate that  $X_{O_1}^0 = 42.39 \text{ cm}^{-1}$  and  $X_{O_1}^{(2)} = 31.71 \text{ cm}^{-1}$ . From these results it appears that if we had observed more combinations of  $R_{Q_{K-1}} - P_{Q_{K+1}}$  and  $R_{Q_K} - P_{Q_K}$  we would be able to include more  $X_{O_j}^{(v)}$  terms and the calculated values of  $X_{O_1}^0$  and  $X_{O_1}^{(2)}$  would be slightly larger. However, we have neglected  $\delta_K''$  and  $\delta_K'$  of Equations (12) and (14). For HNC0 we calculated that  $\delta_K'' < -0.10 \text{ cm}^{-1}$ . Since the centrifugal stretching terms of HNCS are about four times those of HNC0, we should perhaps subtract  $\sim 0.40 \text{ cm}^{-1}$  from our calculated value of  $X_{O_1}^0$ . The neglect of  $X_{O_j}^0$  for  $j > 3$  and the neglect of  $\delta_K''$  tend to compensate each other. Therefore, we shall report

$$\begin{aligned} X_{O_1}^0 &= 43.1 \pm 0.4 \text{ cm}^{-1} \\ X_{O_1}^{(2)} &= 32.2 \pm 0.3 \text{ cm}^{-1} \end{aligned}$$

From Table XXIV and Equations (7)  $\nu_0$  is calculated to be  $6914 \pm 1 \text{ cm}^{-1}$ .

#### J. Molecular Structure of HNCS

The parameters reported by Beard and Dailey (39), from the microwave spectrum of HNCS, are

$$\begin{aligned} r_{C-S} &= 1.57 \pm 0.01 \text{ \AA} \\ r_{N-C} &= 1.21 \pm 0.01 \text{ \AA} \\ r_{N-H} &= 1.2 \pm 0.1 \text{ \AA} \\ \angle \text{HNC} &= 112^\circ \pm 10^\circ \end{aligned}$$

The N-H distance and HNC bond angle are anomalous, but the C-S and N-C distances are reasonable and probably much more reliable as the large moments of inertia are determined principally by the N-C and C-S distances.

In the previous section we have found that for HNCS

$$X_{01}^0 = A_0 - \frac{1}{2}(B_0 + C_0) = 43.1 \pm 0.4 \text{ cm}^{-1} .$$

From the N-C and C-S distances of Beard and Dailey,  $B_0$  is calculated to be  $0.20 \pm 0.02 \text{ cm}^{-1}$  regardless of the position of the hydrogen atom.  $C_0$  is not very different from  $B_0$ , so  $\frac{1}{2}(B_0 + C_0) = 0.2 \text{ cm}^{-1}$ . Therefore,  $A_0 = 43.3 \pm 0.4 \text{ cm}^{-1}$ .

From this,  $(I_A)_0 = (0.646 \pm .005) \times 10^{-40} \text{ gm cm}^2$ .

$(I_A)_0$  is the "effective" moment of inertia in the ground vibrational state. Strictly speaking

$$(I_A)_0 = \frac{1}{(1/I_A)_0} ,$$

$(1/I_A)_0 =$  the time average of  $1/I_A$  in the ground vibration state.

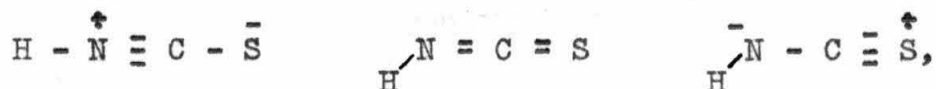
From the N-H stretching frequency with the use of Badger's rule (23) we have calculated that the N-H distance is  $0.99 \text{ \AA}$ , as in HNC $\overset{\circ}{\text{O}}$ . Using this N-H distance and the N-C and C-S distances of Beard and Dailey we have calculated that the HNC angle is  $138^\circ 40'$ , in order to agree with the observed value of  $A_0$ . It was found that an uncertainty of  $0.4 \text{ cm}^{-1}$  in  $A_0$  leads to an uncertainty of about  $12'$  in the HNC angle. Also an uncertainty of

0.01 Å in  $r_{\text{N-H}}$  leads to an uncertainty of 41' in the HNC angle. Small changes in the N-C and C-S distances have little effect on  $I_A$ .

From the above results, for  $r_1 = 0.99 \pm .01$  Å, the HNC angle =  $138^\circ 40' \pm 1^\circ$ .

If we had assumed an N-H distance of 1.2 Å, as reported by Beard and Dailey, an even larger HNC angle would be required to agree with the observed rotational constant.

The angle of  $138^\circ 40'$  is about  $10^\circ$  larger than the HNC angle of HNCO. This indicates that, of the three resonance structures



the third structure is less important than the analogous structure of HNCO. This is in agreement with general chemical experience which suggests that structures with a carbon-sulfur triple bond are less important than others (48).

The larger HNC angle in HNCS than in HNCO is in agreement with the lower frequency of the hydrogen bending vibration -  $660 \text{ cm}^{-1}$  for HNCS and  $780 \text{ cm}^{-1}$  for HNCO.

**APPENDICES**

Appendix I

Derivation of a formula for the shift in vibrational frequency of a polar bond, due to electrostatic interaction of a solute with a solvent of dielectric constant D.

Kirkwood (3) has derived a relation for the electrostatic interaction of zwitterions with a solvent medium, assuming that the zwitterions have spherical boundaries. In the special case of the interaction of zwitterions with a medium of zero ionic strength Kirkwood found that

$$W_0 = \frac{1}{2} \sum_{n=1}^{\infty} \left\{ \frac{(n+1)Q_n}{b^{2n+1}} \right\} \left\{ \frac{(1-D)}{(n+1)D+n} \right\}.$$

$W_0$  is the electrostatic interaction of the solvent with the zwitterions.  $Q_1 = \mu^2$ ,  $\mu$  = dipole moment of solute molecule. Succeeding  $Q_n$ 's involve higher multipole moments,

$b$  = radius of spherical molecule,

$D$  = dielectric constant of solvent.

Kirkwood has pointed out that a zwitterion is a molecule with a large dipole moment, and that his relation should be satisfactory for a solute molecule having a much larger dipole moment than the solvent. He suggested that it should thus hold for the electrostatic interaction of a polar molecule with non-polar solvents.

For methanol the main electrostatic interaction of the solvent with the alcohol is with the polar O-H bond. The higher multipole

moments will be negligible compared to the dipole moment. Therefore we can approximate the change in vibrational energy of the O-H bond, due to the electrostatic interaction with the solvent, by the relation

$$\Delta V = \frac{\mu^2}{b^3} \left( \frac{1 - D}{2D + 1} \right)$$

or

$$V = V_0 + \frac{\mu^2}{b^3} \left( \frac{1 - D}{2D + 1} \right) \quad \text{I-1}$$

$V_0$  = vibrational energy of O-H bond in the vapor state.

If we treat the O-H bond as a harmonic oscillator,

$$V = 2\pi^2 m \nu^2 X^2 \quad \text{I-2}$$

$\nu$  = vibrational frequency

$X$  = displacement coordinate

Differentiating (I-2) twice with respect to  $X$ ,

$$\frac{d^2 V}{dX^2} = 4\pi^2 \nu^2 = 4\pi^2 m (\nu_0 + \Delta \nu)^2 \quad \text{I-3}$$

Differentiating I-1 twice with respect to  $X$ ,

$$\frac{d^2 V}{dX^2} = \frac{d^2 V_0}{dX^2} + C \frac{1-D}{2D+1} \quad \text{I-4}$$

$$C = \frac{2}{b^3} \left[ \mu \frac{d^2 \mu}{dX^2} + \left( \frac{d\mu}{dX} \right)^2 \right]$$

Equating I-3 and I-4

$$4\pi^2 m \nu^2 = \frac{d^2 V_0}{dX^2} + C \frac{1-D}{2D+1}$$

$$\text{But } \frac{d^2 v_0}{dx^2} = 4\pi^2 m v_0^2 .$$

Thus, neglecting  $(\Delta v)^2$ , which is  $\ll v_0 \Delta v$ ,

$$4\pi^2 m v_0 \Delta v = C \frac{1 - D}{2D + 1}$$

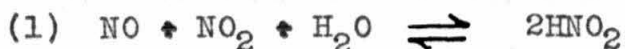
$$\Delta v = A \frac{1 - D}{2D + 1}$$

A is a constant in the approximation that  $\frac{d\mu}{dx}$  and  $\frac{d^2\mu}{dx^2}$  are constants.

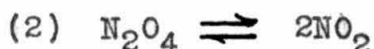
Appendix II

Equilibrium concentrations of various components in a mixture of NO, NO<sub>2</sub>, and H<sub>2</sub>O.

In a gaseous equilibrium mixture of NO, NO<sub>2</sub> and H<sub>2</sub>O there are several equilibria to consider.

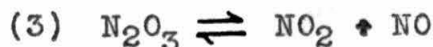


$$K_1 = 1.65 \text{ atm}^{-1}$$



$$K_2 = 0.1426 - 0.7588 C_{\text{N}_2\text{O}_4}^0 \text{ atm.}$$

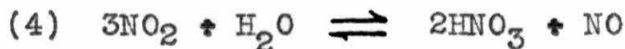
$C_{\text{N}_2\text{O}_4}^0$  = concentration of N<sub>2</sub>O<sub>4</sub> in moles/liter if all NO<sub>2</sub> were in that form.



$$K_3 = 2.105 - 45.63 C_{\text{N}_2\text{O}_3}^0 \text{ atm.}$$

$$C_{\text{N}_2\text{O}_3}^0 = \frac{1}{2} \frac{(P_{\text{NO}_2} + P_{\text{NO}} + 2P_{\text{N}_2\text{O}_3})}{RT}$$

$P_{\text{NO}}$ ,  $P_{\text{NO}_2}$ , and  $P_{\text{N}_2\text{O}_3}$  are the partial pressures at equilibrium



$$K_4 = 1.05 \times 10^{-2} \text{ atm}^{-1}.$$

$K_1$  is reported by Wayne and Yost (13).  $K_2$  and  $K_3$  are from the work of Verhoek and Danials (12).  $K_4$  is from the work of Forsythe and Glaugue (14).

In the mixture there are seven constituents present in appreciable concentration -  $\text{NO}$ ,  $\text{NO}_2$ ,  $\text{H}_2\text{O}$ ,  $\text{N}_2\text{O}_4$ ,  $\text{N}_2\text{O}_3$ ,  $\text{HNO}_2$ , and  $\text{HNO}_3$ . If we add a known amount of a mixture of  $\text{NO}_2$  and  $\text{N}_2\text{O}_4$ , and a known amount of  $\text{NO}$ , and saturate with  $\text{H}_2\text{O}$  so that we know the equilibrium pressure of  $\text{H}_2\text{O}$ , we have three data to go with the four equilibrium relations given above from which we can solve for the partial pressures of all the components.

If we add 600 mm of  $\text{NO}$  to 40 mm of a mixture of ( $\text{NO}_2 + \text{N}_2\text{O}_4$ ) at  $25^\circ\text{C}$ , and then add  $\text{H}_2\text{O}$  vapor to saturation we calculate that:

$P_{\text{HNO}_2}$	=	21.3 mm
$P_{\text{N}_2\text{O}_4}$	=	2.05 mm
$P_{\text{N}_2\text{O}_3}$	=	8.4 mm
$P_{\text{NO}_2}$	=	15 mm
$P_{\text{NO}}$	=	570 mm
$P_{\text{HNO}_3}$	=	.04 mm

Appendix III

An attempt to justify the use of the approximate symmetric top Equation, (1), for nitrous acid.

The approximate relation we have used is

$$T = G(v_1, v_2, \dots) + \frac{1}{2}(B_V + C_V)J(J + 1) + \left[ A_V - \frac{1}{2}(B_V + C_V) \right] K^2$$

A more correct expression derived by Ray (27) is

$$T = G(v_1, v_2, \dots) + \frac{1}{2}(A_V + C_V)J(J + 1) + \frac{1}{2}(A_V - C_V)E_{\lambda}$$

$E_{\lambda}$  is a function of an asymmetry parameter,  $K$

$$K = \frac{2B - \frac{1}{2}(A + C)}{A - C}$$

$\lambda$  takes integral values, including zero, from  $-J$  to  $+J$ .

King, Hainier, and Cross (21) have given a very convenient tabulation of values of  $E_{\lambda}$  for  $J = 0$  up to  $J = 10$  and for

$K = 0, -0.1, -0.2, \dots, -1.0$ . It is interesting to remark that

$$E_{\lambda}(K) = E_{-\lambda}(-K).$$

We wish to apply the more correct energy levels to the band  $2\nu_1^c$  of nitrous acid. The "perpendicular" type structure of this band arises from the component of the changing electric moment parallel to the intermediate axis of inertia. This is called a type B band of an asymmetric top molecule. Herzberg (20) gives the selection rules for this type of transition, which,

together with his figure XVII (28) correlating the energy levels of the asymmetric top with those of the symmetric top, indicate that the transitions of interest, for which  $\Delta K = \pm 1$  and  $\Delta J = 0$ , correspond to  $\Delta \tau = \pm 2$ , and  $\Delta J = 0$ .

If we know the values of  $E_{\tau}$  for the different rotational levels,  $J_{\tau}$ , we can solve for  $(A_0 - C_0)$  from the usual combination,

$$R_{Q_{K-1}} - P_{Q_{K+1}} = \frac{1}{2} (A_0 - C_0) \left( E_{\tau_{K+1}} - E_{\tau_{K-1}} \right)$$

$E_{\tau_K}$  is the value of  $E_{\tau}$  corresponding to the quantum number  $K$  of the nearby symmetric top.

For the most suitable model of nitrous acid, the first one in Table VI,

$$K = \frac{2 \left[ B - \frac{1}{2}(A + C) \right]}{A - C} = -0.95$$

$$A - C = 2.44 \text{ cm}^{-1}$$

To avoid interpolation and to allow plenty of leeway we shall use values of  $E_{\tau}$  for  $K = -0.90$ .

From the intensity formulae given by Herzberg (29) the  $J$  value of maximum intensity for nitrous acid is about 18.

In the tables of King, Hainier, and Cross (21) we found the values of  $(E_{\tau_{K+1}} - E_{\tau_{K-1}})$  for all different  $J$  values up to  $J = 10$ . Then we were forced to extrapolate to  $J = 18$  to determine  $(E_{\tau_{K+1}} - E_{\tau_{K-1}})$  for the line of maximum intensity. The values arrived at together with the resulting calculated

values of  $(A_0 - C_0)$  are given in Table XXV.

Table XXV

Calculation of  $(A_0 - C_0)$  from Asymmetric  
Top Energy Levels for Nitrous Acid, Assuming  $K = -0.90$

$K$	$2(R_{Q_{K-1}} - P_{Q_{K+1}})$	$E_{\tau_{K+1}} - E_{\tau_{K-1}}$	$A_0 - C_0$
5	93.84 $\text{cm}^{-1}$	38.66	2.42 $\text{cm}^{-1}$
6	115.18	46.65	2.46
7	134.26	54.49	2.46

These results compare favorably with the value  $(A_0 - C_0) = 2.44 \text{ cm}^{-1}$  found using the approximate symmetric top equation.

The  $R_{Q_K}$  and  $P_{Q_K}$  maxima are made up of all  $J$  values. The observed maxima of the envelopes of these bands will actually be at a  $J$  value somewhat less than 18, due to the small splitting of lines of different  $J$  value, which increases as  $J$  increases. Our approximation is even better for smaller  $J$  values.

Furthermore, the actual asymmetry is only half as great as that assumed in the above calculations.

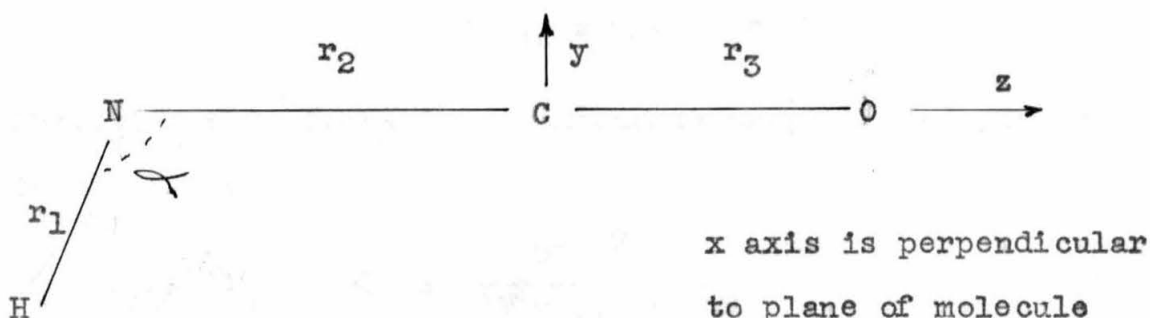
Though the extrapolations involved above are rather rough, they do serve to justify the use of the approximate symmetric top energy levels.

Appendix IV

Classical Treatment of Centrifugal Distortion for HNC O

In this section we shall follow a method analogous to that used by P. C. Cross (49) for H<sub>2</sub>S.

We shall employ the model



The center of gravity is close to the carbon atom and the least axis of inertia is almost parallel to the NCO axis. We shall treat the molecule in the approximation that the least axis of inertia is along the NCO axis.

For the rotating molecule the centrifugal force is

$$F_c = \sum_{s=x,y,z} \sum_{i=1}^4 m_i s_i \omega_s^2$$

$$\omega_z^2 = \frac{K^2 h^2}{4\pi^2 I_{zz}^2}, \quad \omega_y^2 + \omega_x^2 = \frac{\{J(J+1) - K^2\} h^2}{4\pi^2 I_{yy}^2}$$

$$I_{zz} \ll I_{yy}, \text{ so } \omega_z^2 \gg \omega_y^2 + \omega_x^2$$

Therefore, we shall neglect  $\omega_y^2$  and  $\omega_x^2$ . In this approximation the centrifugal forces in the x and z direction are negligible.

$\omega_z$  gives rise to centrifugal force in the y direction. If we let  $\varphi = \mathcal{L} - \pi/2$

$$f_y = m_H r_1 \cos \varphi \omega_z^2$$

$$= \frac{K^2 h^2}{4\pi^2 m_H r_1^3 \cos^3 \varphi}$$

$$\text{as } I_{zz} = m_H r_1^2 \cos^2 \varphi \quad \text{IV-1}$$

Resolving this force into components parallel and perpendicular to the N-H bond

$$f_{//} = f_y \cos \varphi = \frac{h^2 K^2}{4\pi^2 m_H r_1^3 \cos^2 \varphi} \quad \text{IV-2}$$

$$f_{\perp} = f_y \sin \varphi = \frac{h^2 K^2 \tan \varphi}{4\pi^2 m_H r_1^3 \cos^2 \varphi}$$

These forces must be in equilibrium with the restoring forces of the distorted molecule. If we assume Hooke's Law forces

$$f_{//} = k_1 \Delta r_1, \quad f_{\perp} = k_2 r_1 \Delta \varphi \quad \text{IV-3}$$

$k_1$  = N-H bond stretching force constant,  $k_2$  = HNC bond bending force constant units of  $k_1$  and  $k_2$  are dynes/cm.

From Equations (IV-2) and (IV-3)

$$\Delta r_1 = \frac{h^2 K^2}{4\pi^2 m_H r_1^3 \cos^2 \varphi k_1} \quad \text{IV-4}$$

$$\Delta \varphi = \frac{-h^2 K^2 \tan \varphi}{4\pi^2 m_H r_1^4 \cos^2 \varphi k_2}$$

The kinetic energy, without distortion, is

$$E_K = \frac{1}{2} I_{zz} \omega_z^2 = \frac{K^2 h^2}{8\pi^2 I_{zz}}, \text{ again neglecting } \omega_x^2 + \omega_y^2.$$

$$\Delta E_K = \frac{K^2 h^2}{8\pi^2} \left\{ -\frac{1}{I_{zz}^2} \right\} \left\{ \frac{I_{zz}}{r_1} \Delta r_1 + \frac{I_{zz}}{r_1} \Delta \phi \right\} \quad \text{IV-5}$$

From equations (IV-1), (IV-3), (IV-4), and (IV-5)

$$\Delta E_K = -\frac{K^4 h^4}{16 \pi^4 m_H^2 r_1^6 \cos^4 \phi} \left\{ \frac{1}{k_1} + \frac{\tan^2 \phi}{k_2} \right\} \text{ ergs}$$

The change in potential energy is

$$\Delta E_P = \frac{1}{2} k_1 (\Delta r_1)^2 + \frac{1}{2} k_2 r_1^2 (\Delta \phi)^2 \quad \text{IV-6}$$

From Equation (IV-4) and (IV-6)

$$\Delta E_P = \frac{K^4 h^4}{32 \pi^4 m_H^2 r_1^6 \cos^4 \phi} \left\{ \frac{1}{k_1} + \frac{\tan^2 \phi}{k_2} \right\}$$

As before we shall assume  $r_1 = 0.99 \text{ \AA}$

$$\frac{h^4}{32 \pi^4 m_H^2 r_1^6} = 2.385 \times 10^{-13} \text{ (dynes)}^2$$

Then the total change in energy due to centrifugal distortion is

$$\begin{aligned} (\Delta E)_c &= \Delta E_K + \Delta E_P = -2.385 \times 10^{-13} \frac{K^4}{\cos^4 \phi} \frac{1}{k_1} + \frac{\tan^2 \phi}{k_2} \text{ ergs} \\ &= -1.2 \times 10^3 \frac{K^4}{\cos^4 \phi} \left\{ \frac{1}{k_1} + \frac{\tan^2 \phi}{k_2} \right\} \text{ cm}^{-1} \end{aligned}$$

$\phi$  is near  $40^\circ$  so  $\tan^2 \phi$  is  $> 0.5$ ,  $k_1$  is of the order of

$7.5 \times 10^5$  dynes/cm,  $k_2$  is of the order of  $0.4 \times 10^5$  dynes/cm.

Therefore,  $\frac{1}{k_1} \ll \frac{\tan^2 \varphi}{k_2}$

We shall approximate  $(\Delta E)_c$  by

$$-(\Delta E)_c = \frac{1.2 \times 10^3 K^4}{k_2} \left\{ \frac{\tan^2 \varphi}{\cos^4 \varphi} \right\} \quad \text{IV-7}$$

$(\Delta E)_c$  is the change in energy due to centrifugal distortion.

$\varphi$  is the equilibrium angle, and decreases as  $K$  increases,

$\varphi = \varphi_0 + \Delta \varphi$  where  $\varphi_0$  is the angle for zero rotation.

We can expand  $\left(\frac{\tan^2 \varphi}{\cos^4 \varphi}\right)$  in a Taylor's Series about  $\Delta \varphi = 0$ ,

$\varphi_0 = 40^\circ$ . This expansion gives

$$\begin{aligned} \frac{\tan^2 \varphi}{\cos^4 \varphi} &= 1.912 + 14.11 \Delta \varphi + 56.9 (\Delta \varphi)^2 + 176 (\Delta \varphi)^3 \\ &+ 450 (\Delta \varphi)^4 + \dots \end{aligned} \quad \text{IV-8}$$

As seen in Equation (IV-4),  $\Delta \varphi$  itself is a function of  $\varphi$ .

However, it is not as critical as  $\tan^2 \varphi / \cos^4 \varphi$  so we shall

approximate  $\Delta \varphi$  using  $\varphi_0$  for  $\varphi$ .

From Equation (IV-4),  $\Delta \varphi = -97.5 \times \frac{K^2}{k_2}$  radians

If we assume  $k_2 = 4\pi^2 \nu^2 m_H$ ,  $\nu = 800 \times 3 \times 10^{10} \text{ sec}^{-1}$

Then  $k_2 = 0.378 \times 10^5$  dynes/cm and  $\Delta \varphi = -2.58 \times 10^{-3} K^2$

IV-9

and from Equation (IV-8)

$$(\Delta E)_c = -3.17 \times 10^{-2} K^4 (\tan^2 \varphi / \cos^4 \varphi)$$

Then using Equations (IV-8) and (IV-9)

$$(\Delta E)_c = -.061K^4 + 1.15 \times 10^{-3}K^6 - 1.2 \times 10^{-5}K^8 + 9.6 \times 10^{-8}K^{10} \text{ - - - - -} \quad \text{IV-10}$$

It was found experimentally, in Section III-B, that

$$(\Delta E)_c = -.224K^4 + 9.05 \times 10^{-3} K^6 - 2.6 \times 10^{-4} K^8 + 3 \times 10^{-6} K^{10} \text{ - - - - -} \quad \text{IV-11}$$

In comparing the approximate theoretical result with the experimental result, Equations (IV-10) and IV-11), we notice that the theoretical coefficients are considerably lower than the experimental. One reason for this discrepancy is that we have assumed that the least axis of inertia is along the NCO axis and thus have neglected the centrifugal bending of the linear NCO group. It is shown in Appendix X, in a more accurate treatment, that if this is taken into account the coefficient of  $K^4$  in  $(\Delta E)_c$  is about -0.10.

Even with the more accurate treatment for the  $K^4$  coefficient, in Appendix X, we are still off by a factor of 2. There are several reasons for this discrepancy. First, we are not really justified in calculating the HNC bending force constant by treating the HNC bending vibration as an independent harmonic oscillation. The true force constant may be much lower; a normal coordinate treatment would probably be helpful in assigning the true force constant. Also we have neglected the stretching of the N-H bond, however, this has been shown to have a second order effect. Perhaps the neglect of the interaction of rotation with vibration is the largest source of error.

In spite of the lack of agreement of the coefficients in Equations (IV-10) and (IV-11), this treatment has served to show that the centrifugal stretching terms for HNC0 must be represented by a power series in  $K^2$ , having appreciable coefficients for the higher powers of K, which become more and more important for higher K levels.

Appendix V

Calculation of the J value having the observed maximum intensity in  $Q_{0K}$ ,  $P_{0K}$ , and  $R_{0K}$  maxima.

The formulae for the line intensities in the bands of a symmetric top molecule are quoted by Herzberg (29). They were derived on the basis of the old quantum theory by Honl and London and later on the basis of wave mechanics by Dennison, Reiche and Rademaker, and others (50). These formulae are:

$$I = CA_{KJ} \nu \xi_{KJ} e^{-F(K,J) \frac{hc}{KT}} \quad V-1$$

$$\begin{aligned} \xi_{KJ} &= \text{statistical weight} = 2(2J+1) \text{ for } K \neq 0 \\ &= 2J+1 \quad \text{for } K = 0 \end{aligned}$$

$$F(K,J) = B_0 J(J+1) + (A_0 - B_0) K^2$$

$$\text{For } Q_{0K}: A_{KJ} = \frac{K^2}{J(J+1)}$$

$$\text{For } R_{0K} \text{ and } P_{0K+1}: A_{KJ} = 1 - \frac{K(K+1)}{J(J+1)} \quad V-2$$

C is a constant independent of J and K but dependent on the vibrational transition.  $\nu$ , the frequency, can be considered as a constant in Equation (V-1) within a given  $\Delta K$  transition having  $\Delta J = 0$ . J and K are the J and K values of the lower vibrational state. I is the intensity of an individual line, corresponding to one value of J. Actually the  $Q_{0K}$ ,  $R_{0K}$ , and  $P_{0K}$  maxima are made up of many unresolved but slightly separated lines. For an infinitely narrow slit, if the grating will not

resolve the J structure of the Q maxima, the envelope of the observed band would have a maximum at the maximum value of  $I / d\nu$ , where  $I$  is given by Equation (V-1) and  $d\nu$  is the average spacing of the J line at a given J.

We shall now define some new quantities:

$\nu_{OK}$  = frequency of a hypothetical  $Q_K$  transition for which  $J = 0$

$\nu_K$  = frequency of the  $Q_K$  transition of lowest J value having any intensity.

$\nu_m$  = frequency of the  $Q_K$  transition having the maximum observed intensity.

$$f_J = \nu_{JK} - \nu_{OK}$$

$$f_K = \nu_K - \nu_{OK}$$

$$f_m = \nu_m - \nu_{OK}$$

V-3

From Equations (7), if we neglect all members of the sum having  $i > 1$ , we see that for different J values within the same  $Q_K$  transition

$$f_J = aJ(J+1)$$

V-4

a is a proportionality constant.

Therefore the average spacing between lines at a given J value is

$$(df_J)_J = a(2J+1).$$

Thus, for an infinitely narrow slit, the intensity of the envelope of absorption at a given J is proportional to  $\frac{I_J}{2J+1}$ .

The  $(2J + 1)$  in the denominator just cancels out the statistical factor,  $g_{JK}$ .

We can now write, from Equations (V-1) and (V-2),

$$I_{Q_K} = \frac{G_1 e^{-\sigma J(J+1)}}{J(J+1)}$$

$$I_{Q_K}^R = G_2 \left( 1 - \frac{K(K+1)}{J(J+1)} \right) e^{-\sigma J(J+1)}$$

V-5

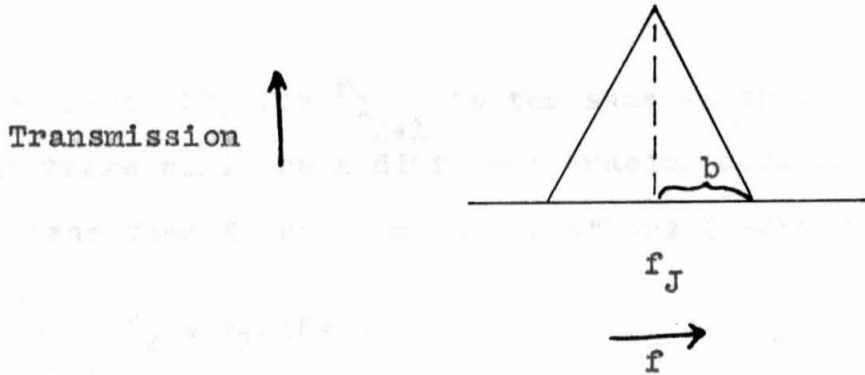
$$I_{Q_{K+1}}^P = G_3 \left( 1 - \frac{K(K+1)}{J(J+1)} \right) e^{-\sigma J(J+1)}$$

$$\sigma = \frac{B_0 hc}{kT}$$

$G_1$ ,  $G_2$ , and  $G_3$  are functions of  $K$  and  $\nu$ , but not of  $J$ .

Due to the finite slit width the observed maxima will not be given by Equations (V-5). To arrive at the observed relative intensity at a given  $f_J$ , the  $I_{Q_K}$  given above must be multiplied by a factor which allows for the slit transmitting certain fractions of nearby wavelengths. The resulting function must then be integrated over the range included by the slit. Differentiation of the result with respect to  $f_J$  and equation to zero will give an equation to solve for the  $f_J$  at which the maximum appears in the observed spectrum.

For a fairly wide slit we can approximate the slit function by the symmetrical diagram shown below.



The slit function will then be

$$s_+ = 1 - \frac{f - f_J}{b} \quad f \geq f_J$$

$$s_- = 1 + \frac{f - f_J}{b} \quad f \leq f_J$$

We can now set up the relations for the observed intensities, expressing  $J(J+1)$  as  $f_J/a$

$$\left\{ I_{Q_K}^{(obs)} \right\}_J = \int_{f_J}^{f_J+b} G_1 \frac{a_1 e^{-\sigma f/a_1}}{f} \left( 1 - \frac{f-f_J}{b} \right) df$$

$$+ \int_{f_K}^{f_J} G_1 \frac{a_1 e^{-\sigma f/a_1}}{f} \left( 1 + \frac{f-f_J}{b} \right) df$$

V-6

$$\left\{ I_{R_K}^{(obs)} \right\}_J = \int_{f_J}^{f_J+b} G_2 \left\{ 1 - \frac{a_2 K(K+1)}{f} \right\} e^{-\sigma f/a_2} \left( 1 - \frac{f-f_J}{b} \right) df$$

$$+ \int_{f_K}^{f_J} G_2 \left\{ 1 - \frac{a_2 K(K+1)}{f} \right\} e^{-\sigma f/a_2} \left( 1 + \frac{f-f_J}{b} \right) df$$

The observed intensity for  ${}^P Q_{K+1}$  is the same as that for  ${}^R Q_K$  except that there will be a different spacing constant,  $a_3$ . J is never less than K, so from the equations (V-3) and (V-4),

$$\text{for } {}^Q Q_K, f_K = a_1 K(K+1)$$

$${}^R Q_K, f_K = a_2 (K+1)(K+2)$$

V-7

$${}^P Q_{K+1}, f_K = a_3 (K+1)(K+2)$$

This is not correct for  $f_K < f_J - b$ . However, we shall see that b is about  $2 \text{ cm}^{-1}$  and  $f_K$  is much larger than  $(f_m - b)$ , and we are attempting to determine  $f_m$  only.

Using the above values for  $f_K$  and performing the integrations in Equations (V-6) we obtain the observed intensities as functions of  $f_J$ . These observed intensities are then differentiated with respect to  $f_J$ . The resulting expressions are equated to zero to solve for  $f_m$ . From this procedure we arrive at the following results:

${}^Q Q_K$ :

$$\ln \frac{f_K(f_m + b)}{(f_m)^2} + \sum_{n=1}^{\infty} \left(-\frac{\sigma}{a_1}\right)^n \frac{1}{n \cdot n!} \left\{ (f_m + b)^n - 2f_m^n + f_K^n \right\}$$

V-8

$$= 0$$

$$\begin{aligned}
 R_{Q_K}: & e^{-\frac{\sigma}{a_2}(f_m+b)} - 2e^{-\frac{\sigma}{a_2}f_m} + e^{-\frac{\sigma}{a_2}f_K} \\
 & + \sigma K(K+1) \{ \ln(f_m+b) + \ln f_K - 2 \ln f_m \} \\
 & + \sigma K(K+1) \sum_{n=1}^{\infty} \left(-\frac{\sigma}{a_2}\right)^n \left(\frac{1}{n \cdot n!}\right) \{ (f_m+b)^n - 2f_m^n + f_K^n \} = 0
 \end{aligned}$$

V-8

For  $P_{Q_{K+1}}$  the results are the same except that  $a_2$  is replaced by  $a_3$ . The  $f_K$  are given by Equation (V-7).

Application to HNC0:

From the geometry of the spectrograph, the effective  $b$  used for the observed spectra was about  $1.5 \text{ cm}^{-1}$ . However, it will be somewhat greater than this due to imperfections in the grating. The appearance of the rotational lines of water vapor suggest that  $b$  is about  $2 \text{ cm}^{-1}$ .

$$\text{For HNC0, } \sigma = .367hc/kT = .00176$$

In Appendix VI it is shown that  $(X_{01}^{(v)} - X_{01}^0)$  is about  $-.002 \text{ cm}^{-1}$ . This is the major contribution to the spacing constants,  $a_1$ ,  $a_2$ , and  $a_3$ , so we have calculated  $f_m$  from Equations (V-8) for values of  $a$  in the neighborhood of  $-.002 \text{ cm}^{-1}$ . These results are listed in Table XXVI.

Table XXVI  
 Values of  $f_m/a$  for Different a

a	$R_{Q_K}$ and $P_{Q_{K+1}}$		$Q_{Q_K}$		
	K = 3	K = 4	K = 3	K = 4	K = 5
-.002	390	410	65	88	
-.0025	366	386			
-.003	343	360	63	85.2	107.3
-.004	305	325			

We shall now investigate the difference in spacing, a, for  $Q_{Q_K}$ ,  $P_{Q_K}$ , and  $R_{Q_K}$  transitions. We shall neglect  $(X_{20}^{(v)} - X_{20}^0)$  and higher terms. Then from Equations (7),

$$\text{For } Q_{Q_K}: a_1 = X_{10}^{(v)} - X_{10}^0 + (X_{11}^{(v)} - X_{11}^0)K^2$$

$$R_{Q_K}: a_2 = X_{10}^{(v)} - X_{10}^0 + (X_{11}^{(v)} - X_{11}^0)K^2 + X_{11}^{(v)} (2K+1)$$

$$P_{Q_K}: a_3 = X_{10}^{(v)} - X_{10}^0 + (X_{11}^{(v)} - X_{11}^0)K^2 - X_{11}^{(v)} (2K-1)$$

In Appendix VI it is shown that  $(X_{10}^{(2)} - X_{10}^0)$  is about  $-.002 \text{ cm}^{-1}$ . In Appendix VII it is shown that  $X_{11}^0$  is about  $10^{-4}$ . In Section III-B we found that  $X_{02}^{(2)}$  is about  $\frac{1}{3} X_{02}^0$ . Therefore, we shall make the approximate assumption that:

$X_{11}^{(2)} - X_{11}^0 = -5 \times 10^{-5}$ . From these approximate results we have calculated the results listed in Table XXVII.

Table XXVII

Approximate Values of Spacing Constants,  $a$

K	$a_1, \text{cm}^{-1}$	$a_2, \text{cm}^{-1}$	$a_3, \text{cm}^{-1}$
2	-.0022	-.00195	-.00235
3	-.00245	-.00210	-.00270
4	-.00280	-.00235	-.00315
5	-.00325	-.00270	-.00370
6	-.00380	-.00315	-.00435

Now we are able to determine the approximate magnitude of terms such as  $(\gamma_K + \gamma_{K+1} - \beta_{K+1} - \alpha_K)$ , to be used in Appendix VIII. As defined in section II-B,

$$\alpha_K = J_R^{(K)} (J_R^{(K)} + 1)$$

$$\beta_K = J_P^{(K)} (J_P^{(K)} + 1)$$

$$\gamma_K = J_Q^{(K)} (J_Q^{(K)} + 1)$$

$J_R^{(K)}$ , etc., are the J values of observed maximum intensity in  $R_{Q_K}$ , etc., bands. Thus:

$$\alpha_K = (f_m/a_1) R_{Q_K}$$

$$\beta_K = (f_m/a_2) P_{Q_K}$$

$$\gamma_K = (f_m/a_3) Q_{Q_K}$$

Making extrapolations from Table XXVI and combining these results with Table XXVII, we have obtained the results of Table XXVIII.

Table XXVIII

Calculate Values of  $\alpha_K$ ,  $\beta_K$ , and  $\gamma_K$

K	$\alpha_K$	$\beta_K$	$\gamma_K$
2	375		43
3	385	342	64
4	390	340	85
5	395	335	107
6	400	330	127

From Table XXVIII we have derived the approximate relations.

$$\gamma_K + \gamma_{K+1} - \beta_{K+1} - \alpha_K = -690 + 40K$$

$$\alpha_{K-1} - \beta_{K+1} = 10(1 + K)$$

$$\alpha_{K-1} + \beta_{K+1} = 720$$

$$\beta_K - \gamma_K = 350 - 25K$$

$$\alpha_K - \gamma_K = 365 - 15K$$

$$\alpha_K - \beta_K = 15 + 10K$$

$$\alpha_K + \beta_K = 730$$

Appendix VI

Calculation of an Approximate Value of  $(X_{10}^{(2)} - X_{10}^0)$  for HNC $\bar{O}$

In part II-B it was found that

$$A_0 - \frac{1}{2} (B_0 + C_0) = 30.30 \text{ cm}^{-1}$$

$$A_2 - \frac{1}{2} (B_2 + C_2) = 24.75 \text{ cm}^{-1}$$

Schulman and Shoolery (47) found that  $\frac{1}{2} (B_0 + C_0) = 0.367 \text{ cm}^{-1}$ .  $\frac{1}{2} (B_2 + C_2)$  will be only slightly different, so

$$A_0 = 30.67$$

$$A_2 = 25.12$$

The subscript 2 signifies that the second excited level of  $\nu_{\text{N-H}}$  is excited, all other levels being unexcited.

In good approximation, A is proportional to  $1/r_1^2 \cos^2(\alpha - \frac{\pi}{2})$ , where  $\alpha$  is the HNC angle and  $r_1$  is the N-H distance. For the vibration  $2\nu_{\text{N-H}}$ ,  $\alpha$  remains constant but the effective value of  $r_1$  increases. Thus,

$$\frac{A_0}{A_2} = \frac{(r_1)_2^2}{(r_1)_0^2}$$

From Badger's rule we previously found that  $(r_1)_0 = 0.99 \text{ \AA}$ .

From this and the above values for  $A_0$  and  $A_2$  we find that

$(r_1)_2 = 1.097 \text{ \AA}$ . This is the effective value of  $r_1$  in the second excited state of the N-H vibration.

In HNC $\bar{O}$  the center of gravity is very close to the carbon atom; therefore,  $1/B_v$  is approximately proportional to

$$m_O (r_{C-O})^2 + m_N (r_{N-C})^2 + m_H \left\{ (r_1)_v \sin (\alpha - \pi/2) + r_{N-C} \right\}^2 .$$

Using the C-O and N-C distances of Eyster, Gillette, and Brockway (36), given in section II-C, and an angle of  $128^\circ$  for  $\alpha$ , as found in section II-C, with the values given above for  $(r_1)_0$  and  $(r_1)_2$  it is found that  $B_2/B_0 = 0.994$ .

$C_2$  is only slightly different than  $B_2$  for HNCO, so

$$\frac{X_{01}^{(2)}}{X_{01}^0} = 0.994$$

Since  $X_{01}^0 = 0.367$ ,  $X_{01}^{(2)} = 0.365$  and

$$X_{01}^{(2)} - X_{01}^0 = -.002 \text{ cm}^{-1}.$$

Appendix VII

Calculation of an Approximate Value of  $X_{11}^0$

It was shown by Wilson and Howard (51) that the rotational energy of a vibrating rotator can be expressed as

$$W_R = \frac{1}{2} \sum_{\alpha\beta} \mu_{\alpha\beta}^{(0)} P_\alpha P_\beta - \frac{1}{8} \sum \lambda_{\alpha\beta\gamma\delta} P_\alpha P_\beta P_\gamma P_\delta$$

The second term is the contribution of centrifugal distortion.

$$\lambda_{\alpha\beta\gamma\delta} = \sum_k \frac{\mu_{\alpha\beta}^{(k)} \mu_{\gamma\delta}^{(k)}}{\lambda_k}$$

$$\lambda_k = 4\pi^2 \nu_k^2$$

$\mu_{\alpha\beta}^{(0)}$   $\mu_{\alpha\beta}^{(k)}$  is the first derivative of the rotational constant with respect to the normal coordinate  $k$ .  
 $\alpha, \beta, \gamma,$  and  $\delta$  are the coordinates of  $x, y,$  and  $z$ .  
 $P_\alpha, P_\beta,$  etc., are the angular momenta  $P_x, P_y,$  and  $P_z$ .

$$P_z = Kh/2\pi$$

$$P_x^2 + P_y^2 + P_z^2 = J(J+1) h^2/4\pi^2.$$

For HNC0 the largest  $\mu_{\alpha\beta}^{(k)}$  are  $\mu_{zz}^{(1)}$  and  $\mu_{zz}^{(4)}$ , where (1) and (4) represent the hydrogen stretching and bending

vibrations respectively. Furthermore, since  $\lambda_1$  is very much larger than  $\lambda_4$  the terms containing  $\mu_{zz}^{(4)}$  have a much larger effect. Therefore we shall attempt to calculate  $X_{11}^0$  in the approximation that only terms containing  $\mu_{zz}^{(4)}$  are appreciable. The centrifugal distortion term then becomes

$$(\Delta E)_C = -\frac{1}{8} \left\{ \tau_{zzzz} P_z^4 + \tau_{yyzz} P_y^2 P_z^2 + \tau_{xxzz} P_x^2 P_z^2 \right\}$$

But  $P_z = Kh/2\pi$  ,  $P_x^2 + P_y^2 = \{J(J+1) - K^2\} h^2/4\pi^2$

and  $\tau_{yyzz} \approx \tau_{xxzz}$

$$(\Delta E)_C = -\frac{1}{8} \left\{ \frac{h^4}{16\pi^4} \right\} \left\{ [\tau_{zzzz} - 2\tau_{yyzz}] K^4 + \tau_{yyzz} J(J+1) K^2 \right\} \quad \text{VII-1}$$

In our approximation,  $\tau_{yyzz} = \frac{\mu_{yy}^{(4)} \mu_{zz}^{(4)}}{\lambda_4}$

In order to express  $W_R$  in ergs  $\mu_{zz}^{(0)}$  and  $\mu_{yy}^{(0)}$  are the reciprocals of the moments of inertia  $I_{zz}$  and  $I_{yy}$ . For HNC0 the center of gravity is very close to the VII-4 carbon atom so these moments of inertia are approximated by,

$$I_{zz} = m_H r_{N-H}^2 \cos^2 \varphi$$

$$I_{yy} = m_O r_{C-O}^2 + m_N r_{C-N}^2 + m_H (r_{N-H} \sin \varphi + 1.21)^2$$

$$\varphi = \angle \text{HNC} - \pi/2.$$

In order that the centrifugal distortion,  $(\Delta E)_C$ , be

expressed in ergs, the normal coordinate,  $Q_4 = \sqrt{m} r_{N-H} \varphi$ .

$$\mu_{zz}^{(4)} = \frac{d\mu_{zz}^{(0)}}{d\varphi} \frac{d\varphi}{dQ_4}$$

$$\mu_{yy}^{(4)} = \frac{d\mu_{yy}^{(0)}}{d\varphi} \frac{d\varphi}{dQ_4}$$

Substituting in the parameters of section II-C,

$$\mu_{zz}^{(4)} = 1.338 \times 10^{60} \text{ gm}^{-3/2} \text{ cm}^{-3}$$

$$\mu_{yy}^{(4)} = -6.21 \times 10^{56} \text{ gm}^{-3/2} \text{ cm}^{-3}$$

$$\lambda_4 = 4\pi^2 \nu_4^2 = 2.276 \times 10^{28} \text{ sec}^{-2}$$

$$\tau_{yyzz} = \frac{\mu_{zz}^{(4)} \mu_{yy}^{(4)}}{\lambda_4} = -3.66 \times 10^{88} \text{ gm}^{-3} \text{ cm}^{-6} \text{ sec}^2$$

$$\tau_{zzzz} = \frac{\{\mu_{zz}^{(4)}\}^2}{\lambda_4} = 7.88 \times 10^{91} \text{ gm}^{-3} \text{ cm}^{-6} \text{ sec}^2$$

Then from Equation (VII-1),

$$\begin{aligned} (\Delta E)_C &= -1.218 \times 10^{-17} K^4 + 5.65 \times 10^{-21} K^2 J(J+1) \text{ ergs} \\ &= -0.061 K^4 + 2.84 \times 10^{-5} K^2 J(J+1) \text{ cm}^{-1} \end{aligned}$$

Thus, in the approximation that the bending of the HNC angle is the main contribution to centrifugal distortion,

$$X_{02}^0 = -0.061 \text{ cm}^{-1}$$

$$X_{11}^0 = 2.84 \times 10^{-5} \text{ cm}^{-1}$$

The experimental value for  $X_{02}^0$  is  $-.22 \text{ cm}^{-1}$ , so  $X_{11}^0$  is probably larger than calculated above. Thus,  $X_{11}^0$  is probably about  $10^{-4} \text{ cm}^{-1}$ .

Appendix VIII

Approximate Calculation of  $\delta_K''$  of Equation (12)  
for HNC0

From Equation (11)

$$\begin{aligned} \Delta_K &= \overset{Q}{Q}_K - \overset{P}{Q}_{K+1} - \overset{R}{Q}_K + \overset{Q}{Q}_{K+1} \\ &= \left\{ X_{11}^{(v)} - X_{11}^0 + (X_{11}^{(v)} - X_{11}^0) K^2 \right\} \gamma_K + \gamma_{K+1} - \beta_{K+1} - \alpha_K \\ &\quad + X_{11}^{(v)} (2K + 1) (\gamma_K - \alpha_K) + X_{11}^0 (2K + 1) (\beta_{K+1} - \gamma_{K+1}) \\ &\quad + (X_{20}^{(v)} - X_{20}^0) (\gamma_K^2 + \gamma_{K+1}^2 - \beta_{K+1}^2 - \alpha_K^2) \end{aligned}$$

$X_{20}^{(v)}$  is a second order term compared with  $X_{10}^{(v)}$ . Furthermore  $X_{20}^{(v)}$  depends mainly on the change of the large moment of inertia with rotation and will not be affected much by changes in the quantum number of the N-H vibration. Therefore we shall neglect  $X_{20}^{(v)} - X_{20}^0$ .

In Appendix VII it is shown that  $X_{11}^0$  is expected to be about  $10^{-4}$ .  $X_{11}^{(2)}$  will be smaller than  $X_{11}^0$ . As shown in Appendix V,  $(\beta_{K+1} - \gamma_{K+1})$  is positive and somewhat smaller than  $(\alpha_K - \gamma_K)$  which is also positive. Therefore, the second and third terms will have a compensating effect and the sum of the two will be small. The first term will be positive and much larger than the rest, so we shall write -

$$X_{10}^{(v)} - X_{10}^0 + (X_{11}^{(v)} - X_{11}^0) K^2 \left\{ \gamma_K + \gamma_{K+1} - \beta_{K+1} - \alpha_K \right\} < \Delta_K$$

In Appendix V it is shown that

$$\gamma_K + \gamma_{K+1} - \beta_{K+1} - \alpha_K = -690 + 40K$$

Therefore,

$$-\left\{ X_{10}^{(v)} - X_{10}^0 + (X_{11}^{(v)} - X_{11}^0) K^2 \right\} < \frac{\Delta_K}{690-40K} \quad \text{VIII-1}$$

From Equation ( 13 ),

$$\begin{aligned} \int_K'' &= \left\{ X_{10}^{(v)} - X_{10}^0 + (X_{11}^{(v)} - X_{11}^0) K^2 \right\} \left\{ \alpha_{K-1} - \beta_{K+1} \right\} \\ &+ X_{11}^0 (2K) \left\{ \beta_{K+1} + \alpha_{K-1} \right\} + X_{11}^0 \left\{ \beta_{K+1} - \alpha_{K-1} \right\} \end{aligned}$$

again neglecting  $X_{20}^{(v)} - X_{20}^0$ .

The last term will be small compared to the others. Then, using Equation (VIII-1),

$$\int_K'' < \left( \frac{-\Delta_K}{690-40K} \right) (\alpha_{K-1} - \beta_{K+1}) + X_{11}^0 (2K) (\beta_{K+1} + \alpha_{K-1})$$

Using the results of Appendix V,

$$\int_K'' < \frac{-\Delta_K (K+1)}{69 - 4K} + (4K) 360X_{11}^0 \quad \text{VIII-2}$$

From the values of  $\Delta_K$  given in Table (XIII ), the first term on the right is approximated by  $(-.01)4K$ . In Appendix VII it is shown that  $X_{11}^0$  is expected to be about  $10^{-4}$ .

Substituting these values in Equation VIII-2,

$$\int_K^{\infty} 4K(.026) \text{ cm}^{-1}$$

The assumptions made are good enough to say with confidence that

$$\int_K^{\infty} 4K(0.10) \text{ cm}^{-1}.$$

This will allow  $X_{11}^0$  to be as high as  $3 \times 10^{-4}$ .

Appendix IX

Calculation of the change in the smallest moment of inertia of HNC0 with small changes in the HNC and NCO angles from the values  $129^\circ$  and  $180^\circ$  respectively.

For this calculation we shall define the following quantities:

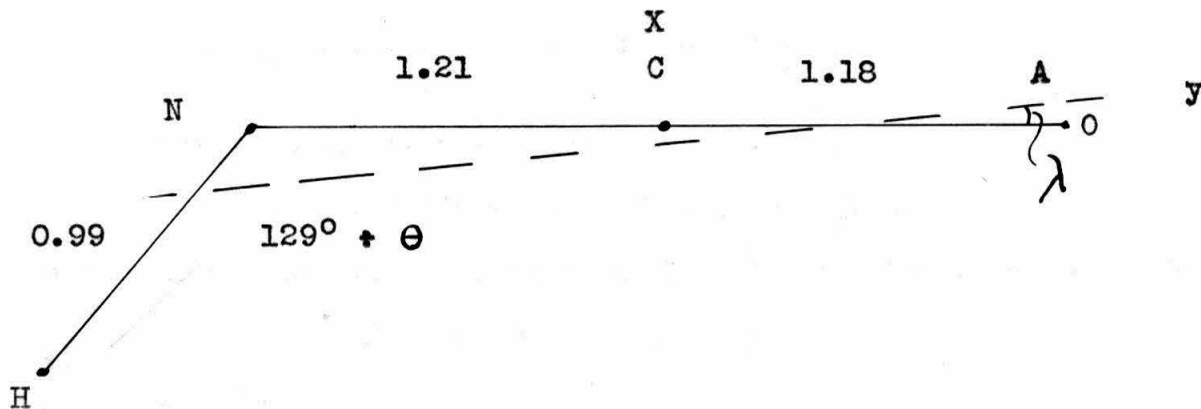
$\Theta$  = change in HNC angle from  $129^\circ$

$\gamma$  = change in NCO angle from  $180^\circ$

$\lambda$  = angle least axis of inertia makes with the C-O axis

$\beta = \Theta - \gamma$

We shall assume the model indicated below, for the reasons presented in section II-B



We are interested only in small displacements, and  $\lambda$  is small, so  $\sin \lambda = \lambda$ ,  $\cos \lambda = 1$ ,  $\lambda = \gamma, \Theta, \beta, \lambda$ .

In this approximation we calculate the center of gravity coordinates, relative to the carbon atom as origin,

$$\bar{y} = -.01804 - 0.4226 \gamma + 0.0146 \beta \lambda$$

$$\bar{x} = 0.00186 - .01804 \beta \lambda$$

Knowing  $\bar{x}$  and  $\bar{y}$  we can set up the expression for the moment of inertia about the least axis of inertia, A.

$$\begin{aligned}
 6.023 \times 10^{39} I_A = & 1.008 [ .7514 + .787 \gamma - .608 \beta - 1.83 \lambda - .7694 \beta \lambda ]^2 \\
 & + 14.008 [ .01804 - .787 \gamma - .0146 \beta + 1.21 \lambda ]^2 \\
 & + 12.010 [ .01804 + .423 \gamma - .0146 \beta ]^2 \\
 & + 16.000 [ -.01804 - .423 \gamma + .0146 \beta + 1.18 \lambda ]^2
 \end{aligned}$$

Since  $\beta$  and  $\lambda$  are both small, in first approximation we shall neglect  $0.7694 \beta \lambda$ . If we now take  $\frac{\partial I_A}{\partial \lambda} = 0$  and solve for  $\lambda$  thus giving  $\lambda$  for the least axis of inertia we find that

$$\lambda = .03077 + .494 \gamma - .0250 \beta$$

We can now correct for our neglect of  $\lambda \beta$ , giving

$$\lambda = .03077 + .494 \gamma - .0260 \beta$$

We now shall put this expression for  $\lambda$  in the expression for  $I_A$ , and also substitute  $\theta - \gamma$  for  $\beta$ .

The result is

$$\begin{aligned}
 6.023 \times 10^{39} I_A = & 1.008 [ .6953 + .467 \gamma - .585 \theta ]^2 \\
 & + 14.008 [ .0552 - .144 \gamma - .0460 \theta ]^2 \\
 & + 12.010 [ .0180 + .437 \gamma - .0146 \theta ]^2 \\
 & + 16.000 [ .0183 + .176 \gamma - .0160 \theta ]^2
 \end{aligned}$$

From this expression:

$$(I_A)_{\substack{\theta = 0 \\ \gamma = 0}} = 0.8946 \times 10^{-40} \text{ gm cm}^2$$

$$\left( \frac{\partial I_A}{\partial \theta} \right)_{\substack{\theta = 0 \\ \gamma = 0}} = -1.506 \times 10^{-40} \text{ gm cm}^2/\text{radian}$$

$$\left( \frac{\partial I_A}{\partial \gamma} \right)_{\substack{\theta = 0 \\ \gamma = 0}} = +1.202 \times 10^{-40} \text{ gm cm}^2/\text{radian}$$

Appendix X

Calculation of the coefficient of the  $K^4$  term in the energy expression for HNC0, taking account of centrifugal distortion of the HNC and NCO angles.

We shall equate the centrifugal force on the oxygen and carbon atoms to the restoring force on the respective atoms.

$$f_O = m_O R_O \omega^2 = k_\gamma \delta / r_3 \quad \text{X-1}$$

$$f_C = m_C R_C \omega^2 = k_\gamma \left\{ \frac{1}{r_2} + \frac{1}{r_3} \right\} + k_\theta \theta / r_3 \quad \text{X-2}$$

$m_O$  and  $m_C$  are the masses of the oxygen and carbon atoms.

$R_O$  and  $R_C$  are the distances of the oxygen and carbon atoms from the least axis of inertia.

$r_2$  is the N-C distance

$r_3$  is the C-O distance

$k_\gamma$  and  $k_\theta$  are the force constants for the bending of the NCO and HNC angles respectively.

From Equations (X-1) and (X-2),

$$\delta = m_O R_O r_3^2 / k \quad \text{X-3}$$

$$\theta = \left\{ m_C R_C r_2 - m_O R_O (r_2 + r_3) \right\} \omega^2 / k_\theta$$

For  $\text{CO}_2$ ,  $k_\gamma = 0.77 \times 10^{-11}$  dynes cm/radian, and the bending frequency is  $667 \text{ cm}^{-1}$ . For NCO the bending frequency is  $540 \text{ cm}^{-1}$ , so we shall make the approximation,

$k_{\gamma} = \frac{(0.77 \times 10^{-11})(550)^2}{(667)^2} = 0.52 \times 10^{-11}$  dynes cm/  
radian and the bending frequency is  $667 \text{ cm}^{-1}$ .

The HNC bending is primarily an oscillation of the hydrogen atom so we shall make the approximation

$$k_{\theta} = 4\pi^2 \frac{m_H r_1^2}{I} \nu^2 = 0.36 \times 10^{-11} \text{ dynes cm/radian.}$$

We shall attempt to calculate only the coefficient of  $K^4$ , which is the centrifugal distortion as the molecule begins to rotate. Therefore,  $R_O$  and  $R_C$  will be the distances of the oxygen and carbon atoms, respectively, from the least axis of inertia for the non-rotating molecule. Without rotation  $\gamma = 0$  and  $\theta = 41' = .012$  radians (see Section II-C).

Then from Appendix IX,

$$R_O = .0181 \times 10^{-8} \text{ cm}$$

$$R_C = .0178 \times 10^{-8} \text{ cm}$$

From Section II-B,

$$r_3 = 1.18 \times 10^{-8}$$

$$r_2 = 1.21 \times 10^{-8}$$

Substituting in Equation X-3 we find,

$$\gamma = 1.09 \times 10^{-29} \quad 2$$

$$\theta = -2.00 \times 10^{-29} \quad 2$$

$$\omega^2 = K^2 h^2 / 4\pi^2 I_A^2 = 1.337 \times 10^{26} K^2$$

Thus,  $\gamma = 1.457 \times 10^{-3} K^2$

$$\theta = -2.674 \times 10^{-3} K^2$$

The change in kinetic energy due to rotation is,

$$\Delta E_K = -\frac{K^2 h^2}{8\pi^2 I_A^2} \left\{ \frac{d I_A}{d \gamma} \gamma + \frac{d I_A}{d \theta} \theta \right\} \quad \text{ergs}$$

Using the above values of  $\gamma$  and  $\theta$  and the values of  $\frac{d I_A}{d \theta}$  and  $\frac{d I_A}{d \gamma}$  from Appendix IX, we calculate that

$$\Delta E_K = -1.17 \times 10^{-17} K^4 - 2.68 \times 10^{-17} K^4$$

The change in potential energy is

$$\Delta E_P = \frac{1}{2} k_\gamma \gamma^2 + \frac{1}{2} k_\theta \theta^2$$

Using the values of  $k_\gamma, k_\theta, \gamma,$  and  $\theta$  given above

$$\Delta E_P = .55 \times 10^{-17} K^4 + 1.28 \times 10^{-17} K^4$$

The total change in energy due to centrifugal distortion is then

$$(\Delta E)_C = -0.62 \times 10^{-17} K^4 - 1.40 \times 10^{-17} K^4 \text{ ergs}$$

$$= -.031 K^4 - .070 K^4 \text{ cm}^{-1}$$

$$= -.101 K^4 \text{ cm}^{-1}.$$

Thus the contribution of the NCO bending to the centrifugal distortion,  $-.031 K^4 \text{ cm}^{-1}$ , is almost half that of the HNC bending, in this approximation for small rotations.

Appendix XI

Mixing of eigenfunctions of three interacting energy levels.

For three close-lying levels, A, B, and C, having wave functions  $\psi_A$ ,  $\psi_B$ , and  $\psi_C$ , there will be resonance, depending on the magnitude of the interaction energy. The wave functions of the resulting levels are represented by:

$$\psi_{I, II, III} = a \psi_A + b \psi_B + c \psi_C$$

where the coefficients a, b, and c may have different values for  $\psi_I$ ,  $\psi_{II}$ , and  $\psi_{III}$ . Also, for normalization,  $a^2 + b^2 + c^2 = 1$ .

A solution to this problem is found from the wave equation :

$$\int \psi_{I,II,III}^* H \psi_{I,II,III} d\tau = E_{I,II,III} \int \psi_{I,II,III}^* \psi_{I,II,III}$$

Upon expanding this equation in terms of  $\psi_A$ ,  $\psi_B$ , and  $\psi_C$ , and minimizing the energy with respect to a, b, and c, we can set up the secular determinant:

$$\begin{vmatrix} H_{AA} - E & H_{AB} & H_{AC} \\ H_{AB} & H_{BB} - E & H_{BC} \\ H_{AC} & H_{BC} & H_{CC} - E \end{vmatrix} = 0$$

This is a rather cumbersome equation to solve except in certain special cases. We shall choose the special case for which

$$H_{BB} = H_{CC} \neq H_{AA}$$

$$H_{AB} = H_{AC} .$$

The solution of the secular determinant now gives

$$E_I = H_{BB} - H_{BC}$$

$$E_{II,III} = \frac{1}{2} \left\{ H_{AA} + H_{BB} + H_{BC} \pm \sqrt{(H_{AA} - H_{BB} - H_{BC})^2 + 8H_{AB}^2} \right\}$$

and

$$\psi_I = \frac{1}{\sqrt{2}} \psi_B - \frac{1}{\sqrt{2}} \psi_C$$

$$\psi_{II,III} = \frac{1}{\sqrt{4H_{AB}^2 + 2(H_{AA} - E_{II,III})^2}} \left\{ -2H_{AB} \psi_A + (H_{AA} - E_{II,III}) (\psi_B + \psi_C) \right\}$$

We wish to investigate the intensities of infrared absorption bands involving transitions to each of the levels I, II, and III. The intensity of a transition is given by

$$\left\{ \int \psi_U \psi_L \text{Md}\tau \right\}^2 = M_{UL}^2$$

where  $M$  is the electric moment of the molecule and  $\psi_L$  and

$\psi_U$  are the wave functions for the lower and upper level respectively. We wish to apply the results of these calculations to the perturbed band at  $5790 \text{ cm}^{-1}$ . We believe most of the intensity in this band comes from one transition,  $\nu_1 + \nu_2$ .

Therefore we shall make the following assumptions:

$\nu_1 + \nu_2$  is referred to as level A before perturbation.

$$M_{AL} \neq 0$$

$$M_{BL} = M_{CL} = 0$$

Due to the interaction, the levels I, II, and III may all have some of the character of  $\psi_A$ , in which case  $M_{IL}$ ,  $M_{II L}$ , and  $M_{III L}$  may all be  $\neq 0$ . The intensities of the three transitions to levels I, II, and III will be  $M_{I L}^2$ ,  $M_{II L}^2$ , and  $M_{III L}^2$  respectively. These intensities will be proportional to the squares of the coefficients of  $\psi_A$  in  $\psi_I$ ,  $\psi_{II}$ , and  $\psi_{III}$ .

From the expressions given above for  $\psi_I$ ,  $\psi_{III}$ , and  $\psi_{III}$  we find that

$$M_{I L}^2 = 0$$

$$M_{II L}^2 = \frac{4H_{AB}^2}{4H_{AB}^2 + 2(H_{AA} - E_{II})^2}$$

$$M_{III L}^2 = \frac{4H_{AB}^2}{4H_{AB}^2 + 2(H_{AA} - E_{III})^2}$$

Thus, after the interaction one of the transitions still has no intensity. The ratio of the intensities of the other two transitions is

$$\frac{I_{II}}{I_{III}} = \frac{4H_{AB}^2 + 2(H_{AA} - E_{III})^2}{4H_{AB}^2 + 2(H_{AA} - E_{II})^2}$$

Using the expressions given above for  $E_{II}$  and  $E_{III}$  we find that

$$\frac{I_{II}}{I_{III}} = 1 + \frac{2(E_{II} - E_{III})(H_{AA} - H_{BB} - H_{BC})}{4H_{AB}^2 + 2(H_{AA} - E_{III})^2}$$

It is arbitrary which of these two levels we call II and which we call III. Let us consider  $E_{II} > E_{III}$ .

Then  $I_{II} > I_{III}$  if  $H_{BC} < H_{AA} - H_{BB}$

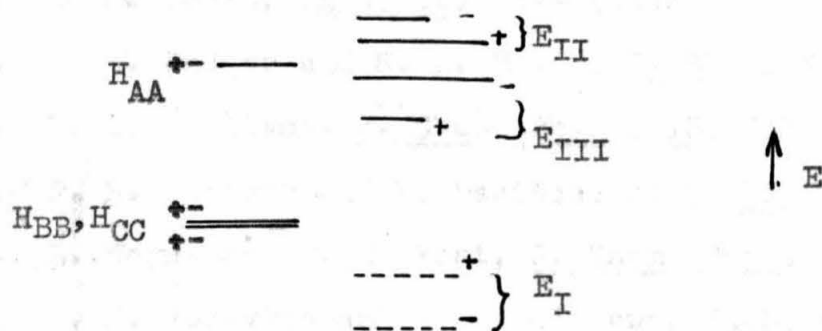
$I_{II} < I_{III}$  if  $H_{BC} > H_{AA} - H_{BB}$

Since HNC0 is not a symmetric top, the  $+$  and  $-K$  levels are not degenerate and may have different interaction integrals,

$$H_{BC}^+ \text{ and } H_{BC}^- .$$

If  $H_{BC}^+ < H_{AA} - H_{BB}$  and  $H_{BC}^- > H_{AA} - H_{BB}$

we may obtain the following levels as a result of the perturbations, assuming  $H_{BC}^+$  and  $H_{BC}^-$  are positive and  $H_{AA} > H_{BB}$ .



The lengths of the full lines on the right represent qualitatively the magnitude of the intensity of absorption for the transition to the levels indicated.

The same pattern is obtained in reverse, of course, if  $H_{BC}^+$  and  $H_{BC}^-$  are negative and  $H_{AA} < H_{BB}$ .

This pattern is qualitatively the same as the observed vibrational-rotational transitions,  $R_{Q,K}$  and  $P_{Q,K}$ , of the band at  $5790 \text{ cm}^{-1}$ , shown in Fig. XVII.

REFERENCES

1. R. M. Badger and S. H. Bauer, J. Chem. Phys., 4, 469 (1936).
2. R. M. Badger and S. H. Bauer, J. Chem. Phys., 5, 839 (1937).
3. J. G. Kirkwood, J. Chem. Phys., 2, 358 (1934).
4. W. Gordy, Phys. Rev., 50, 1151 (1936).  
JACS, 60, 605 (1938).  
Nature, 142, 831 (1938).
5. W. Gordy, J. Chem. Phys., 7, 93 (1939).
6. Kreuzer and R. Mecke, Z. physik. Chem., series B, 49, 309 (1942).
7. J. J. Fox and A. E. Martin, Proc. Roy. Soc. London, A, 162, 419 (1937).
8. E. H. Melvin and O. R. Wulf, J. Chem. Phys., 3, 755 (1935).
9. E. J. Jones, JACS, 65, 2274 (1943).
10. R. M. Badger and S. H. Bauer, J. Chem. Phys., 5, 852 (1937).
11. V. Z. Williams, J. Chem. Phys., 15, 232 (1947).
12. F. H. Verhoek and F. Daniels, JACS, 53, 1250 (1931).
13. L. Wayne and D. M. Yost, J. Chem. Phys., 8, 767 (1950).
14. W. R. Forsythe and W. F. Giaugue, JACS, 64, 48 (1942).
15. R. M. Badger, L. R. Zumwalt, and P. A. Giguere, Rev. of Sci. Inst., 19, 861 (1948).
16. W. F. Meggers and C. J. Humphreys, Bureau of Standards Journal of Research, 10, 427 (1933).
17. R. C. Nelson, Atlas and Wavelength Tables, Summary Report No. IV, Dept. of Physics, Northwestern Univ., Evanston, Illinois.
18. G. Herzberg, Infrared and Raman Spectra, pp. 48, 460, (D. Van Nostrand, New York, 1947).
19. L. O. Brockway, J. Y. Beach, and L. Pauling, JACS, 55, 2693(1935).

20. G. Herzberg, Infrared and Raman Spectra, pp. 463, 468,  
(D. Van Nostrand, New York, 1947).
21. G. W. King, R. M. Hainier, and P. C. Cross, J. Chem. Phys.,  
11, 27 (1943).
22. Stig Claesson, J. Donahue, and V. Schomaker, J. Chem. Phys.,  
16, 207 (1948).
23. R. M. Badger, J. Chem. Phys., 2, 128 (1934).  
J. Chem. Phys., 3, 710 (1935).
24. F. Rogowski, Ber. 75B, 244 (1942).
25. V. Schomaker and D. P. Stevenson, JACS, 63, 37 (1940).
26. R. M. Badger, J. Chem. Phys., 8, 288 (1940).
27. B. S. Ray, Z. Physik., 78, 74 (1932).
28. G. Herzberg, Infrared and Raman Spectra, p. 45,  
(D. Van Nostrand, New York, 1947).
29. G. Herzberg, Infrared and Raman Spectra, pp. 421, 426,  
(D. Van Nostrand, New York, 1947).
30. G. Herzberg, Infrared and Raman Spectra, p. 300,  
(D. Van Nostrand, New York, 1947).
31. G. Herzberg, Infrared and Raman Spectra, p. 206,  
(D. Van Nostrand, New York, 1947).
32. E. B. Wilson, Jr., J. Chem. Phys., 7, 1047 (1939).
33. Franklin, Nitrogen System of Compounds, p. 108, Reinhold  
Publishing Co., 1935.
34. G. Herzberg and H. Verleger, Z. Physik., 37, 444 (1936).
35. E. H. Eyster, J. Chem. Phys., 8, 135 (1940).
36. E. H. Eyster, R. H. Gillette, and L. O. Brockway,  
JACS, 62, 3236 (1940).
37. J. Goubeau, Ber. d. d. Chem. Ges., 68, 912 (1935).
38. J. Goubeau and O. Gott, Ber. 73, 127 (1940).
39. Beard and Dailey, J. Chem. Phys., 15, 762 (1947).
40. L. Pauling, Nature of the Chemical Bond, p. 84, 168,  
(Cornell University Press, Ithaca, New York) 1945.

41. G. Herzberg, Infrared and Raman Spectra, p. 279,  
(D. Van Nostrand Co., Inc., New York, 1947).
42. P. E. Martin and E. F. Barker, Phys. Rev., 41, 291 (1932).
43. G. Herzberg, Infrared and Raman Spectra, p. 414,  
(D. Van Nostrand Co., Inc., New York, 1947).
44. Slawsky and D. M. Dennison, J. Chem. Phys., 7, 509 (1939).
45. L. Zumwalt and P. Giguere, J. Chem. Phys., 9, 458 (1941)
46. G. Herzberg, Infrared and Raman Spectra, p. 439,  
(D. Van Nostrand Co., Inc., New York, 1947).
47. J. Schulman and P. G. Shooley, to be published in J. Chem. Phys.
48. L. Pauling, Nature of the Chemical Bond, p. 197,  
(Cornell University Press, Ithaca, New York, 1947).
49. P. C. Cross, Phys. Rev., 47, 7 (1935).
50. H. Honl and F. London, Z. Physik., 33, 803 (1925).  
Ann. d. Phys., 79, 273 (1926).
- D. M. Dennison, Phys. Rev., 28, 318 (1926).
- F. Reiche and H. Rademaker, Z. Physik., 39, 444 (1926).  
Z. Physik., 41, 453 (1927).
51. E. B. Wilson and J. B. Howard, J. Chem. Phys., 4, 260 (1936).

PROPOSITIONS

1. The structure of fulminic acid is usually given as HONC (1). I propose that the most important structure for fulminic acid is HCNO, due to increased resonance stabilization. This could be readily determined from the infrared spectrum of fulminic acid vapor. I would predict a very large HCN-angle, of the order of  $150^\circ$ .

2. The infrared spectrum of nitrous acid vapor (Part II of this thesis) gives no indication of a dimer of nitrous acid analogous to that in formic acid. It is proposed that an infrared investigation of a mixture of  $H_2O$  and  $NO_2$  with several atmospheres of NO would reveal absorption bands due to a dimer of cis-nitrous acid.

Perhaps a cis-trans dimer is an intermediate in the decomposition of nitrous acid.

3. In studying the spectrum of nitrous acid it was observed that  $N_2O_3$  has a strong absorption band at  $1835\text{ cm}^{-1}$ . This frequency is only slightly lower than the vibrational frequency of NO,  $1879\text{ cm}^{-1}$ . I propose that this indicates that the important structure for  $N_2O_3$  has a long  $N\cdots N$  three-electron bond.

This structure is in accord with the crystal structure of  $N_2O_4$  (2), indicating a long N - N bond of  $1.64\text{ \AA}$ , which may be a three-electron bond.

4. In observing the infrared spectrum of HNCS it was noticed that HNCS decomposes slowly, forming HCN. It is proposed that an investigation of the rate of the decomposition through the use of infrared spectroscopy would be of interest. Probably the molecule decomposes unimolecularly, as  $\text{HNCS} \rightarrow \text{HCN} + \text{S}$ . If so, HNC may be an intermediate in the decomposition. Perhaps an infrared spectrum of a long path length of decomposing HNCS would reveal absorption bands due to HNC.

5. In the infrared spectrum of HNCS a few bands were observed which may arise from the isomer HSCN (thesis, Part III-H). It is proposed that if the band at  $2847 \text{ cm}^{-1}$  were observed under fairly high dispersion, an analysis of the rotational structure would determine whether this is the S-H frequency of HSCN, a combination band of HNCS, or a band from an impurity.

There is no evidence of HOCN in the spectrum of HNCO. However, it is expected that the stability of HSCN with respect to HNCS would be greater than the stability of HOCN with respect to HNCO.

6. For a mixture of high polymers made up of the same sub-molecules but having a statistical distribution of molecular weights the following properties may exist: (a) conformance to the law for intrinsic viscosity,  $[\eta] = KM^\alpha$ ; and (b) mechanism of degradation involves complete peeling off of monomer units when a bond is ruptured. For such a polymer mixture the following simple experiment can be performed to determine the constant  $\alpha$ .

A known weight of the polymer mixture, of known intrinsic viscosity, is partially degraded by heating. The monomer is removed as soon as it is formed. The remaining polymer is weighed and its intrinsic viscosity is measured. It can be shown that

$$\alpha = 2 \frac{\log [\eta]_o - \log [\eta]_f}{\log W_o - \log W_f} .$$

$W_o$  and  $W_f$  are the weights before and after degradation.  $[\eta]_o$  and  $[\eta]_f$  are the intrinsic viscosities before and after degradation.

7. A simple calculation shows that for a symmetrical, linear triatomic molecule,  $XYX$ , in which the bending mode performs harmonic oscillations and only one of the mutually degenerate pairs of vibrations is excited, the quantum mechanical average of the moment of inertia about the least axis of inertia increases linearly with the quantum number of the bending vibration, while the quantum mechanical average of the reciprocal of this moment of inertia is infinity for all even levels, and a constant for all odd levels. For odd levels,

$$(1/I_A)_{n = \text{odd}} = 8 \pi^2 \nu_o / h.$$

8.  $^R Q_K$  and  $^P Q_K$  branches which are observed in the infrared vibration-rotation spectra of perpendicular bands of symmetric top molecules are made up of many, usually unresolved lines arising from transitions of different  $J$  value, having slightly different frequencies. The observed maxima in these  $Q$  branches occur at a  $J$  value which is a function of: (a) the matrix element of the transition electric moment; (b) the difference in

frequency for transitions of different J value; (c) the resolution of the spectrometer.

For a given  $R_{Q_K}$  or  $P_{Q_K}$  transition, an expression can be derived relating the J value of observed maximum intensity to the small rotational constant, the effective slit width, and the difference in rotational constants of the two levels. (See Appendix V, page 123.)

9. If two energy levels, A and B, with the same zero order wave functions interact with another level, C, with a slightly different zero order wave function, it can be shown that of the resulting three mixed wave functions one is a mixture of A and B only, while the other two are mixtures of all three zero order wave functions. (See Appendix XI of thesis.)

10. The assignments of the vibrational frequencies of formic acid are still in great doubt. Bonner and Hofstadter (3) have assigned the frequency at  $1090\text{ cm}^{-1}$  to the C-O stretching frequency. The reason for this assignment is not clear. I propose that this band at  $1090\text{ cm}^{-1}$ , or  $1105\text{ cm}^{-1}$  according to V. Z. Williams (4), can equally well be a C-H bending frequency, and that the C-O frequency is probably a good deal lower.

V. Z. Williams (4) has investigated the spectra of  $\text{HCOOH}$ ,  $\text{HCOOD}$ ,  $\text{DCOOH}$ , and  $\text{DCOOD}$ . His results are rather incomplete. It is proposed that a thorough investigation of the spectra of these four isotopic species should certainly yield the correct assignments of frequencies to the vibrations of formic acid.

11. Herzberg and Reid (5) have made a vibrational analysis of the infrared spectrum of HNC $\bar{O}$ . They explain the large divergence of the Q branches of the hydrogen-bending vibration by Coriolis interaction with the out of plane bending vibration. I propose that such an interaction cannot take place.

12. I propose that two new units be defined for moments of inertia, to replace gm cm<sup>2</sup> and (atomic weight units) $\text{\AA}^2$ .

#### REFERENCES

1. P. Karrer, Organic Chemistry, p. 212, (Nordeman Publishing Inc., New York, 1938).
2. J. S. Broadley and J. M. Robertson, Nature, 164, 915 (1949).
3. L. G. Bonner and R. H. Hofstadter, J. Chem. Phys., 6, 531 (1938).  
R. Hofstadter, J. Chem. Phys., 6, 540 (1938).
4. V. Z. Williams, J. Chem. Phys., 15, 5 (1947).
5. G. Herzberg and C. Reid, Private communication to Professor R. M. Badger.

Supplementary Propositions by Llewellyn H. Jones

13. Consider two unfractionated high polymer mixtures, A and B, made up of the same kind of monomer units. If each mixture has a normal statistical distribution of molecular weights but A and B are polymerized to different degrees, it can be shown that  $(M_n)_A / (M_n)_B \cong (M_w)_A / (M_w)_B \cong (M_z)_A / (M_z)_B$ .

$M_n$  is the number average molecular weight.

$M_w$  is the weight average molecular weight.

$M_z$  is the "z" average molecular weight.

14. In discussing various types of molecular weight distributions of high polymers the evaluation of  $\sum_{n=1}^{\infty} n^x p^n$  is of some interest. It can be shown that

$$\sum_{n=1}^{\infty} n^x p^n = \frac{1}{(1-p)^{x+1}} \sum_{r=1}^x \left\{ \sum_{s=0}^{x+1} \frac{(-1)^s (x+1)(x)(x-1)\dots(x-s+2)}{s!} (r-s)^x \right\} p^r$$